

In presenting the dissertation as a partial fulfillment of the requirements for an advanced degree from the Georgia Institute of Technology, I agree that the Library of the Institute shall make it available for inspection and circulation in accordance with its regulations governing materials of this type. I agree that permission to copy from, or to publish from, this dissertation may be granted by the professor under whose direction it was written, or, in his absence, by the Dean of the Graduate Division when such copying or publication is solely for scholarly purposes and does not involve potential financial gain. It is understood that any copying from, or publication of, this dissertation which involves potential financial gain will not be allowed without written permission.

*S. J. ...*

7/25/68

MOBILITIES, LONGITUDINAL DIFFUSION COEFFICIENTS,  
AND REACTION RATES OF MASS-IDENTIFIED  
POSITIVE IONS IN CARBON MONOXIDE

A THESIS

Presented to

The Faculty of the Division of Graduate  
Studies and Research

by

John Herman Schummers


In Partial Fulfillment  
of the Requirements for the Degree  
Doctor of Philosophy  
in the School of Physics

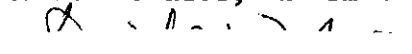
Georgia Institute of Technology


July, 1972

MOBILITIES, LONGITUDINAL DIFFUSION COEFFICIENTS,  
AND REACTION RATES OF MASS-IDENTIFIED  
POSITIVE IONS IN CARBON MONOXIDE

Approved:

  
\_\_\_\_\_  
Earl W. McDaniel, Chairman

  
\_\_\_\_\_  
David W. Martin

  
\_\_\_\_\_  
Ian R. Gatland

Date approved by Chairman: July 11, 1972

This thesis is gratefully  
dedicated  
to my wife, Ann

## ACKNOWLEDGMENTS

It is with pleasure that acknowledgment is made of the interest and assistance of those who have contributed to the work described in this dissertation. The author wishes to acknowledge the guidance, encouragement, and teaching of his thesis advisors, Dr. Earl McDaniel and Dr. David Martin, throughout this research. The help, comments, and instruction of Dr. Ian Gatland, who also served on the thesis reading committee, were appreciated.

The assistance of Dr. George Thomson, Dr. Don Volz, Mr. Randy James, Mr. Edward Graham, and Mr. Richard Laser, who aided the author in obtaining the data presented here and with whom many fruitful discussions were held, is greatly appreciated. The contributions of those who preceded the author in this laboratory, Dr. Dan Albritton, Dr. Tom Miller, Dr. John Moseley, and Dr. Bob Snuggs, are acknowledged.

A special acknowledgment is made of the contribution of Dr. Ian Gatland to the analysis presented in Chapter III.

The research reported here was sponsored in part by the U. S. Air Force Office of Scientific Research and in part by the Office of Naval Research in Project SQUID, Purdue University.

## TABLE OF CONTENTS

	Page
ACKNOWLEDGMENTS. . . . .	iii
LIST OF TABLES . . . . .	vi
LIST OF ILLUSTRATIONS. . . . .	vii
SUMMARY. . . . .	ix
Chapter	
I. INTRODUCTION. . . . .	1
General Considerations	
Review of Past Research on Ion Swarms	
in Carbon Monoxide	
Goals of Present Research	
II. APPARATUS . . . . .	14
General Description	
Modifications Incorporated for the Present	
Research	
III. ANALYSIS. . . . .	39
The Transport Equations and Their Solution	
Mobilities	
Longitudinal Diffusion Coefficients	
Transverse Diffusion Coefficients	
Reaction Rates	
IV. MOBILITIES. . . . .	75
Production of Ions	
Method of Data Analysis	
Experimental Procedures	
Experimental Results	
Error Analysis	
Comparison with Existing Data	

## TABLE OF CONTENTS (Concluded)

Chapter	Page
V. LONGITUDINAL DIFFUSION COEFFICIENTS . . . . .	106
Method	
Experimental Procedures	
Experimental Results	
Error Analysis	
VI. ION-MOLECULE REACTIONS. . . . .	119
Method	
Experimental Procedures	
Experimental Results	
Error Analysis	
Comparison with Existing Data	
VII. CONCLUSIONS . . . . .	135
Mobilities	
Longitudinal Diffusion Coefficients	
Ion-Molecule Reactions	
Appendices	
I. TABULATION OF THE MOBILITY RESULTS. . . . .	138
II. TABULATION OF THE LONGITUDINAL DIFFUSION COEFFICIENT RESULTS . . . . .	144
III. TABULATION OF THE ION-MOLECULE REACTION RATES . . . . .	148
IV. IONIC FLUX NEAR THE GUARD RINGS . . . . .	150
BIBLIOGRAPHY . . . . .	155
VITA . . . . .	159

## LIST OF TABLES

Table	Page
1. Summary of the Errors Involved in the Mobility Measurements . . . . .	101
2. Pure Polarization Force Mobilities versus Experimental Data . . . . .	103
3. Mobility and Drift Velocity Results for $\text{CO}^+$ Ions in Carbon Monoxide . . . . .	139
4. Mobility and Drift Velocity Results for $\text{CO}^+\cdot\text{CO}$ Ions in Carbon Monoxide . . . . .	141
5. Mobility and Drift Velocity Results for $\text{C}^+$ Ions in Carbon Monoxide . . . . .	142
6. Mobility and Drift Velocity Results for $\text{K}^+$ Ions in Carbon Monoxide . . . . .	143
7. Longitudinal Diffusion Results for $\text{CO}^+$ Ions in Carbon Monoxide. . . . .	145
8. Longitudinal Diffusion Results for $\text{K}^+$ Ions in Carbon Monoxide. . . . .	147
9. Reaction Rate Coefficient Results for the Reaction $\text{CO}^+ + 2 \text{CO} \rightarrow \text{CO}^+\cdot\text{CO} + \text{CO}$ . . . . .	149



## LIST OF ILLUSTRATIONS

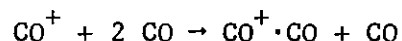
Figure		Page
1.	Sectioned View of the Drift Tube, the Outer Vacuum Enclosure, and the Analysis Chamber. . . . .	15
2.	Perspective Drawing of the Drift Region and the Mass Analysis and Detection Components. . . . .	17
3.	Schematic Diagram of the Ion Source . . . . .	19
4.	Schematic Drawing of the Analysis Region. . . . .	24
5.	Schematic Drawing of the Refrigerated Vapor Bath Cold Trap. . . . .	28
6.	Sample Arrival-Time Spectrum and Curve-Fitted Theoretical Profile. . . . .	56
7.	Mobility Results for $\text{CO}^+$ and $\text{CO}^+\cdot\text{CO}$ in Carbon Monoxide. . . . .	90
8.	Mobility Results for $\text{C}^+$ in Carbon Monoxide. . . . .	93
9.	Mobility Results for $\text{K}^+$ in Carbon Monoxide. . . . .	95
10.	Pressure Recalibration Data; Mobility of $\text{K}^+$ in Nitrogen Gas . . . . .	99
11.	Mobility Comparison for Potassium Ions Drifting in Carbon Monoxide and Nitrogen. . . . .	105
12.	Sample Experimental Arrival-Time Spectrum Showing Fit to Computer-Generated Analytical Profile . . . . .	108
13.	Longitudinal Diffusion Coefficient Results for $\text{K}^+$ and $\text{CO}^+$ in Carbon Monoxide . . . . .	110
14.	Longitudinal Diffusion Coefficient Results for $\text{K}^+$ in Carbon Monoxide and Nitrogen. . . . .	117
15.	Product Ion Arrival-Time Spectrum at High Pressure. . . . .	126

## LIST OF ILLUSTRATIONS (Concluded)

Figure		Page
16.	Product Ion Arrival-Time Spectrum at Low Pressure. . . . .	127
17.	Plot of the Percentage of Ions within a Given Radius versus $(4D_T t)$ . . . . .	153

## SUMMARY

The drift velocities and mobilities of mass-identified  $C^+$ ,  $CO^+$ ,  $CO^+\cdot CO$ , and  $K^+$  ions in carbon monoxide gas at 300°K and at pressures on the range from 0.03 to 0.80 Torr have been determined as a function of  $E/N$ , where  $E$  is the electric field strength and  $N$  is the gas molecule number density. The longitudinal diffusion coefficient for  $CO^+$  and  $K^+$  ions in carbon monoxide has been measured as a function of  $E/N$  at the same temperature and on the same pressure range. The rate of the ion-molecule reaction



has been obtained over an intermediate range of  $E/N$ .

The measurements were made using a drift tube mass spectrometer of ultra-high vacuum construction. The measurements were made by a time-of-flight method, using a pulsed electron-impact ion source combined with an electric shutter to create, repetitively, bursts of ions of accurately known initial spatial extent and temporal duration. Potassium ions can be produced by a thermionic emitter. The ion swarm migrates down the drift tube under the influence of a weak uniform electric field. During this migration the swarm spreads due to diffusion, and may undergo ion-molecule reactions with the neutral gas. The ion population is sampled on the axis at the end of the drift tube by a small exit aperture and mass-selected by an rf quadrupole spectrometer. The ions are individually

detected. The time of arrival of an ion at the detector is recorded by a 256-channel time analyzer. By repetitive pulsing of the ion source, a histogram of arrival times can be built up. From such time profiles, the drift velocities, longitudinal diffusion coefficients, and ion-molecule reaction rates were obtained.

Transport equations describing the drift, diffusion, and reaction of two ion swarms were solved and these solutions used in the quantitative studies made. The drift velocity values were obtained basically from the mean arrival times of the profiles. The longitudinal diffusion coefficients were determined from the shape (basically the width) of the profiles. The reaction rate coefficients were obtained from the detailed shape of the reaction-influenced profiles.

The mobility of  $\text{CO}^+$  in CO was obtained over an  $E/N$  range from 13 to 667 Td. Due to the ion-molecule reaction with the CO gas molecules, data at sufficiently low values of  $E/N$  to determine a zero-field mobility for  $\text{CO}^+$  could not be taken. The mobility of  $\text{CO}^+\cdot\text{CO}$  in CO was measured over an  $E/N$  range from 9 to 92 Td and the zero-field mobility was measured to be  $1.90 \pm 0.03 \text{ cm}^2/\text{V}\cdot\text{sec}$ . The mobility of  $\text{C}^+$  in CO was obtained over the  $E/N$  range from 14 to 745 Td and the zero-field mobility was measured to be  $2.7 \pm 0.1 \text{ cm}^2/\text{V}\cdot\text{sec}$ . The mobility of  $\text{K}^+$  in CO was measured over an  $E/N$  range from 4 to 640 Td and the zero-field mobility was determined to be  $2.30 \pm 0.04 \text{ cm}^2/\text{V}\cdot\text{sec}$ .

The longitudinal diffusion coefficients of both  $\text{CO}^+$  and  $\text{K}^+$  in CO were measured over a wide range of  $E/N$ .  $\text{ND}_L$  for  $\text{CO}^+$  increased rather slowly with increasing  $E/N$ , possibly due to the effects of resonant charge

exchange, whereas  $ND_L$  for  $K^+$  rose very rapidly with increasing  $E/N$ . The predictions of the theory of Wannier concerning the relation between the mobility and diffusion coefficients for a polarization force interaction were in excellent agreement with the  $ND_L$  data for  $K^+$  in CO, up to an  $E/N$  of about 200 Td.

The rate coefficient for the reaction given earlier was determined over an  $E/N$  range from 75 to 150 Td. The rate coefficient was found to vary from  $1.35 \pm 0.16 \times 10^{-28} \text{ cm}^6/\text{sec}$  at an  $E/N$  of 75 Td to  $1.10 \pm 0.13 \times 10^{-28} \text{ cm}^6/\text{sec}$  for values of  $E/N$  between 110 and 150 Td. The data clearly indicate that this reaction is three-body over the  $E/N$  range of these measurements.

## CHAPTER I

## INTRODUCTION

General Considerations

As a slow ion moves through a gas under the influence of a static, uniform electric field, on the average it gains energy from the field between collisions with molecules and loses energy during collisions. Since the ionic mass is usually comparable to the molecular mass, only a few collisions are normally required for ions to attain a steady-state condition after they are produced in the gas. The ratio of the electric field intensity to the gas number density,  $E/N$ , is the parameter that determines the average ionic energy acquired from the field in steady-state drift, above the energy associated with the thermal motion. In this thesis, the quantity  $E/N$  shall be expressed in units of  $10^{-17}$  Volt-cm<sup>2</sup>, called the Townsend (abbreviated Td).

If the value of  $E/N$  is small and constant, and if steady-state conditions have been achieved, the motion of an ensemble, or swarm, of ions of a given kind consists of a slow uniform drift in the field direction superimposed on the much faster random motion which produces diffusion. Under such conditions, the average energy the ions have acquired from the field is small with respect to their thermal energy, and their mean drift velocity,  $v_d$ , in the field direction is proportional to the field strength  $E$ . Thus

$$v_d = K E \quad (1-1)$$

where the constant  $K$  is called the mobility of the ions and is usually expressed in units of  $\text{cm}^2/\text{V}\cdot\text{sec}$ .

At higher values of  $E/N$ , where the ions are no longer in thermal equilibrium with the gas, the drift velocity may no longer be proportional to the electric field strength. However, the mobility, defined as the ratio of drift velocity to electric field strength, still serves as a convenient quantity to describe the transport of ions through the gas.

The mobility  $K$  is inversely proportional to the molecular number density  $N$ , and in order to facilitate comparisons between data taken at various temperatures and pressures, experimental results are usually presented as the mobility which would result if  $N$  were  $2.69 \times 10^{19} \text{ cm}^{-3}$ , which corresponds to  $0^\circ\text{C}$  and 760 Torr. This practice leads to the definition of a reduced mobility  $K_0$ :

$$K_0 = K(p/760)(273.16/T) \quad (1-2)$$

where  $p$  and  $T$  are the pressure in Torr and temperature in degrees Kelvin at which the measurement is performed.

The zero-field reduced mobility is defined as the limiting (constant) value which  $K_0$  approaches as  $E/N$  approaches zero.

Whenever a number density gradient of ions exists in a gas of uniform total pressure, there will be a motion of the ions to eliminate the gradient, the process known as diffusion. If the gradient is small, and if the value of  $E/N$  is very low, the ionic flux will be proportional to the magnitude of the gradient and opposite in direction. The constant of

proportionality, known as the diffusion coefficient,  $D$ , can be related to the ionic mobility by a classical relation known as the Einstein equation<sup>1</sup>:

$$\frac{D}{K} = \frac{kT}{e}, \quad (1-3)$$

where  $k$  is Boltzmann's constant,  $T$  is the absolute temperature, and  $e$  is the ionic charge. Equation (1-3) is exact in the limit of small ionic concentrations and vanishing electric field strength, and approximately correct so long as the ions are close to being in thermal equilibrium with the gas molecules.

At values of  $E/N$  where the ions acquire an average energy appreciably above the thermal energy of the gas molecules, the ionic flow due to diffusion becomes anisotropic and the diffusion current density is given by

$$\vec{j}_d = - \vec{D} \cdot \vec{\nabla} n(\vec{r}, t), \quad (1-4)$$

where  $n(\vec{r}, t)$  is the ionic number density and  $\vec{D}$  is the diffusion tensor.  $\vec{D}$  has the form<sup>2</sup>

$$\vec{D} = \begin{vmatrix} D_T & 0 & 0 \\ 0 & D_T & 0 \\ 0 & 0 & D_L \end{vmatrix} \quad (1-5)$$

where  $D_T$  is the (scalar) transverse diffusion coefficient which describes



the rate of diffusion in directions perpendicular to the electric field and  $D_L$  is the (scalar) longitudinal diffusion coefficient characterizing diffusion in the field direction.

During the drift of the ions, collisions between ions and gas molecules can produce chemical reactions. Within the ion swarm, ions of a particular species may be disappearing and appearing due to conversion to and from other species. The rate (per ion) at which a given reaction occurs is denoted by the reaction frequency,  $\alpha$ , in units of  $(\text{sec})^{-1}$ . The reaction frequency depends on the collision frequency and hence on the number density,  $N$ , of the gas. The dependence of  $\alpha$  on  $N$  is determined by the interactions involved. If  $\alpha$  is proportional to  $N$ , the reaction is said to be two-body, while if  $\alpha$  is proportional to  $N^2$ , the reaction is said to be three-body. The constant of proportionality,  $k$ , is called the reaction rate coefficient. The units of  $k$  will depend on the  $N$ -dependence of  $\alpha$ .

Data on ionic mobilities, diffusion coefficients, and reaction rates are of both theoretical and practical interest. First of all, experimental values of these quantities, and particularly their dependence on  $E/N$  and the gas temperature, can provide information about ion-molecule interaction potentials at greater separation distances than are accessible in beam scattering experiments. Studies of ion-molecule interactions can also yield important information applicable to neutral-neutral interactions. Mobilities are required for the calculation of ion-ion recombination coefficients and the rate of dispersion of ions in a gas due to mutual repulsion. Finally, information on mobilities, diffusion coefficients, and

reaction rates is required for a quantitative understanding of electrical discharges in gases and various atmospheric phenomena.

### Review of Past Research on Ion Swarms in Carbon Monoxide

#### Mobilities

The mobilities of the alkali ions in carbon monoxide were measured by Mitchell<sup>3</sup> in the 1930's. The apparatus used was the four grid, electrical shutter method developed by Tyndall and his colleagues at Bristol University. The alkali ions were thermionically emitted from a heated cathode, and were periodically gated into a drift region by a pair of closely spaced grids with an ac potential applied between them. These ions drift until they encounter a second pair of grids, biased with the same ac voltage as the first pair. At certain frequencies of the ac voltage, the ions arrive at the second pair of grids during the interval the grids allow ions to pass. The current passing through both pairs of grids was read by an electrometer. The frequency for maximum transmitted current could be related to the mobility of the ions.

When reduced to 760 Torr and 0°C, the measured mobilities were: Li<sup>+</sup>, 2.47 cm<sup>2</sup>/V-sec; Na<sup>+</sup>, 2.29 cm<sup>2</sup>/V-sec; K<sup>+</sup>, 2.18 cm<sup>2</sup>/V-sec; Rb<sup>+</sup>, 1.95 cm<sup>2</sup>/V-sec; and Cs<sup>+</sup>, 1.86 cm<sup>2</sup>/V-sec.

In 1953 Varney<sup>4</sup> reported mobility values for two ions formed by a discharge in carbon monoxide. He used a pulsed Townsend discharge method, in which a field is applied between parallel plate electrodes, and a pulse of electrons is released from the cathode by the radiation from an external spark of short duration. A typical Townsend avalanche results, and an exponential distribution of positive ions is left between the plates. The

time needed to sweep out these ions is measured and thereby the drift velocity is obtained. Because of the high voltage used to create the ions, this technique is limited to high E/N. Of the two ions seen, the one with the lower drift velocity was believed to be  $\text{CO}^+$ . In the region of E/N from 250 to 600 Td, a break in the plot of drift velocity versus E/N was seen and attributed to an ion-molecule reaction forming  $\text{CO}^+\cdot\text{CO}$ . The faster ion seen was suspected of being  $\text{C}^+$ , but the data were of poorer quality for this ion.

In 1968 Saporoschenko<sup>5</sup> reported the mobilities of  $\text{CO}^+$ ,  $\text{CO}_2^+$ , and  $\text{CO}^+\cdot\text{CO}$  ions in carbon monoxide. In this experiment the ions were formed in a glow discharge of about one watt power. The ions passed through a 1.63 cm thermalizing region, entered a double-shutter device for the measurement of their drift velocity, and were extracted through a 0.008 cm diameter pinhole for identification in a magnetic mass spectrometer. The drift space, i.e., the distance between the two electrical shutters, was fixed at one centimeter. The extrapolated zero-field mobilities were determined to be  $1.93 \text{ cm}^2/\text{V-sec}$  for both  $\text{CO}^+$  and  $\text{CO}_2^+$  and  $1.61 \text{ cm}^2/\text{V-sec}$  for  $\text{CO}^+\cdot\text{CO}$ .

The greatest uncertainty in the mobility data obtained on ions in carbon monoxide up to the present time is due to the effect of ion-molecule reactions. Even though the identity of the detected ions may be determined through mass analysis, there is no assurance that the ion had not participated in an ion-molecule reaction during its drift, thus giving rise to an "apparent" drift velocity, that is, an average of the true drift velocities for the ions involved in the reaction. In fact, there

is evidence to attest to the belief that such reactions did occur. Furthermore, the data were not obtained at low enough  $E/N$  to justify the inference of a zero-field mobility.

Before the transport properties of the several ions in carbon monoxide can be determined unambiguously, data must be taken under the following conditions:

1. It must be demonstrated that the data reach low enough  $E/N$  to ensure that  $K_0$  is truly constant, independent of  $E/N$ . There is no guide for determining the zero-field reduced mobility from data which do not meet this requirement.
2. The data must clearly indicate that any drift velocities ascribed to a given ion were not falsified by that ion having spent part of its drift time as another species.
3. The ionic identity must be unambiguously determined.

#### Longitudinal Diffusion Coefficients

There do not appear to be any published data on the longitudinal diffusion coefficients of ions in carbon monoxide. At low values of  $E/N$ , the diffusion coefficient can be obtained from the Einstein relation, Equation (1-3). No experiment has produced data for which the longitudinal diffusion coefficient for ions in carbon monoxide has been shown to be consistent with Equation (1-3).

As will be described in Chapter III, G. H. Wannier has derived expressions relating the mean free time between collisions, as obtained from drift velocity measurements, to the longitudinal and transverse diffusion coefficients. These derivations are applicable to the regime where

polarization forces dominate the interaction between the ions and the molecules. Again, no experimental data have been obtained in carbon monoxide that substantiate the use of the Wannier expressions.

As was the case with mobilities, many criteria must be met before longitudinal diffusion coefficients can be measured accurately. The requirement that ion-molecule reactions must be excluded from the drift region becomes even more important, since the effects of reaction distort the drift-time spectrum, from which the longitudinal diffusion coefficient is determined, more severely than they affect the drift-time averages, from which the drift velocity is calculated. The effects of space charge also tend to affect the measurement of longitudinal diffusion more severely than they affect the measurement of drift velocity.

#### Ion-Molecule Reaction Rates

In 1970 Chong and Franklin<sup>6</sup> measured the reaction rate for the conversion of  $\text{CO}^+$  into  $\text{CO}^+\cdot\text{CO}$ . A mass spectrometer with a high pressure ion source was used. The drift field inside the ion source was fixed at 11.5 V/cm and the pressure was varied from 0.1 to 1.2 Torr.

Reaction rates were obtained by analyzing the variation with pressure in the ion intensity of the observed ions. The influence of several impurities, notably  $\text{CO}_2$  and  $\text{H}_2\text{O}$ , was considered. The forward (attachment) reaction rate was determined from the decrease in  $\text{CO}^+$  intensity along with the increase in  $\text{CO}^+\cdot\text{CO}$  intensity as the pressure was increased. The reaction rate was determined to be  $1.43 \times 10^{-28} \text{ cm}^6/\text{sec}$ . At high pressures an equilibrium constant was determined and thereby a backward (detachment) reaction rate was obtained.

Several important criteria need to be fulfilled when measuring reaction rates:

1. The rate coefficients of many reactions, especially detachment reactions, are very sensitive to the mean energy of the collisions. Hence, a given measurement of a rate coefficient should be made at a fixed value of  $E/N$ . A series of such measurements at various values of  $E/N$  can then provide the rate coefficient as a function of  $E/N$ .

2. If both formation and breakup occur in a reaction scheme, then an analysis involving both the forward and backward reactions needs to be employed. The influence of the production of parent ions due to product ion breakup within the drift region must be considered.

3. If reliable equilibrium constants are to be determined, ion intensity studies need to be made that are independent of mass discrimination. Parkes<sup>7</sup> has analyzed mass discrimination factors in drift tube mass spectrometers, but in most experiments the uncertainty concerning mass discrimination has not been fully resolved.

4. If the product ion species is a weakly bound molecular system, extreme care must be used in the extraction of the ion from the drift region in order to prevent its breakup before mass analysis. The dissociation of weakly bound molecular ions through collisions with gas molecules during extraction has been observed in drift tube mass spectrometric studies in nitrogen by McKnight, et al.<sup>8</sup>

#### Transport and Reaction Analysis

A brief description of some of the recent works concerning the analysis of the transport and reaction processes for ions in gases will

be presented in this section.

1957. Burch and Geballe<sup>9</sup> presented a one-dimensional analysis which applies to transient ion currents in a Townsend discharge. The effects of diffusion are not included, but the forward reaction of primary ions to form two kinds of secondary ions is considered.

1964. Edelson and McAfee<sup>10</sup> discussed the determination of Townsend ionization and electron attachment coefficients, and ionic mobilities in pulsed discharge experiments. The analysis is one-dimensional; the effects of longitudinal diffusion and reactions are considered.

In another one-dimensional analysis of a pulsed Townsend discharge, Edelson, et al.<sup>11</sup> considered ionization, electron attachment and secondary electron production at the cathode. The transport of positive and negative ions is treated, with and without diffusion. The results are useful in the determination of mobilities.

Frommhold<sup>12</sup> discussed electron detachment from negative ions as a process occurring in avalanches in various gases. Experiments involving the study of avalanches to determine various transport properties would have to consider this process along with electron attachment and ionization.

1965. Beaty and Patterson<sup>13</sup> presented an analysis for cylindrical geometry, with the ion source and collector forming the ends of the drift chamber. Drift, diffusion (with  $D_L = D_T$ ), and a depleting reaction to form a secondary species are considered. The analysis was applied to experiments on helium to determine the mobilities of the primary and secondary ions, and the forward reaction rate.

1967. Barnes<sup>14</sup> presented an analysis that is basically one-

dimensional and deals with drift, diffusion, and depleting reactions. Statistical estimates are developed for the mobility, diffusion coefficient, and reaction rate.

Edelson, et al.<sup>15</sup> developed a one-dimensional analytic solution for a system composed of two kinds of drifting, inter-converting ions. Ions of one of the species are introduced initially by a delta-function source. Diffusion is not included in the model. Numerical solutions are also discussed. They contain the effects of diffusion and can be used to determine mobilities and reaction rates.

1968. In another paper, Edelson<sup>16</sup> considered the effects of radial diffusion on the collected ion current due to different residence times. The effect of a reduced collector area is also discussed.

In a paper by Whealton and Woo,<sup>17</sup> a three-dimensional analysis is presented that pertains to the determination of reaction rates. The effects produced by the primary and secondary ions having unequal temperatures are discussed.

In several works by Moseley, et al.<sup>18,19</sup> an analytic solution to the transport of an ion species is given. The effects of drift, longitudinal and transverse diffusion, and a depleting reaction are considered. The geometry is three-dimensional, with the source term being a thin, radially symmetric disk of low ionic density. Techniques for determining the mobility, longitudinal and transverse diffusion coefficients, and depleting reaction rates with high accuracy are presented.

1969. In another paper by Woo and Whealton,<sup>20</sup> a three-dimensional analysis is presented that considers drift, transverse and longitudinal



diffusion and a forward reaction to a secondary species. The source term corresponds to a thin disk with arbitrary radial ion density. Expressions are obtained for both the primary and secondary ion densities.

1970. In a paper by Keller, et al.<sup>21</sup> mathematical modifications to the solution of the Woo-Whealton model are suggested in order to facilitate calculations.

In several publications by Snuggs, et al.<sup>22,23</sup> a comprehensive analysis is made of an inter-reacting system of two ion swarms. The geometry is three-dimensional, and drift, transverse and longitudinal diffusion, and reactions are considered. The reaction from each ionic species to the other is taken into account, as well as other depleting reactions. The ion source is an axially thin disk, and the ion current is measured on the axis of the drift tube. For the primary ion species that undergoes only a depleting reaction, a closed form solution for the time-integrated ion current is obtained and used to determine transverse diffusion coefficients and reaction rates. An analytical solution is presented for the arrival-time spectrum for both primary and secondary ions. Comparison of experimental data with these analytical arrival-time spectra permits the determination of mobilities, diffusion coefficients, and reaction rates. Many simplifying assumptions are also considered, and appropriate formulas to aid in data reduction are obtained.

1971. In an article by Woo and Whealton<sup>24</sup> the error introduced by neglecting transverse diffusion when calculating reaction rates from arrival-time spectra is considered. Three dimensional geometry is used, and various ion source configurations are considered. Longitudinal diffusion is

neglected, and only a forward reaction is included.

Summary. In the light of all the theory contained in the above works, a summary of the current analysis as it pertains to the drift-tube mass spectrometer utilized in the present research is appropriate. This summary is contained in Chapter III.

#### Goals of the Present Research

The general objective of the present research is to evaluate as precisely as possible the drift velocities, longitudinal diffusion coefficients, and reaction rates of ions in carbon monoxide at room temperature. Specifically, this may be broken down into four goals:

1. To measure the variation of the mobilities of ions in carbon monoxide over as wide a range of  $E/N$  as possible.
2. To determine unambiguous zero-field reduced mobilities.
3. To evaluate the longitudinal diffusion coefficients over as wide a range of  $E/N$  as possible.
4. To assess the ion-molecule reaction situation and to determine the reaction rates involved.

## CHAPTER II

### APPARATUS

#### General Description

The apparatus that was used to perform the present research has been described in detail in several reports,<sup>25-28</sup> so a detailed description will not be given here. A brief general description will be given, followed by a detailed discussion of all modifications that were made to the equipment for the present research.

Figure 1 is a sectioned drawing of the apparatus. The main ultrahigh-vacuum chamber is constructed of stainless steel and is evacuated by oil diffusion pumps which are separated from the chamber by water-cooled baffles and molecular sieve traps. Metal gaskets provide the vacuum seals. The vacuum chamber contains the ion source, drift tube, and sampling apparatus.

A very pure sample of carbon monoxide is admitted into the drift tube through a servo-controlled leak valve and the gas continuously flows from the drift tube through the exit aperture, and into the main kettle where it is pumped away by the six inch diffusion pump. An MKS "Baratron" capacitance manometer continuously monitors the pressure in the drift tube and through a Granville-Phillips pressure controller maintains any selected pressure in the range of 0.026 to 0.790 Torr in the drift tube.

Two sources of carbon monoxide were used in this research. The gas

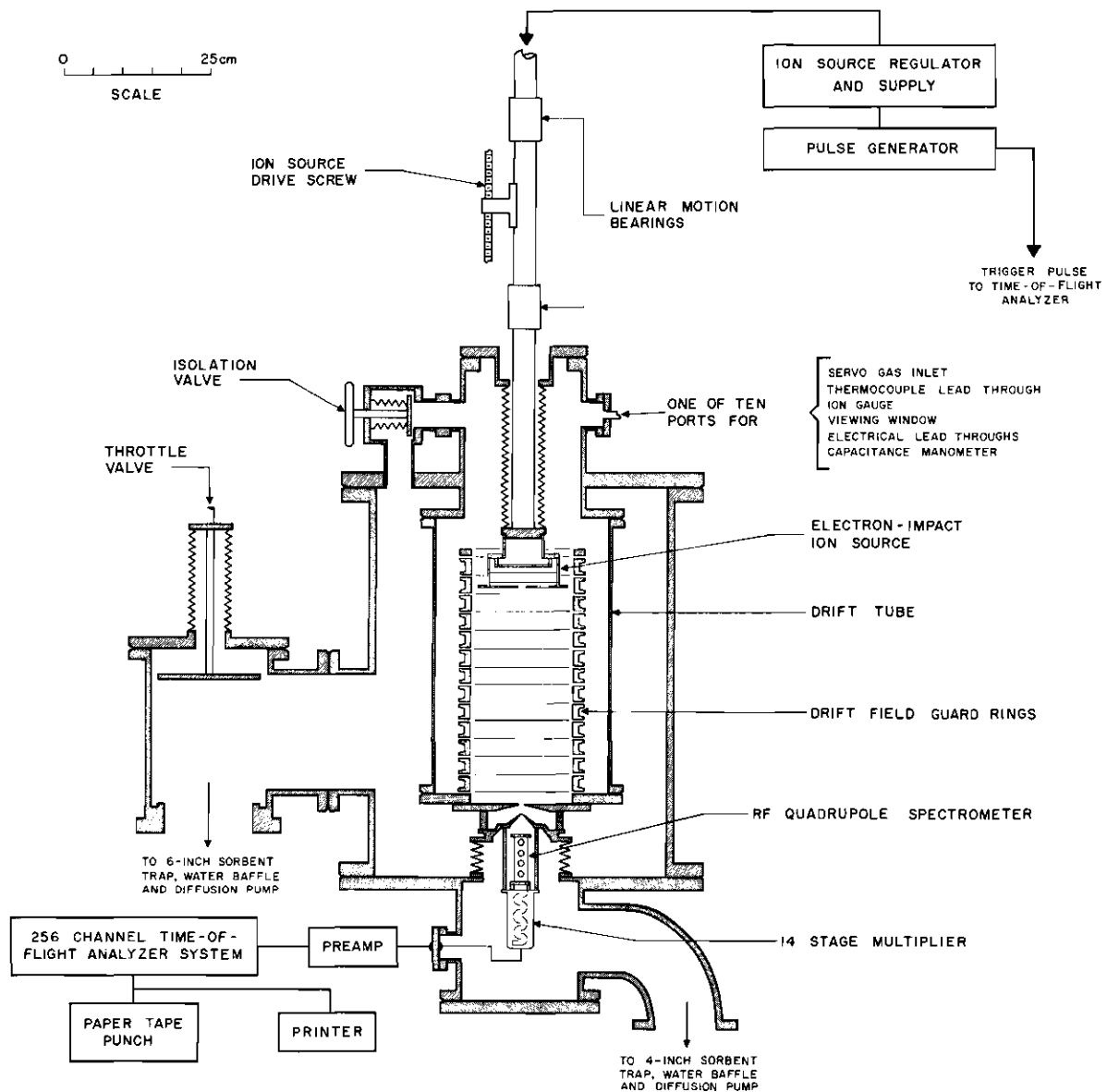


Figure 1. Sectioned View of the Drift Tube, the Outer Vacuum Enclosure and the Analysis Chamber. (The objects connecting the drift tube exit aperture plate to the housing of the conical skimmer above the spectrometer are posts, which do not significantly impede the action of the pump shown at the left in disposing of the gas flowing from the drift tube.)

used for most of the work was the chemically pure grade supplied by Air Products and Chemicals, Inc., Emmaus, Pennsylvania. The only impurities above five parts per million (ppm) were nitrogen, (245 ppm), oxygen and argon, (20 ppm), and carbon dioxide, ( $< 10$  ppm). Research grade carbon monoxide as supplied by Liquid Carbonic Corporation, Chicago, Illinois, was used for the ion-molecule reaction rate studies. The impurity levels of this gas were nitrogen, (124 ppm), oxygen, (39 ppm), carbon dioxide, (15 ppm), and hydrocarbons, (10 ppm).

An ion swarm can be followed from creation to detection in Figure 2. The ion source, which is movable over almost the entire length of the 44 centimeter cylindrical drift tube, creates short bursts (typically 1-5 microseconds) of ions in the drift tube. The ions are created either by electron-impact with the carbon monoxide gas or in the case of alkali ions, by thermionic emission from a filament coated with Kingman feldspar. These ions are gated out of the source into the drift region by a double grid shutter, referred to as the "Tyndall shutter," located at the ion entrance aperture.

Each ion swarm migrates down the drift region under the influence of a weak uniform electric field maintained by the drift field guard rings. During this migration, the swarm spreads due to diffusion, and may undergo ion-molecule reactions with the neutral gas. When the ions reach the bottom of the drift tube, some of those close to the axis are swept out through the exit aperture, and the core of the emerging jet of ions and gas molecules is cut out by a conical skimmer and directed into a radio-frequency quadrupole mass spectrometer. Ions of only a selected charge-to-mass ratio traverse the length of the spectrometer; all other ions are

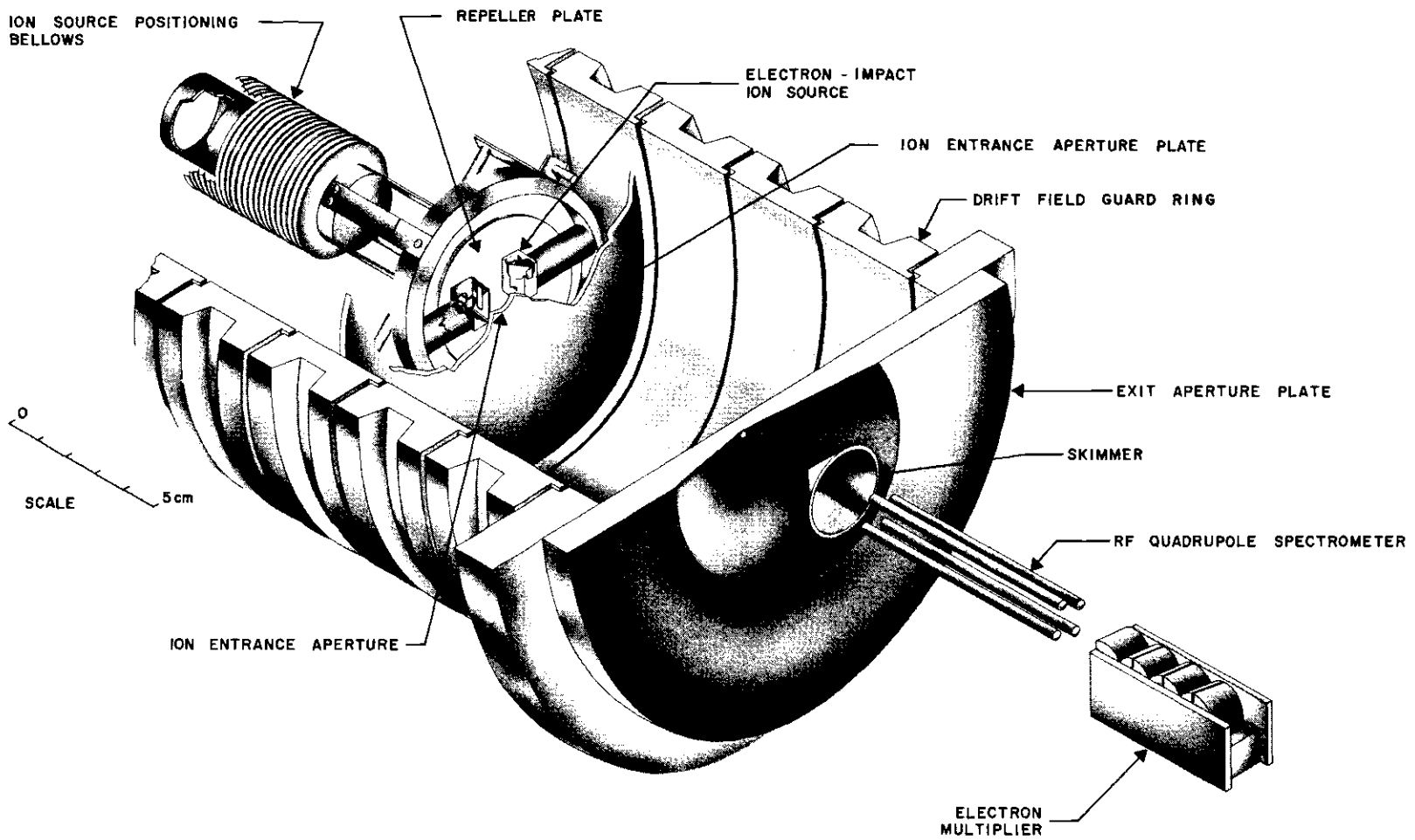


Figure 2. Perspective Drawing of the Drift Region and the Mass Analysis and Detection Components

rejected in the mass selection process. The selected ions are then detected individually by a capillary electron multiplier operated as a pulse counter, and the resulting pulses are electronically sorted as to their arrival time by a 256-channel time-of-flight analyzer.

### Modifications Incorporated for the Present Research

#### Ion Source

The ion source and its method of operation are basically the same as that described by Miller,<sup>26</sup> Moseley,<sup>27</sup> and Snuggs.<sup>28</sup> However, one change had to be made to eliminate an undesirable distortion that showed up in one phase of the present research.

A schematic diagram of the ion source is given in Figure 3. One basic method of producing ions is by electron impact with the carbon monoxide gas. The electron-impact source consists of two nonmagnetic stainless steel boxes mounted on opposite sides of the source fixture, and an ionization region between them. Electrons are evaporated from a thoriated-iridium filament (or BaZrO<sub>3</sub> coated filament when strong oxidants are present at high pressures) contained in one box, are periodically gated into the ionization region, and are collected on a Faraday cup in the box on the opposite side. The electron beam has the shape of a narrow ribbon perpendicular to the drift tube axis, and thus the primary ionization is restricted to a narrow, well-defined region in the gas. Normally, the electron-impact source is mounted between the pole faces of a ring magnet that produces a magnetic field of about 100 gauss across the ionization region. The magnetic field serves to confine the electrons within a narrow beam. However, the penetration of the magnetic field into the drift

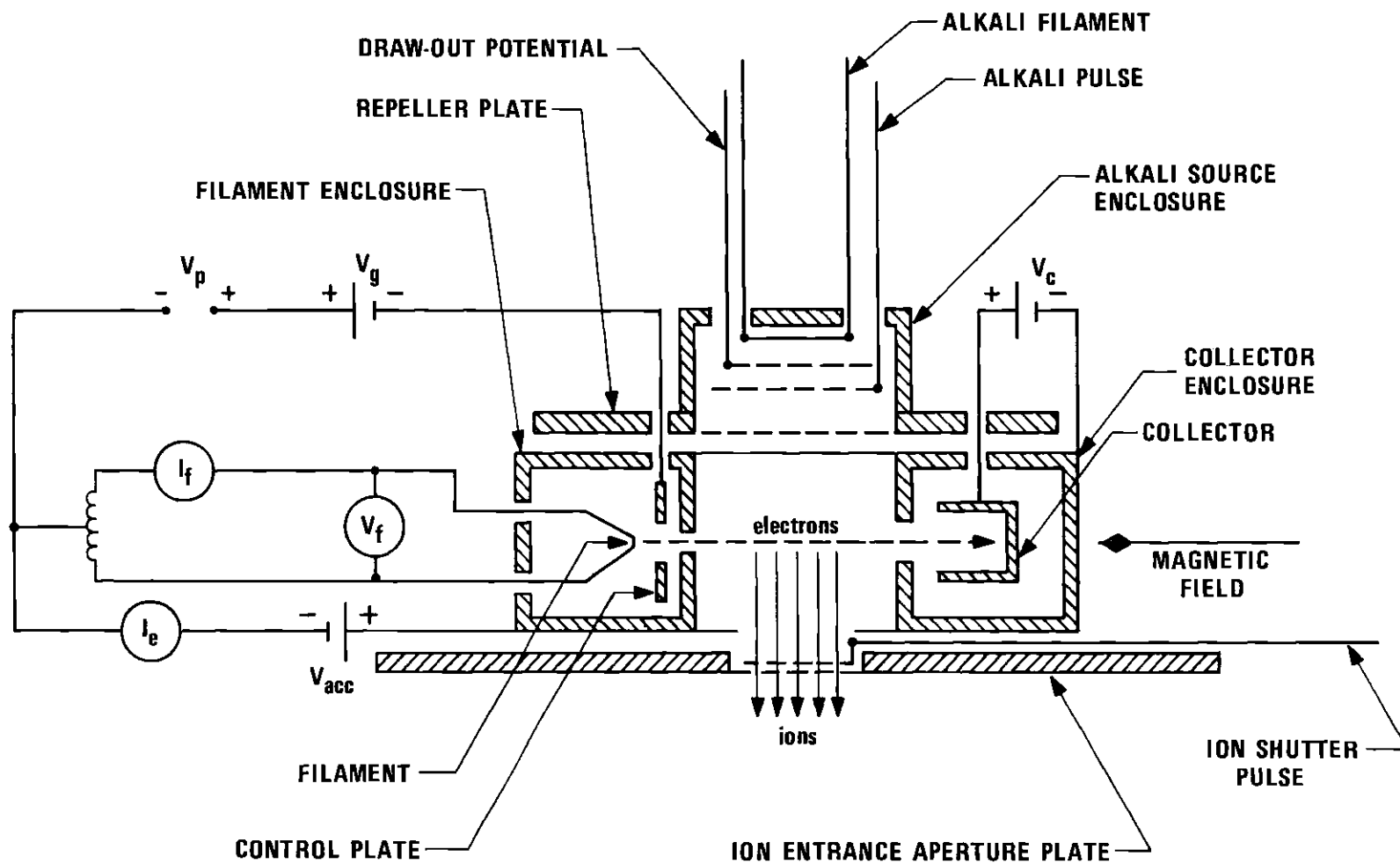


Figure 3. Schematic Diagram of the Ion Source. (The Alkali Source is Mounted Above the Electron Impact Ion Source.)



region caused a problem during the study of reaction rates in carbon monoxide. The entire source was constructed with non-magnetic stainless steel and it therefore provides no shielding from the magnetic field within it. Magnetic fields of several gauss were measured several centimeters from the entrance aperture of the ion source and the magnetic field's effect was very noticeable under certain conditions.

When the time-of-flight profiles of a reaction-produced ion species were studied, the profiles had a distorted shape. These abnormal spectra were traced to an unusual behavior of the reaction process that occurred during the first several centimeters of drift. A more detailed description of the distortion is included in the chapter on ion-molecule reactions.

The cause of the distortion was linked to the presence within the drift tube of the small magnetic field that the ion source magnet produced. In order to eliminate this undesirable effect, the magnet was removed. The two Alnico magnets were replaced by stainless steel pieces of the same shape, and the source was rebuilt in the same manner as before. As stated above, the purpose of the magnetic field was to constrain the electrons to move in helices of small radii across the ionization region. With the magnets removed, the electron beam does spread because of collisions with gas molecules and the short burst of ions produced by electron impact extends over a greater spatial region. Although the Tyndall shutter prevents most of the ions from penetrating into the drift region when they are supposed to be biased out, the leakage into the drift tube is increased by the absence of the magnetic field. This leakage contributes a small background to the data that are taken, and while this background can be

compensated for easily, it does indicate that the magnetic field served a useful purpose. A large group of tests were run to determine the effect of the absence of the magnetic field on the various measurements previously made with the drift tube, but no changes in these measured values were found.

#### Quadrupole Assembly

In order to keep pace with improvements made in radio-frequency quadrupole mass filters, a new quadrupole assembly was installed on the apparatus. This quadrupole replaced the Varian quadrupole that had been used for several years.

The quadrupole installed was manufactured by Extranuclear Laboratories, Pittsburgh, Pennsylvania. It consists of two basic parts, the Quadrupole Mass Filter, Model #324-9, and the Quadrupole Power System, Model #011-1. The Quadrupole Mass Filter contains four stainless steel cylindrical rods, 3/4 inch in diameter, approximately 8 1/2 inches long, mounted in a stainless steel can 2.88 inches in diameter and 9.00 inches long. The four quadrupole rods are very accurately machined to a .750 inch diameter and are spaced on a 0.697 inch radius circle. Precise tolerances are required to achieve maximum resolution with the unit.

The Quadrupole Power System is electronically and physically divided into three major units. The Radio Frequency Power Source produces the rf voltage that powers the mass filter. It has an input power capacity of up to 250 watts and a frequency variable from 1.2 to 4.8 megahertz. The High-Q Head is a high-q tuned transformer used to step up the rf voltage to a level suitable for driving the mass filter. Vacuum diodes are used

to monitor the rf level for feedback control purposes and to provide the dc voltages applied to the mass filter electrodes. The Quadrupole Control Unit is the center for controlling and monitoring the operation of the system. The feedback amplifier used to stabilize the output is located in this unit.

One of the major advantages of the Extranuclear quadrupole system over the Varian system is the ability to vary the rf frequency and the loading of the mass filter. The inductor in the High-Q Head and the capacitance of the quadrupole rods and cable assembly form a resonant circuit. To produce the maximum possible voltages on the mass filter poles, and thereby obtain the maximum mass range, the resonant frequency of the circuit must be determined and the rf power must be loaded properly into the resonant circuit. By having a variable-frequency rf power source and an adjustable loading circuit, this peak rf voltage can be obtained. The Varian quadrupole rf power supply had only two fixed frequencies of operation. Loading of the mass filter circuit was very difficult because the voltage measuring equipment had to be external and would detune the circuit when applied and removed.

The Extranuclear quadrupole system is capable of providing greater mass range (due to its higher voltage capability), increased resolution (especially at the lower masses), greatly increased transmission, greater dependability, and more flexibility in mass sweeping. The Varian quadrupole had a fixed set of sweep speeds that were internally controlled by the quadrupole unit itself. With the Extranuclear system, a voltage ramp from a Tektronix 531A oscilloscope causes a corresponding mass sweep.

Since the quadrupole sweep is tied to the sweep of the oscilloscope, all of the flexibility in triggering and all of the sweep rates of the oscilloscope are available. In addition, the ion current can be displayed directly on the oscilloscope without making any further adjustments.

Once we have the quadrupole sweeping a range of masses repetitively, a very efficient and accurate mass scan can be made by utilizing our TMC time-of-flight analyzer. Since the quadrupole is sweeping at a fixed mass-per-second rate and the time-of-flight analyzer is sweeping at a fixed time-per-channel rate, the output of the analyzer will be a mass-per-channel display. Since the time-of-flight analyzer operates at very fast cycle rates, any variation in the source output will be very uniformly spread over the entire mass spectrum. With the Varian quadrupole, the normal method of obtaining a mass spectrum was to sweep the mass range at a very slow rate and display the count rate on a strip chart recorder. Any change in source output was misinterpreted as a change in the intensity of whatever mass the quadrupole was scanning at that particular time.

At the same time the Extranuclear quadrupole was added, new mounting hardware was installed. Figure 4 shows the new method of installation. One important new feature was the addition of two cylindrical lens elements between the skimmer assembly and the entrance of the quadrupole. Just as applying a small bias to the skimmer gave us greater transmission of ions, appropriate bias to the lens elements has given us greater transmission of ions into the quadrupole. One feature that was built into the Extranuclear quadrupole, and had to be added to the Varian model, was the ability to float all four quadrupole poles at a dc bias with respect to

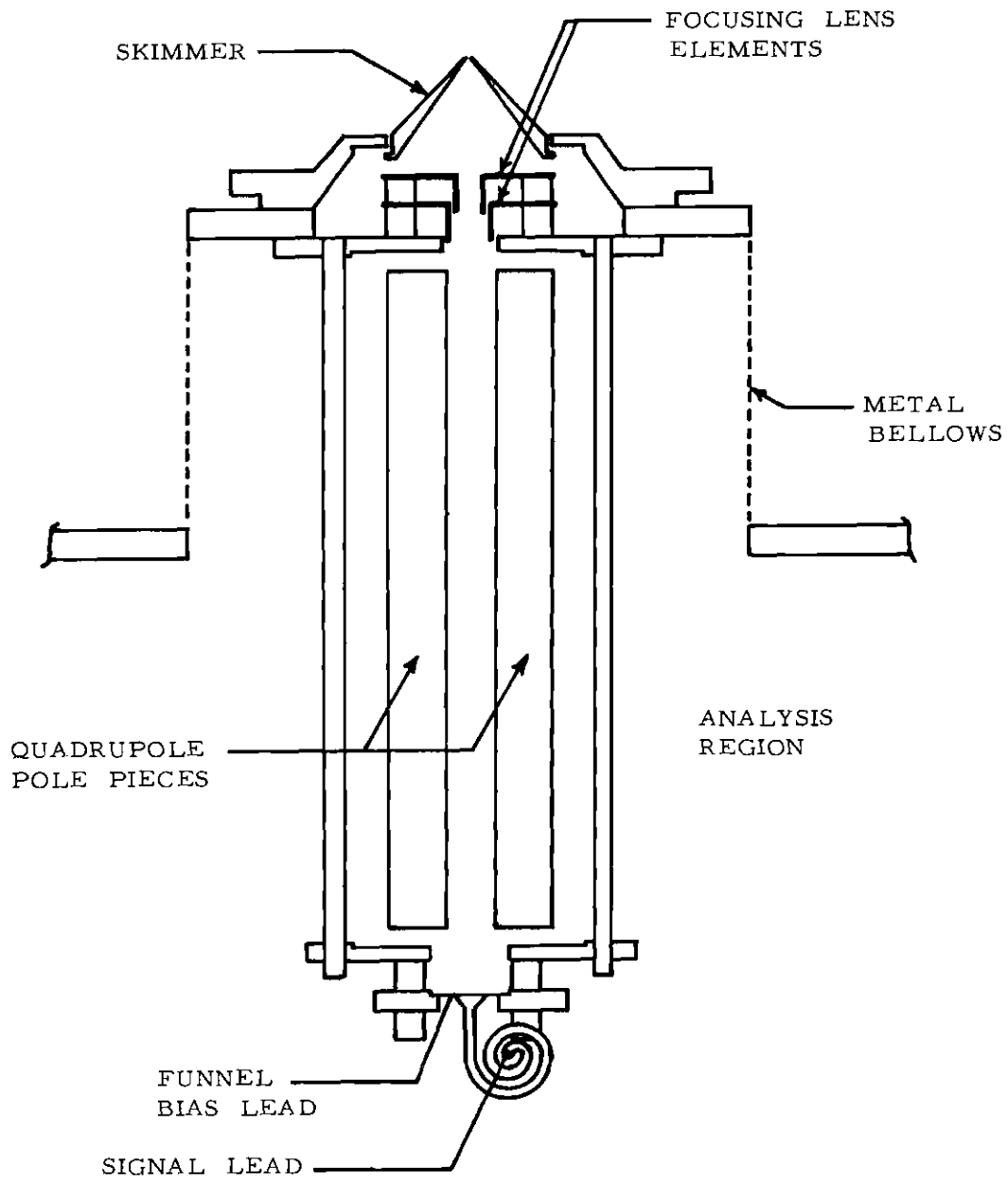


Figure 4. Schematic Drawing of the Analysis Region

ground. This is necessary since the ions enter the analysis region at very nearly ground potential and efficient analysis requires them to pass through the lens and quadrupole with at least several electron volts of energy. The Extranuclear quadrupole has an internal power supply capable of biasing the mass filter up to  $\pm 8$  volts with respect to ground. In addition, this bias can be raised to over 500 volts by utilizing an external power supply. We found the 8 volt power supply to be adequate for all of the work.

A major problem we had with the Quadrupole Mass Filter was the production of electrons and photons by the high voltage radio-frequency potentials applied to the pole pieces. As originally manufactured, our mass filter produced quite large numbers of spurious counts on our channeltron when run at high voltages. A factory modification increased the insulation between the pole pieces and the grounded enclosure. This reduced the number of counts but did not eliminate them.

The source of the spurious counts was finally traced to the connection of the rf voltage to the pole pieces. Heavy rf feedthroughs were substituted for the original feedthroughs used to pass the potentials through the enclosure and the straps that connected the feedthroughs to the pole pieces were more firmly attached. These two modifications now permit us to run the quadrupole at its maximum voltage with only a small number of background counts.

#### Refrigerated Vapor Bath

One of the greatest problems encountered in most of the ion swarm work done is the presence of impurities in the gas. Impurities arise from

two principal sources, the external gas supply and outgassing from the internal surfaces of the apparatus. Outgassing is reduced principally by using ultrahigh-vacuum construction. The background pressure within the drift tube with the isolation valve closed (see Figure 1) is about  $10^{-8}$  Torr, so that at a pressure of 0.1 Torr, the impurities from outgassing are about 0.1 parts per million. With ultrahigh-vacuum techniques adhered to in the construction of the apparatus, the main source of impurities is the gas supply itself. Many gases, even when obtained from the purest sources available, contain appreciable impurities. In the past research with nitric oxide, and in this research with carbon monoxide, the impurities within the source gas were a serious obstacle to the determination of reaction rates.

For the present research, techniques were sought to purify the gas before it was admitted to the drift tube. The most promising technique was refrigeration. With this in mind, the Refrigerated Vapor Bath (RVB) was installed. It is patterned after the vapor bath developed by Puckett, et al.<sup>29</sup> The basic scheme is to refrigerate the gas to a given temperature by passing it through a trap cooled by liquid nitrogen vapor. By adjusting the flow of cold vapor past the trap and the flow of heat leaking into the trap, any desired temperature down to nearly the boiling point of liquid nitrogen can be obtained. Our principal impurities, such as water vapor and carbon dioxide, have an appreciable vapor pressure even at moderately low temperatures, so maintaining the trap as cold as possible while keeping the carbon monoxide gaseous is desired. We found that reducing the temperature of the carbon monoxide from that obtained by an

acetone and dry ice mixture to nearly the boiling point of liquid nitrogen reduced our impurity level quite substantially.

Figure 5 shows the basic construction of the RVB. Basically, the trap consists of a coil of stainless steel tubing inserted into a cryogenic dewar. The dewar is filled to just below the bottom of the coil with liquid nitrogen. The equilibrium temperature of the coil is monitored by a copper-constantan thermocouple through a pyrometer. The pyrometer is manufactured by API Instrument Company, Chesterland, Ohio, and is a double set point optical meter-relay. If the temperature of the coil drops below the desired temperature, a relay sends current through a resistance winding wrapped around the coil to warm it up. If the coil becomes too warm, another relay sends current through a resistance winding immersed in the liquid nitrogen. This causes the liquid nitrogen to boil and sends more cold vapor past the coil to cool it down. With the boiling point of carbon monoxide being just above that of liquid nitrogen, the RVB was run with only the cooling action present.

The results obtained by using the RVB were quite dramatic. The principal impurities in carbon monoxide were clustered around mass 44, presumably  $\text{CO}^+\cdot\text{H}_2\text{O}$ . Without the trap in operation, these impurity ions entered into a reaction with the  $\text{CO}^+$  ions that made any reaction rate determination questionable. With the trap working, the impurity ions were not present at low pressures, and just barely detectable at higher pressures.

After several weeks of operation with the trap cooled, the impurities would begin to reappear. Apparently the ability of the trap to remove condensable impurities decreased during use. This is believed to be



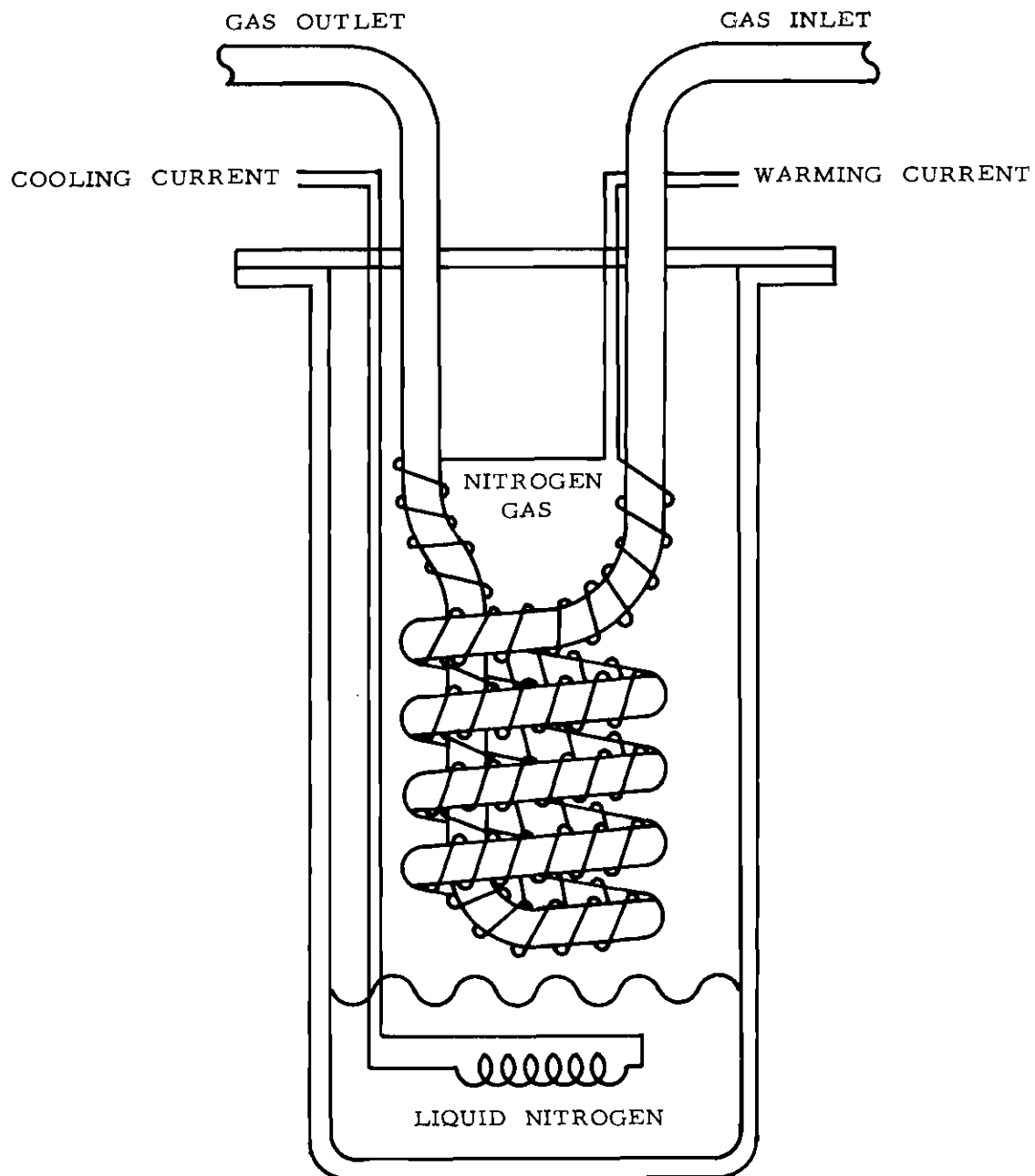


Figure 5. Schematic Drawing of the Refrigerated Vapor Bath Cold Trap

due to an increased concentration of the impurity molecules on the walls of the trap. The presence of impurities would be first noticeable as the gas pressure in the feed line decreased. The relative concentration of the impurity versus carbon monoxide in the feed line would increase as carbon monoxide was admitted to the drift tube, since the impurity was primarily restricted to the trap. As more gas was cleansed by the trap, its load of impurity molecules increased to the point that the trap was no longer effective. Since this time span was the order of one month, a routine procedure of cleaning the trap had to be devised. By attaching a ultrahigh-vacuum diffusion pump directly to the feedline, the trapped impurities could be removed by baking and pumping without releasing the impurities into the still clean drift tube. Since the full bakeout of the drift tube consumes about one week, this necessity for a rapid trap bakeout scheme is apparent.

Once the trap is cleaned out and the gas readmitted to the trap, it takes several days for the impurity level to decrease to a negligible level. Apparently the impurity molecules adhere to the clean walls of the trap reasonably tightly, so that trapping them in the cooled region takes some time. This same phenomenon is noticed in the drift tube, where the impurity level increases with a constant flow of gas into the tube. The impurity molecules are believed to enter the drift tube, and be initially trapped by the clean walls. Once their concentration on the walls grows, an equilibrium between evaporation and condensation is established and the impurity level in the drift tube grows rapidly. Monitoring of the impurity level both before and after the collection of

reaction rate data by taking mass scans is routinely done. Periodic examination of impurity levels during all other data taking is done to insure that the impurity level does not affect those measurements.

#### Preset Counter

In order to increase the resolution of our time-of-flight spectra, a Hewlett-Packard Preset Counter, Model #5330B, was purchased and added to our data analysis scheme. The counter was needed to provide an arbitrary delay between the time when the ions are gated into the drift tube and the start of the time-of-flight analysis scan. Prior to the installation of the preset counter, a timing pulse from the General Radio pulser that opened the Tyndall shutter would trigger the start of the time-of-flight scan. Under most conditions there would be a considerable delay before the first ions released by the Tyndall shutter would begin to arrive at the detector. During this time, a number of channels in the analyzer would be wasted, since no information was ever stored in them. Sometimes this dead time could be eliminated by setting the analyzer to scan through all 256 channels several times before it would begin to record data. In many instances, however, the ions would arrive over an interval of time that overlaps one of these dead periods and the channel width would have to be increased sufficiently to include the entire spectra in one sweep.

The desired solution is to have an arbitrary delay between the time the ions are gated into the drift tube and the time the time analyzer starts its scan. The Hewlett-Packard preset counter does this. In addition the preset counter has enough flexibility to allow it to be the

central timing unit.

The Hewlett-Packard preset counter is basically a 10 megahertz counter having a normalizable gate time and preset limit controls. It can be set up in a variety of configurations to perform several different tasks. The configuration that will be described here is the one that is used to introduce the desired digital delays between the various operations necessary in the data accumulation procedure. The detailed data accumulation procedures that were implemented with the preset counter will be described in Chapter IV.

The preset counter contains an internal one megahertz crystal-controlled clock accurate to better than one part in  $10^5$ . The one microsecond clock pulses are routed through a prescaler, a preset normalizing counter, and then to a displayed counting scaler. The prescaler divides the clock pulses by a factor of 1, 10, 100, or 1000. The output pulses from the prescaler are counted by the preset normalizing counter. Whenever the count reaches the preset value, which can be set from 1 to 100 000, the normalizing counter sends a pulse to the displayed counting scaler. In this manner, the displayed counting scaler receives pulses spaced from 1 to  $10^8$  microseconds apart in time.

The number of counts in the display is monitored by a coincidence detector. Dialed into two sets of limit controls are two preset count values. Whenever the displayed count agrees with one of the preset values, the coincidence detector sets one of three control lines appropriately. The "LO" control line is set to zero volts whenever the displayed count is less than the lower of the two preset values and is set to five volts

otherwise. The "IN" control line is set to zero volts whenever the displayed count contains at least the lower preset value but is less than the high preset value. It is set to five volts otherwise. The "HI" control line is set to zero volts whenever the displayed count is greater than or equal to the high preset value, and five volts otherwise. Thus as the displayed count increases past the two preset control values, the three control lines are appropriately set first to their low level of zero volts and then reset back to their high level of five volts.

There are two additional portions of the preset counter that are of interest. There is a reset control that allows the displayed count to be reset to any count the operator desires. Thus each cycle of counting can begin with from 0 to 99 999 counts in the displayed scaler. Also, there is a fourth control line that monitors whether the displayed counter has overflowed or not. It is held at five volts until an overflow occurs, at which time it is set to zero volts until the displayed count is reset.

The four control lines and the several presettable control switches are used to trigger the pulsers that open the electron gate and the Tyndall grid, and to start the analysis by the time-of-flight analyzer. The cycle is repeated by using the "HI" control line to reset the counter and allow the entire sequence of operations to be repeated.

One very important feature that could be implemented with this new timing system is the drift of several ion swarms in the drift tube at one time. If the drift time of an ion cloud is much greater than the spread in arrival times, there is no reason why several ion swarms can not be drifting in the drift tube at one time. This "multipulsing" allows the

analysis of one ion swarm to be accomplished while another ion swarm is still drifting. A major advantage of multipulsing is that several times as much data can be taken in a given time without increasing the ion density in any one swarm and thereby increasing the possibility of space charge effects causing errors in the determination of the transport properties.

In addition to being able to accumulate data faster than we could previously, measurements tend to be significantly more precise. By delaying the start of the time-of-flight analysis, a smaller channel width can be used, which spreads the ion swarm into more channels. Greater resolution in the arrival-time spectra can be achieved than before. The longitudinal diffusion coefficient measurements depend basically on a determination of the shape of the arrival-time spectra. With the data spread over more channels, the shape is more accurately known and the longitudinal diffusion coefficient can be more accurately computed. In past measurements, a noticeable error arose frequently when the ion arrival-time spectrum was spread over only ten or twenty channels. Now, the data can always be spread over at least 128 channels.

In the determination of reaction rates, one of the methods used is to analyze the shape of the arrival-time spectra of reaction-produced product ions. Here very precise measurements must be made and spreading the spectrum over many channels is imperative. Since the cost of an analyzer with more channels is prohibitive, the full use of the channels in the analyzer is the best solution.

### Electronics For Count-Rate Measurements

In addition to obtaining arrival-time spectra, we make several other measurements in analyzing transport properties of ions. One of these additional measurements is the determination of the attenuation, or "fall-off," of the time-integrated count of ions of the detected species as the drift distance is increased. In the determination of both the transverse diffusion coefficient and the reaction rate, the ratio of ion intensity to drift distance is measured and analyzed.

Previously the method for obtaining the count rate was to accumulate a spectrum in the time-of-flight analyzer for a preset period of time and then integrate this spectrum to obtain the total number of counts. This method has the desirable feature of providing a check of the arrival-time spectra while accumulating the data to see if unforeseen problems are distorting the arrival-time spectra and could lead to errors. It has several undesirable features however. The count rate of the ions must be quite slow. A count that arrives within 16 microseconds after the arrival of a previous count will not be recorded. Even with slow count rates, the possibility of this occurring exists, since the nature of the spectrum is to make many of the counts arrive within narrow time ranges. For mobility determinations, this is not much of a problem, since from the time spectrum most of these lost counts can be compensated for statistically. This analysis for fall-off measurements would require recording the entire arrival-time profile for each measurement, considerably increasing the analysis time and expense. Another undesirable feature of the integration method is that the source must be operated in a pulsed mode, wasting much

of the time during which count rates could be measured. Counts arrive in quantity during only a small fraction of the time, while during the rest of the time no information is being obtained. A third undesirable feature is that the time between count rate determinations is lengthened by the time it takes the analyzer to perform the integration. Because the ion source is intrinsically unsteady, the count rate determinations for each position should be made as close together in time as is possible.

For all of these reasons, it was decided to purchase a Nuclear Counter, Model #1491, from Canberra Industries, Meriden, Connecticut. This Nuclear Counter contains within a single unit a 20 megahertz counter and a 0.1 second timer. The Nuclear Counter can be set to accumulate counts for a preset time, or to determine the time necessary to accumulate a preset number of counts. With the 20 megahertz counting capability, only counts arriving within 50 nanoseconds of each other would cause an error. At the end of the accumulation period, the count is immediately available.

The ion current pulses are normally amplified by a Tennelec Pre-amplifier, Model TC-L-170. This unit provides sufficient amplification and pulse shaping to trigger the time-of-flight analyzer but is not well suited to triggering the Canberra Nuclear Counter. To properly amplify and shape the ion pulses for the counter, a Canberra Preamplifier-Amplifier-Discriminator (PAD), model #814, was purchased. Since the pre-amplifier is part of the same unit as the amplifier and is mounted in an AEC-type bin, the signal from the channeltron was run about fifteen feet before being attached to the preamplifier. This signal line introduced too much noise into the system, so an improved method of signal ampli-



cation was found. The Tennelec preamplifier is now used to initially amplify the signal, this signal is then amplified by the Canberra main amplifier, and the discriminator signal is used to drive the Nuclear Counter. In this manner we obtain the maximum signal level with the minimum noise. The discriminator can be set to pass signals to the Nuclear Counter that are well above the noise and yet not discriminate against an appreciable number of true signal counts.

#### Pressure Recalibration

As described in a paper by McDaniel and Martin,<sup>30</sup> an efficient and accurate method of calibrating our pressure transducer, an MKS Baratron, is to determine the mobility of  $K^+$  in nitrogen. This mobility is well known and can be used as a standard. Since this pressure recalibration needs to be performed at periodic intervals, the source gas feed line was modified to allow a tank of nitrogen to be attached to the system at all times. This tank is valved off whenever another gas is being studied. At this same time, and in conjunction with the pumpout of the refrigerated vapor bath cold trap, a nude ion gauge was attached to the feed line. This gauge allows us to monitor the vacuum in the feed line when the trap and feed line are being baked out in order to improve gas purity. The ion gauge had to be mounted nude, since a glass envelope might not be able to stand the pressures that might exist in the feedline when it is placed in use.

#### Carbon Monoxide Alarms

Because of the poisonous nature of carbon monoxide and the possibility of a leak occurring without anyone's knowledge, two carbon monoxide alarms were purchased. The first alarm was a Model #8010 Carbon Monoxide

Alarm, purchased from Matheson Gas Products, East Rutherford, New Jersey. It worked on the basis of a chemical agent changing color when exposed to carbon monoxide and this color change being picked up by a photocell detector. This unit did not work properly due to poor construction and was returned to the supplier. Because these mechanical defects plagued this type of detector, we purchased another brand of detector. The second detector was a product of Mine Safety Appliances Company, Pittsburg, Pennsylvania, model #701. This detector worked on a different principle. The gas sample is continuously admitted to two chambers, one filled with a catalyst and the second filled with some neutral substance. Any carbon monoxide present in the room air is catalytically burned in the first chamber, raising its temperature slightly. The temperature imbalance between the two chambers is detected by two thermistors in a Wheatstone bridge, amplified and used to sound an alarm. This device, unlike the product sold by Matheson, proved to be fairly reliable. When a large amount of carbon monoxide was pumped out of the vacuum system rapidly as a test, the device responded properly.

To guard against the consequences of a leak in the carbon monoxide gas system, a fan was installed to blow the room air out a window and thereby prevent the carbon monoxide from entering the building air conditioning system. In case the leak was major, gas masks and carbon monoxide filtering canisters were left available both in the laboratory and in one of the offices.

In order to make spot checks of hazardous gas concentrations in locations inaccessible to the MSA detector, and for use in checking out the operation of the MSA detector, a Unico Model 400 Precision Gas Detector

was purchased. This device is a hand-held, mechanical pump for drawing precise gas samples through a chemical detector. By noting the nature and degree of chemical change, normally indicated by a color change, the concentration of the desired poisonous gas can be determined. This detector is useful for a wide range of gases, by simply changing the chemical detector.

## CHAPTER III

## ANALYSIS

The purpose of this chapter is to describe the analytical solution of the transport equations that apply to the drift tube and to describe how the parameters we wish to determine can be calculated from the data we obtain from the experiment. The major portion of the analysis described in this chapter was done by Dr. I. R. Gatland.

The Transport Equations and Their Solution

Consider a population of two ionic species created at one end of a cylindrically symmetric drift space filled with gas of a uniform pressure  $p$ , in which an externally applied electric field  $\vec{E}$  exists directed along the axis. Assume that the number density,  $n(\vec{r}, t)$ , of each of the two species is low enough that ion-ion interactions have a negligible effect. The ionic current densities for the two species (A and B) are, respectively,

$$\vec{j}_A(\vec{r}, t) = \vec{v}_{dA} n_A(\vec{r}, t) - \vec{D}_A \cdot \vec{\nabla}_r n_A(\vec{r}, t) \quad (3-1)$$

$$\vec{j}_B(\vec{r}, t) = \vec{v}_{dB} n_B(\vec{r}, t) - \vec{D}_B \cdot \vec{\nabla}_r n_B(\vec{r}, t). \quad (3-2)$$

Recall that  $\vec{D}$  is a diagonal tensor, the first two components of which are equal. If we consider that these two species may be depleted by ion-molecule reactions to each other or to other species, and that each species

may increase by reaction from the other, the continuity equations are:

$$\frac{\partial n_A}{\partial t} + \nabla \cdot \vec{j}_A + \alpha_A n_A - \alpha_{AB} n_B = 0 \quad (3-3)$$

$$\frac{\partial n_B}{\partial t} + \nabla \cdot \vec{j}_B + \alpha_B n_B - \alpha_{BA} n_A = 0 \quad (3-4)$$

where  $\alpha_i$  is the frequency of reaction for depletion from species  $i$  to all others ( $i=A,B$ ) and  $\alpha_{ij}$  is the frequency of the forward or backward reaction between the two species ( $ij=AB,BA$ ). If we define the differential operator  $\mathcal{D}$  in the form:

$$\mathcal{D} = D_T \left( \frac{\partial^2}{\partial x^2} + \frac{\partial^2}{\partial y^2} \right) + D_L \frac{\partial^2}{\partial z^2} - v_d \frac{\partial}{\partial z} - \alpha \quad (3-5)$$

then by combining Equations (3-1) to (3-4) we obtain

$$\frac{\partial n_A}{\partial t} = \mathcal{D} n_A + \alpha_{AB} n_B \quad (3-6)$$

$$\frac{\partial n_B}{\partial t} = \mathcal{D} n_B + \alpha_{BA} n_A. \quad (3-7)$$

To the above continuity equations we need to add source terms representing the input of ions into the drift tube. We assume that the ion swarm fills the entrance aperture with uniform density and that ions are gated into the drift tube for only a very short time in comparison to the drift time. With these assumptions the source terms are approximated by

$$\beta_A = f_A s S(r_0 - r) \delta(z) \delta(t) \quad (3-8)$$

$$\beta_B = f_B s S(r_0 - r) \delta(z) \delta(t) \quad (3-9)$$

where

$$S(\theta) = 0 \quad \text{if } \theta \leq 0,$$

$$S(\theta) = 1 \quad \text{otherwise.}$$

Here  $s$  is the areal source ion density,  $r_0$  is the entrance aperture radius,  $z = 0$  is the position of the entrance aperture, and  $f_i$  is the fraction of ions that are species  $i$ .

Including the source terms, the pair of coupled partial differential equations we wish to solve are:

$$\frac{\partial n_A}{\partial t} = \mathcal{D}_A n_A + \alpha_{AB} n_B + \beta_A \quad (3-10)$$

$$\frac{\partial n_B}{\partial t} = \mathcal{D}_B n_B + \alpha_{BA} n_A + \beta_B. \quad (3-11)$$

In order to solve these coupled equations, we will break the problem into several parts. First, we will solve a set of differential equations, the first equation describing the drift, diffusion, and depleting reaction of a source produced ion species. Each succeeding differential equation will describe an ion species created from the previous species by reaction. Secondly, we will combine these equations into a form describing two species that can react back and forth, but with only one species created in the source. Finally, we will describe the solution for both

ion species created in the source.

Consider the solution to the following differential equation:

$$\frac{\partial n_1}{\partial t} = \nu_1 n_1 + \beta. \quad (3-12)$$

Since this equation is linear in  $n_1$ , we can use the standard techniques for partial differential equations. The applicable Green's function is

$$G(\vec{x}) = \left[ (4\pi D_T t)^2 4\pi D_L t \right]^{-\frac{1}{2}} \exp \left[ -\alpha t - \frac{x^2 + y^2}{4D_T t} - \frac{(z - v_d t)^2}{4D_L t} \right] \quad (3-13)$$

and the solution is

$$n_1(\vec{x}) = \int d^4 x_0 G_1(\vec{x} - \vec{x}_0) \beta(\vec{x}_0) \quad (3-14)$$

where the time integration runs from  $-\infty$  to  $t$  and the space integrations from  $-\infty$  to  $+\infty$ . (Note that  $\vec{x}$  represents  $x, y, z$ , and  $t$ .)

If this first species  $n_1(\vec{r}, t)$  reacts to form a second ionic species  $n_2(\vec{r}, t)$ , the source term for the second species will be  $\alpha_{21} n_1(\vec{r}, t)$  where  $\alpha_{21}$  is the reaction frequency for producing species  $n_2$  from  $n_1$ . The solution for species  $n_2$  can be obtained by applying a second Green's function:

$$n_2(\vec{x}) = \int d^4 x_1 G_2(\vec{x} - \vec{x}_1) \alpha_{21} \int d^4 x_0 G_1(\vec{x}_1 - \vec{x}_0) \beta(\vec{x}_0). \quad (3-15)$$

Similarly, the differential equation for the  $k^{\text{th}}$  species is

$$\frac{\partial n_k}{\partial t} = \vartheta_k n_k + \alpha_{k,k-1} n_{k-1} \quad (3-16)$$

and the solution is

$$n_k(\vec{x}) = \int d^4x_{k-1} \cdots \int d^4x_1 \int d^4x_0 G_k(\vec{x}-\vec{x}_{k-1}) \alpha_{k,k-1} \quad (3-17)$$

$$\times G_{k-1}(\vec{x}_{k-1}-\vec{x}_{k-2}) \alpha_{k-1,k-2} \cdots \alpha_{21} G_1(\vec{x}_1-\vec{x}_0) \beta(\vec{x}_0).$$

All of the spatial integrations  $\vec{r}_1$  to  $\vec{r}_{k-1}$  can be done immediately. If we assume that  $\beta$  has the general form expressed in Equations (3-8) and (3-9), the integration over  $\vec{x}_0$  can also be carried out and the result is:

$$n_k(\vec{x}) = s \prod_{j=1}^{k-1} \left[ \alpha_{j+1,j} \int_0^{t_{j+1}} dt_j \right] (\pi r_{Lk}^2)^{-\frac{1}{2}} \exp\left[-\gamma_k - (z-r_{dk})^2/r_{Lk}^2\right] \quad (3-18)$$

$$\times \left\{ 1 - \sum_{m=0}^{\infty} \sum_{i=0}^m (m!i!)^{-1} (r^2/r_{Tk}^2)^m (r_0^2/r_{Tk}^2)^i \exp\left[-(r_0^2+r^2)/r_{Tk}^2\right] \right\}$$

where

$$r_{Tk}^2 = \sum_{j=1}^k 4 D_{Tj} (t_j - t_{j-1}) \quad (3-19a)$$

$$r_{Lk}^2 = \sum_{j=1}^k 4 D_{Lj} (t_j - t_{j-1}) \quad (3-19b)$$

$$r_{dk} = \sum_{j=1}^k v_{dj} (t_j - t_{j-1}) \quad (3-19c)$$

$$\gamma_k = \sum_{j=1}^k \alpha_j (t_j - t_{j-1}) \quad (3-19d)$$



with  $t_k = t$  and  $t_0 = 0$ .

Each of these parameters has a definite physical interpretation. The variable  $r_{Tk}$  is a measure of the average distance that the ions observed as the  $k^{\text{th}}$  species will travel due to the transverse diffusion of themselves and all the other species in their history. Similarly,  $r_{Lk}$  is a measure of the distance the ions observed as the  $k^{\text{th}}$  species will travel due to longitudinal diffusion,  $r_{dk}$  is a measure of the average distance traveled due to the drift introduced by the electric field, and  $\gamma_k$  is a measure of the survival probability for the ions observed as the  $k^{\text{th}}$  species.

In the present experiment, the ion swarm is sampled on axis, and the result of interest is the axial ionic number density,  $n_k(0, z, t)$ :

$$n_k(0, z, t) = s \prod_{j=1}^{k-1} \left[ \alpha_{j+1, j} \int_0^{t_{j+1}} dt_j \right] (\pi r_{Lk}^2)^{-\frac{1}{2}} \quad (3-20)$$

$$\times \exp \left[ -\gamma_k - (z - r_{dk})^2 / r_{Lk}^2 \right] \left[ 1 - \exp(-r_0^2 / r_{Tk}^2) \right].$$

Now we return to consideration of the forward-backward reaction problem. If we consider all of the species with odd indices to be species A and those with even indices to be species B, each term,  $n_k$ , represents ions that have undergone a specified number of reactions. Physically the term  $n_{2m+1}$  represents the density of ions of species A that has been converted from species A to species B and back again  $m$  times. The term  $n_{2m+2}$  represents the number density of ions converted into species B and then reacted from species B into species A and back into species B  $m$  times. We therefore define  $n_A$  and  $n_B$  as follows:

$$n_A = \sum_{m=0}^{\infty} n_{2m+1} \quad (3-21)$$

$$n_B = \sum_{m=0}^{\infty} n_{2m+2} \quad (3-22)$$

and arrive at the solution for the forward-backward reaction equations, (3-10) and (3-11), with only species  $n_A$  formed in the source.

With this definition of the identity of the  $k^{\text{th}}$  species kept in mind, we consider the solution for  $n_k$ . Since  $G_{2m-1}(\vec{x})$  equals  $G_A$  and  $G_{2m}(\vec{x})$  equals  $G_B$ , for  $m=1,2,3,\dots$ , equations (3-19) can be simplified to:

$$r_T^2 = 4 D_{TA}(t-u) + 4 D_{TB}u \quad (3-23a)$$

$$r_L^2 = 4 D_{LA}(t-u) + 4 D_{LB}u \quad (3-23b)$$

$$r_d = v_{dA}(t-u) + v_{dB}u \quad (3-23c)$$

$$\gamma = \alpha_A(t-u) + \alpha_B u \quad (3-23d)$$

where  $u$  is the time the ion spends as species B. For  $k$  odd,  $u$  equals  $u_k$  and for  $k$  even,  $u$  equals  $(t-u_k)$ , where

$$u_k = \sum_{j=1}^{k-1} (-1)^{k+j+1} t_j. \quad (3-24)$$

Since all the  $t_j$  occur in only one combination, all but one of the time integrations in equation (3-18) reduce to geometrical factors. Using the appropriate change of variables:

$$\int_0^{t_{i+1}} dt_i \int_0^{t_i} du_i f(t_i - u_i) \frac{u_i^n}{n!} \frac{(t_i - u_i)^m}{m!} \quad (3-25)$$

$$= \int_0^{t_{i+1}} du_{i+1} f(u_{i+1}) \frac{(t_{i+1} - u_{i+1})^{n+1}}{(n+1)!} \frac{u_{i+1}^m}{m!}$$

one obtains:

$$n_{2k+1}(\vec{x}) = s \int_0^t du (\alpha_{AB} \alpha_{BA})^k \frac{u^{k-1}}{(k-1)!} \frac{(t-u)^k}{k!} (\pi r_L^2)^{-\frac{1}{2}} \quad (3-26)$$

$$\times \exp\left[-\gamma - (z - r_d)^2 / r_L^2\right] \left[1 - \exp(-r_0^2 / r_T^2)\right]$$

$$n_{2k+2}(\vec{x}) = s \alpha_{BA} \int_0^t du (\alpha_{AB} \alpha_{BA})^k \frac{u^k}{k!} \frac{(t-u)^k}{k!} (\pi r_L^2)^{-\frac{1}{2}} \quad (3-27)$$

$$\times \exp\left[-\gamma - (z - r_d)^2 / r_L^2\right] \left[1 - \exp(-r_0^2 / r_T^2)\right]$$

for  $k = 0, 1, 2, \dots$ . Species  $n_1$  must be treated as a unique case, since it has no reaction-produced input. It can be included in the above equations if one replaces the  $u^{k-1}/(k-1)!$  with a delta function at  $u = 0$ , since the ions represented by this term spend no time as species B. The delta function is treated as lying entirely within the range of integration in order to obtain the correct result.

When equations (3-26) and (3-27) are inserted into equations (3-21) and (3-22), two infinite sums result. These infinite sums result from the possibility of an ion reacting back and forth between species A and species B any number of times. These infinite sums can be related to the power series expansion of the zero and first order modified Bessel func-

tions:

$$I_1(\eta) = \left(\frac{1}{2}\eta\right) \sum_{j=0}^{\infty} \left(\frac{1}{4}\eta^2\right)^j / (j!(j+1)!) \quad (3-28)$$

$$I_0(\eta) = \sum_{j=0}^{\infty} \left(\frac{1}{4}\eta^2\right)^j / (j!)^2 \quad (3-29)$$

with 
$$\eta = \left[4\alpha_{AB}\alpha_{BA}u(t-u)\right]^{\frac{1}{2}}. \quad (3-30)$$

Carrying through the algebra, one obtains:

$$n_A(0, z, t) = s \int_0^t du \left[ \delta(u) + \alpha_{AB}\alpha_{BA}(t-u)2I_1(\eta)/\eta \right] (\pi r_L^2)^{-\frac{1}{2}} \quad (3-31)$$

$$\times \exp\left[-\gamma - (z-r_d)^2/r_L^2\right] \left[1 - \exp(-r_0^2/r_T^2)\right]$$

$$n_B(0, z, t) = s\alpha_{BA} \int_0^t du I_0(\eta) (\pi r_L^2)^{-\frac{1}{2}} \quad (3-32)$$

$$\times \exp\left[-\gamma - (z-r_d)^2/r_L^2\right] \left[1 - \exp(-r_0^2/r_T^2)\right].$$

Using the same analysis, but assuming that all ions in the source term belong to species B, one can obtain

$$n_A(0, z, t) = s\alpha_{AB} \int_0^t du I_0(\eta) (\pi r_L^2)^{-\frac{1}{2}} \quad (3-33)$$

$$\times \exp\left[-\gamma - (z-r_d)^2/r_L^2\right] \left[1 - \exp(-r_0^2/r_T^2)\right]$$

$$n_B(0, z, t) = s \int_0^t du \left[ \delta(t-u) + \alpha_{AB} \alpha_{BA} u \frac{2I_1(\eta)}{\eta} \right] (\pi r_L^2)^{-\frac{1}{2}} \quad (3-34)$$

$$\times \exp \left[ -\gamma - (z-r_d)^2 / r_L^2 \right] \left[ 1 - \exp(-r_0^2 / r_T^2) \right],$$

where  $r_L$ ,  $r_T$ ,  $r_d$ , and  $\gamma$  are the same as before. Combining fraction  $f_A$  of the terms considering species A as the source, and fraction  $f_B$  of the terms considering species B as the source, one obtains:

$$n_A(0, z, t) = s \int_0^t du \left[ f_A \left\{ \delta(u) + \alpha_{AB} \alpha_{BA} (t-u) \frac{2I_1(\eta)}{\eta} \right\} \right. \quad (3-35)$$

$$\left. + f_B \alpha_{AB} I_0(\eta) \right] \exp \left[ -\gamma - (z-r_d)^2 / r_L^2 \right]$$

$$\times \left[ 1 - \exp(-r_0^2 / r_T^2) \right] (\pi r_L^2)^{-\frac{1}{2}}$$

$$n_B(0, z, t) = s \int_0^t du \left[ f_B \left\{ \delta(t-u) + \alpha_{AB} \alpha_{BA} u \frac{2I_1(\eta)}{\eta} \right\} \right. \quad (3-36)$$

$$\left. + f_A \alpha_{BA} I_0(\eta) \right] \exp \left[ -\gamma - (z-r_d)^2 / r_L^2 \right]$$

$$\times \left[ 1 - \exp(-r_0^2 / r_T^2) \right] (\pi r_L^2)^{-\frac{1}{2}}.$$

Equations (3-35) and (3-36) represent the solutions to the partial differential equations (3-10) and (3-11). The quantity measured experimentally is the flux of ions leaving the drift tube through the exit aperture of area  $a$  at a fixed distance  $z$  from the source plane:

$$\bar{\phi}(0, z, t) = a j(0, z, t) \quad (3-37)$$

where  $j(0, z, t)$  is the  $z$ -component of the ionic current density in the drift tube, on the axis, at the end of the drift distance  $z$ . The ionic current density is related to the ionic number density by equations (3-1) and (3-2). If equations (3-35) and (3-36) are substituted for  $n_A$  and  $n_B$  and the required differentiation is performed to obtain the gradient, we obtain:

$$\bar{\phi}_A(0, z, t) = as \int_0^t du \left[ f_A \left\{ \delta(u) + \alpha_{AB} \alpha_{BA} (t-u) \frac{2I_1(\eta)}{\eta} \right\} \right] \quad (3-38)$$

$$+ f_B \alpha_{AB} I_0(\eta) \left[ \left\{ \frac{2D_{LA}(z-r_d)}{r_L^2} \right\} + v_{dA} \right]$$

$$\times \exp \left[ -\gamma - (z-r_d)^2 / r_L^2 \right] \left[ 1 - \exp(-r_0^2 / r_T^2) \right] (\pi r_L^2)^{-\frac{1}{2}}$$

$$\bar{\phi}_B(0, z, t) = as \int_0^t du \left[ f_B \left\{ \delta(t-u) + \alpha_{AB} \alpha_{BA} u \frac{2I_1(\eta)}{\eta} \right\} \right] \quad (3-39)$$

$$+ f_A \alpha_{BA} I_0(\eta) \left[ \left\{ \frac{2D_{LB}(z-r_d)}{r_L^2} \right\} + v_{dB} \right]$$

$$\times \exp \left[ -\gamma - (z-r_d)^2 / r_L^2 \right] (\pi r_L^2)^{-\frac{1}{2}} \left[ 1 - \exp(-r_0^2 / r_T^2) \right].$$

The experimental data obtained from the drift tube are spectra of arrival times for various values of drift distance, electric field, gas pressure, and ion mass. From these "arrival-time spectra" we extract the transport and reaction properties we desire to measure, namely the mobility, the diffusion coefficient, and ion-molecule reaction rate.

### Mobilities

When data are taken for mobility or diffusion coefficient measurements, the pressure and  $E/N$  are set so that the ionic species under consideration is formed essentially only in the source. For ion species that are created in the source, and may be depleted by ion-molecule reactions, but do not gain ions due to other species reacting with the gas, the equation for the ionic flux is given by:

$$\begin{aligned} \Phi(0, z, t) = & as (v_d + z/t) \exp\left[-\alpha t - (z - v_d t)^2 / 4D_L t\right] \\ & \times \left[4(\pi D_L t)^{\frac{1}{2}}\right]^{-1} \left[1 - \exp(-r_0^2 / 4D_T t)\right]. \end{aligned} \quad (3-40)$$

The drift velocity, and hence the mobility from equation (1-1), can be obtained from the mean arrival time. If one were able to determine the spatial distribution of the ions at one instant of time, the mean distance the ions drifted would be exactly  $v_d t$ , the drift velocity times the time of drift. However, the only quantity we can measure is the distribution of drift times of the ions arriving at one specific distance. The mean arrival time is shifted from the desired ratio of drift distance to drift velocity due to the effects of diffusion and reaction on ions staying in the drift tube for longer times.

In the report by Moseley, et al.,<sup>31</sup> these effects were considered for two special cases, an infinite plane source and a point source. From these results, one can obtain information pertaining to the disk source that was used in this research. The experimental quantity we wish to study is the mean arrival time,  $\bar{T}$ , given analytically by

$$\bar{t} = \frac{\int_0^{\infty} t \Phi(0, z, t) dt}{\int_0^{\infty} \Phi(0, z, t) dt}. \quad (3-41)$$

For the infinite plane source, we let  $r_0 \rightarrow \infty$ , while keeping the plane source density  $s$  constant. The solution for the flux becomes

$$\Phi(0, z, t) = \frac{as(v_d + z/t)}{2(4\pi D_T t)^{\frac{1}{2}}} \exp\left[-\alpha t - (z - v_d t)^2 / 4D_L t\right]. \quad (3-42)$$

If one proceeds through the integration, making approximations where necessary to give a first order correction to the "true arrival time," the result is

$$\bar{t} = \frac{z}{v_d} \left[ 1 + \frac{D_L}{v_d z} - \frac{2\alpha D_L}{v_d^2} \right]. \quad (3-43)$$

One can see the reason for both of the correction terms on a physical basis. Because of the infinite radial extent of the source, there is no radial density gradient to cause transverse diffusion. Only longitudinal diffusion occurs. The first term,  $D_L/v_d z$ , is due to longitudinal diffusion alone and accounts for the fact that ions diffusing back, toward the source, remain in the drift tube longer and are allowed a chance to diffuse further. The ions diffusing away from the source are swept out of the drift tube early and do not have a chance to diffuse for as long a period of time. The mean arrival time is thereby increased. The second term,  $2\alpha D_L/v_d^2$ , is due to both longitudinal diffusion and reaction and accounts for the fact that ions drifting for longer times suffer more attenuation from reactions than do the ions that are collected early. The



mean arrival time is reduced due to this effect.

For the second limiting case, the point source, we let  $r_0 \rightarrow 0$ , but keep the total number of ions  $b = s(\pi r_0^2)$  constant. The solution for the flux of ions becomes

$$\Phi(0, z, t) = \frac{ab(v_d + z/t)}{2(4\pi t)^{\frac{3}{2}} D_T D_L^{\frac{1}{2}}} \exp\left[-\alpha t - \frac{(z - v_d t)^2}{4D_L t}\right]. \quad (3-44)$$

For this case, the first order correction terms come out as

$$\bar{t} = \frac{z}{v_d} \left[ 1 - \frac{D_L}{v_d z} - \frac{2\alpha D_L}{v_d} \right]. \quad (3-45)$$

Again, one can see the reason for these corrections on a physical basis. For a point source, the ion density is not constant in the radial direction, and both longitudinal and transverse diffusion occur. Due to the nature of the point source approximation, diffusion causes the ion density to decrease very rapidly at very early times (the ion density gradient is infinite for a point source) and then decay steadily for later times. The fact that transverse diffusion is occurring (independent of the value of the diffusion coefficient) means that both reactions and transverse diffusion are removing ions from the ion swarm near the axis. Longitudinal diffusion causes some ions to drift for longer times than others, and those ions drifting longer suffer more attenuation near the axis by both mechanisms than do those that drift for shorter times. Thus, both terms reduce the mean arrival time.

Drift velocities in the present experiment were not obtained directly

from  $v_d = z/\bar{t}$ , however. In order to reduce time errors caused by end effects in the source and analysis region, a differencing technique was used. Drift velocities are calculated from the relation:

$$v_d = (z_i - z_j) / (\bar{t}_i - \bar{t}_j), \quad (3-46)$$

If we write the first order correction for the measured drift velocity as

$$\bar{t}_i = \frac{z_i}{v_d} \left[ 1 \pm \frac{D_L}{v_d z_i} - \frac{2\alpha D_L}{v_d^2} \right], \quad (3-47)$$

and substitute this into equation (3-46), we obtain for the measured drift velocity,  $v_d'$ ,

$$v_d' = \frac{v_d}{\left[ 1 - \frac{2\alpha D_L}{v_d^2} \right]} \approx v_d \left[ 1 + \frac{2\alpha D_L}{v_d^2} \right] \quad (3-48)$$

The diffusion term has canceled and only the reaction term has remained.

Although this analysis indicates that no diffusion error remains in the experimental drift velocities calculated by differencing mean drift times, this conclusion is not entirely true. Equations (3-43) and (3-45) contain only the first order correction terms. However, in the report by Moseley, et al.<sup>31</sup> he showed that, for values of  $v_d$ ,  $D_L$ ,  $D_T$ , and  $\alpha$  that represent the motion and reaction of  $N_2^+$  in  $N_2$ , the errors between the "measured" drift velocity and the "true" drift velocity are near that estimated by the above calculations. He demonstrated this result by constructing an "experimental" arrival-time spectrum from Equation (3-40) and

then calculating the mean arrival time from this spectrum. The difference in mean arrival times agreed quite well with predictions based on the known difference in drift distances and the drift velocity used to calculate the spectra.

### Longitudinal Diffusion Coefficients

We have not been able to find a statistical characteristic of the arrival-time spectra that measures the longitudinal diffusion coefficient as accurately as the mean arrival time measures the drift velocity. Qualitatively, the width of the spectra is a function of the longitudinal diffusion coefficient, but the only way we have found to determine  $D_L$  accurately is by a computerized curve-fitting procedure.

The work of Moseley, et al.<sup>31</sup> showed that the shape of the arrival-time spectra is relatively insensitive to the amount of transverse diffusion or reaction occurring. The time dependence of these effects is sufficiently weak so as to affect most of the arriving ions about the same amount. The variation of  $D_T$  and  $\alpha$  does have a significant effect on the overall intensity of the spectra. However, the curve-fitting technique normalizes both experimental and theoretical spectra to the same value in the manner described below, so any effects of absolute intensity are eliminated.

The first step in the computerized curve fitting is normalization of the experimental data. The most obvious procedure is to make the count in the experimental channel with the maximum number of counts equal to the peak of the theoretical curve (both are normalized to a value of unity). This choice frequently turns out to be in error. All of the

experimental data have some random scatter, no matter how long we collect data. The channel with the maximum number of counts will frequently have more counts than normal because of the scatter, while others will have less. The normalization will therefore be consistently high. This is especially true for spectra where counts are spread over very many channels, with relatively few counts in each channel. The statistical scatter is then larger and the improper normalization is emphasized. An example of this effect can be seen in Figure 6. The histogram represents the experimental data and the smooth curve represents a theoretical profile curve fitted to the experimental data. Normalization of the theoretical profile to the peak of the experimental data would obviously be in error.

To eliminate this effect, a smoothing procedure is performed. Each channel is averaged with both adjacent channels twice in order to eliminate much of the statistical scatter. This produces a peak that is much smoother and a peak value that is much closer to the true value. This procedure does have a drawback, however. For spectra that have not been spread over many channels and therefore have a large number of counts in their peak channels, the statistics are good enough to need no smoothing. The result of smoothing is to lower the peak, since channels adjacent to the peak must have fewer counts.

Because smoothing causes erroneously low normalizations in narrow peaks, and no smoothing causes erroneously high normalizations in wide peaks, much of the data taken early in this research was analyzed with both normalizations and the analysis that produced the best fit was used. The sum of squared deviations was calculated for each spectrum and this sum was used to determine which fit was superior. Many times this was

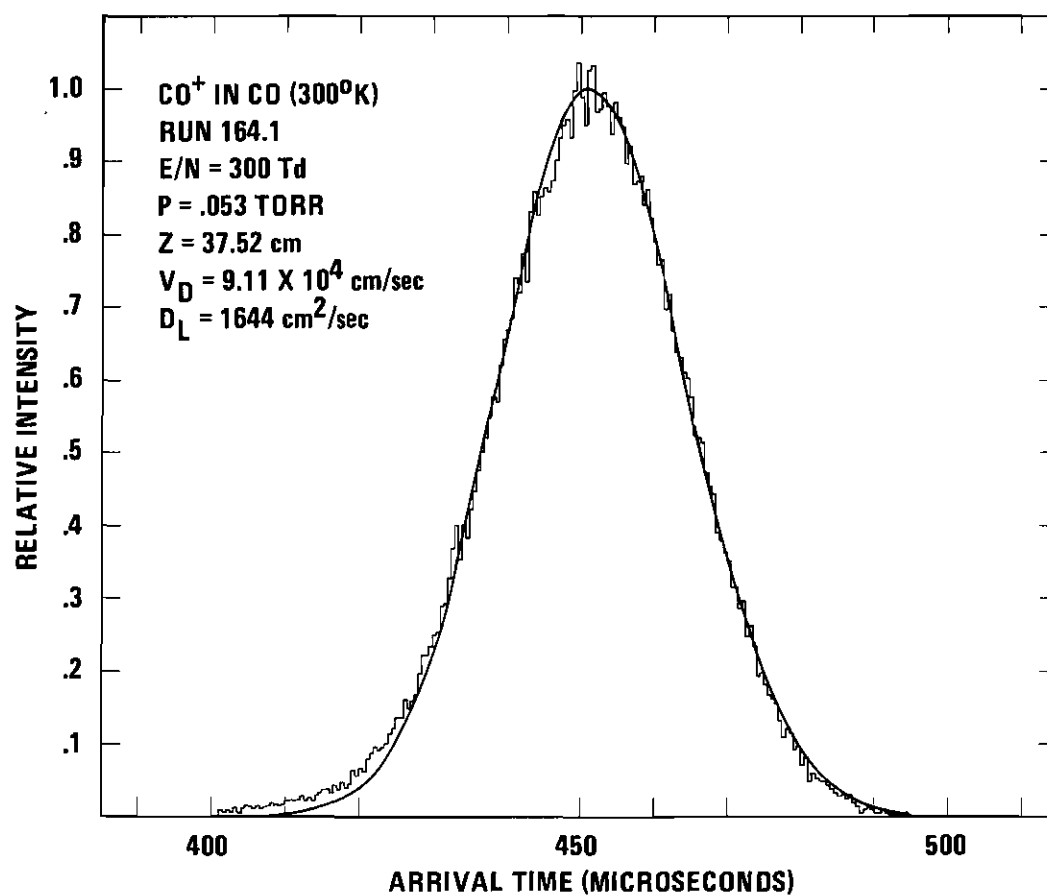


Figure 6. Sample Arrival-Time Spectrum and Curve-Fitted Theoretical Profile

obvious from the computer-printed graphs as well. Once the Hewlett-Packard preset counter was installed to introduce a variable delay before analysis was begun, all of the spectra could be spread over a large number of channels and the smoothing technique was always used. Any data analyzed without both types of normalization before the preset counter was installed were not used in final  $D_L$  determinations.

The next step in the computer analysis is the calculation of the theoretical curve from Equation (3-40). Initially  $D_L$  and  $D_T$  are set equal to the Einstein value and  $\alpha$  is set equal to zero. The theoretical curve is normalized to a value of unity at its peak. A second normalization is now necessary. The experimental data contain an additive analysis time, i.e., the time the ions spend traveling between the exit aperture and the detector plus any end effects produced by the source and exit aperture. The theoretical curve includes no analysis time so it must be shifted in time to agree with the experimental data. The point of agreement is again at the peak, which is arranged to lie in the same channel.

Once the two spectra are normalized and aligned, they are compared. The sum of the cubed differences between the experimental and theoretical values is calculated for the regions on either side of the peak. If the experimental spectrum lies basically above the theoretical spectrum (the net differences are positive), the assumed  $D_L$  is too small. The value of  $D_L$  is doubled, and the process is repeated. If the experimental spectrum lies below the theoretical (the net differences are negative), the assumed value for  $D_L$  is too large. In this case  $D_L$  is cut in half. One of these two steps takes place until one value of  $D_L$  that is too large and another value that is too small have been obtained.

Once the desired value of  $D_L$  has been bounded, the program uses a process of linear interpolation to obtain the successive trial values for  $D_L$ . Since the sum of cubed differences will be positive for small values of  $D_L$  and negative for large values, the value of  $D_L$  that would give a net zero difference is calculated. The unknown function that gives net differences versus  $D_L$  cannot be assumed to be linear, so several iterations are necessary to closely approach the value of  $D_L$  that produces zero net difference.

As values of  $D_L$  are found that produce smaller differences, the gap between values of  $D_L$  that are too small and those that are too large is made smaller. Once this "bound" on  $D_L$  is made sufficiently small, the iterative process is stopped. Even though the net differences are now quite small, they can cancel each other out since the sign of each difference is kept. If the sum of differences on one side of the peak is of one sign and the sum for the other side is the opposite, then often shifting the theoretical curve in the proper direction will bring about a better fit. When this is done the entire searching procedure for  $D_L$  is repeated.

Once a point is reached where the net difference is small and the differences for each side of the peak the same sign, or the respective signs have shifted, no further realignment of the two spectra is necessary. The value of  $D_L$  that has given the smallest net difference is printed out and recorded.

Longitudinal diffusion coefficients can be estimated from drift velocity measurements by the use of the theory of Wannier.<sup>2</sup> By use of the model of constant mean free time, typical of the polarization force

between an ion and a neutral molecule, the following expression for the longitudinal diffusion coefficient can be derived:

$$D_L(E) = D(0) + \frac{(M+3.72m)M}{3(M+1.908m)} \frac{v_d^3}{eE} \quad (3-49)$$

where  $D(0)$  is the zero-field value of  $D$ , which can be calculated from the Einstein equation, (1-3),  $m$  is the mass of the ion,  $M$  is the mass of the molecule,  $e$  is the ionic charge, and  $E$  is the electric field intensity. For ions drifting in a gas where resonant charge transfer is not a dominant interaction, this formula agrees quite well with the existing data.<sup>32</sup>

#### Transverse Diffusion Coefficients

As mentioned in the previous section of this chapter, the transverse diffusion coefficient does not have a strong effect on the shape of the arrival-time spectra. We cannot determine  $D_T$  by curve fitting to the arrival-time spectra. The quantity we can measure that is strongly affected by  $D_T$  is the intensity of the flux of ions. We cannot measure the flux of ions absolutely and thereby determine  $D_T$ . The quantity we can measure is the relative flux of ions on the axis for various drift distances.

For an ion species that is entirely source-created, the flux of ions is given by equation (3-40). To eliminate the necessity of considering the entire arrival-time spectrum for each drift distance, we perform a time integration to obtain the integrated flux on axis. Theoretically, this means that we need to consider the expression

$$I(z) = \int_0^{\infty} \Phi(0, z, t) dt. \quad (3-50)$$



In the report by Snuggs, et al.<sup>33</sup> this integral is evaluated and shown to be equal to

$$I(z) = \frac{as \exp(zv_d/2D_L)}{4D_L^{\frac{1}{2}}} \left\{ \left[ 2D_L^{\frac{1}{2}} + \frac{v_d}{(\alpha + v_d^2/4D_L)^{\frac{1}{2}}} \right] \exp \left[ \frac{-z}{D_L^{\frac{1}{2}}} \left( \frac{v_d^2}{4D_L} + \alpha \right)^{\frac{1}{2}} \right] \right. \\ \left. - \left[ \frac{z}{(z^2/4D_L + r_0^2/4D_T)^{\frac{1}{2}}} + \frac{v_d}{(\alpha + v_d^2/4D_L)^{\frac{1}{2}}} \right] \right. \\ \left. \times \exp \left[ -2 \left( \frac{z^2}{4D_L} + \frac{r_0^2}{4D_T} \right)^{\frac{1}{2}} \left( \frac{v_d^2}{4D_L} + \alpha \right)^{\frac{1}{2}} \right] \right\} \quad (3-51)$$

This equation is compared for various values of  $D_T$  with the experimental determination of the relative intensity versus drift distance.

In order to calculate the theoretical intensity on axis, we must have values for the drift velocity, drift distance, longitudinal and transverse diffusion coefficients, and the reaction rate. The drift velocity and longitudinal diffusion coefficients can be considered known from previous measurements, as described in the previous sections of this chapter. The drift distances are fixed and well known. The transverse diffusion coefficient and reaction rate are coupled and must be determined from relative intensity data.

At low  $E/N$ ,  $D_T$  can be calculated from the Einstein equation. The data can be analyzed to give the thermal reaction frequency,  $\alpha_t$ , directly. For non-thermal  $E/N$ 's, one can calculate both  $D_T$  and  $\alpha$  by an iterative scheme. If data can be taken at the same  $E/N$  but at different pressures, one can make use of the pressure dependence of  $D_T$  and  $\alpha$ . Since  $D_T$  varies

as  $1/N$  and  $\alpha$  varies as either  $N$  or  $N^2$ , the high pressure data should be used to determine  $\alpha$ , since reactions are favored at high pressure. At low pressure,  $D_T$  should be determined, since diffusion is accentuated at low pressures.

The iterative scheme proceeds as follows. First, the thermal value of  $\alpha$  is used, if available, and from the low pressure data an initial value for  $D_T$  is determined. With this value of  $D_T$ , a better value for  $\alpha$  is calculated from the high pressure data. One then uses this improved  $\alpha$  to obtain an improved value for  $D_T$  from the low pressure data. This process is repeated until stationary values of  $\alpha$  and  $D_T$  are found. Frequently data can be obtained over a pressure range large enough to make the first iteration sufficient for reasonable accuracy.

In order to determine  $D_T$  and  $\alpha$  from the experimental data, two computer programs were written. The program for determining  $D_T$  will be described in this section. The data experimentally obtained are ionic count-rates for each of seven drift distances. Since one position must be used for normalization, six ionic intensity ratios are obtained. The program is given the value of mobility, longitudinal diffusion, and reaction rate for the particular  $E/N$  being studied.

For each of the six positions that has a non-trivial ionic intensity ratio, an iterative process is performed to determine the value of  $D_T$  that produces the proper ratio. An assumed value for  $D_T$  is used in equation (3-51) to determine the ratio for the corresponding position. If this ratio indicates that this value of  $D_T$  is too small,  $D_T$  is doubled and the ratio recalculated. If the ratio indicates the value of  $D_T$  is too

large,  $D_T$  is cut in half and the ratio recalculated. This procedure continues until the experimental ratio is bounded by ratios from values of  $D_T$  that are too large and too small. Then a linear interpolation between the values of  $D_T$  is performed until the ratio is very closely matched.

With all six ratios matched this way, and an average value of  $D_T$  calculated, a second procedure is begun. Here we try to find a value for  $D_T$  that simultaneously fits all six ratios closely. The procedure is similar to that for determining the value of  $D_L$  as described in the previous section. A value of  $D_T$  is found that produces ratios whose cubed differences indicate it is too large. A lower value is found that is too small. Linear interpolation is performed using the sum of cubed differences until these differences become quite small. This value of  $D_T$  is known as the "best fit" value.

By comparison of the six values of  $D_T$  that correspond to each of the non-reference positions, and the average and "best fit" values of  $D_T$ , one can determine the uncertainty and statistical error involved in the measurement of  $D_T$ .

As was the case for longitudinal diffusion, the transverse diffusion coefficient can be estimated from drift velocity measurements by the use of the theory of Wannier.<sup>2</sup> Again by use of the model of constant mean free time, the following expression for the transverse diffusion coefficient can be derived:

$$D_T(E) = D(0) + \frac{(M+m)M}{3(M+1.908m)} \frac{v_d^3}{dE} \quad (3-52)$$

where  $D(0)$  is the zero-field value of  $D$ ,  $m$  is the mass of the ion,  $M$  is the mass of the molecule,  $e$  is the ionic charge, and  $E$  is the electric field intensity. For ions drifting in a gas where resonant charge exchange is not a dominant interaction, this formula agrees well with existing data.<sup>32</sup>

### Reaction Rates

The determination of reaction rates involves measurements of both the shape of the arrival-time spectra as well as the change in ionic intensity with varying drift distance. The discussion of reaction rate measurement will be divided into two categories: reactions that only deplete one ion species into another, i.e., a "one-way" reaction, and those reactions that link together two species with a forward and backward reaction. Methods will be described that determine reaction rates for both of these cases.

#### Depleting Reactions

Depleting reactions can be characterized by a reaction equation of the form:



where  $C^+$  does not break up and form  $A^+$  in the drift tube.

The reaction rate can be measured by determining the rate at which the parent ionic flux decreases as the drift distance is increased. The study of this "fall-off" is basically the same as the method used to determine  $D_T$ . Both transverse diffusion and a depleting reaction reduce the ion intensity along the axis of the drift tube as long as the ions are drifting.

As described in the last section on  $D_T$  determination, the analysis involves matching the experimental count rate for a given position to the corresponding ionic intensity as calculated from the solution to the transport equation. Each of these values is normalized by dividing by the corresponding ion flux intensity at a reference position. Because both  $D_T$  and  $\alpha$  strongly determine the ionic ratios, both must be determined simultaneously. For thermal values of  $E/N$ , the value for  $D_T$  can be obtained from the Einstein equation and  $\alpha$  can be determined directly. For intermediate and high values of  $E/N$ , the iterative solution between  $D_T$  and  $\alpha$  that was described in the previous section must be used. The different pressure dependences of  $D_T$  and  $\alpha$  are used to separate the effect of each. The computer program for determining  $\alpha$  is identical to the  $D_T$  program except that the value of  $D_T$  is kept constant and the value of  $\alpha$  is varied to give the best fit to the experimental data.

A second method of determining  $\alpha$  involves the examination of the arrival-time spectra of the product ion species. This method will be called "product ion curve-fitting." Equation (3-39) gives the solution to the transport equation for the product ion species. Since, in the present case of a depleting-only reaction, we are assuming the backward reaction rate,  $\alpha_{AB}$ , is zero, this equation reduces to:

$$\begin{aligned} \Phi_B(0, z, t) = & as \int_0^t du \left[ f_B \delta(t-u) + f_A \alpha_{BA} \right] (\pi r_L^2)^{-\frac{1}{2}} \quad (3-54) \\ & \times \left\{ \frac{2D_{LB}(z-r_d)}{r_L^2} + v_{dB} \right\} \exp \left[ -\gamma - \frac{(z-r_d)^2}{r_L^2} \right] \left[ 1 - \exp \left( -\frac{r_0^2}{r_T^2} \right) \right]. \end{aligned}$$

In practice, the experimental arrival-time spectra are compared with this equation for various values of the parameters, and  $\alpha$  and  $D_T$  are adjusted until good agreement is obtained.

Two examples of typical product ion spectra calculated from Equation (3-54) can be seen in Chapter VI, Figures 15 and 16. As can be seen, each spectrum represents ions spending from almost all to almost none of their arrival-time as the product ion species. The slope of the arrival-time profile from the point where ions are spending almost all of their drift as the parent ion species to the point where the ions are spending almost all of their time as the product ion species is a sensitive measure of the reaction frequency. The slope of this "shoulder" can be analyzed to give the reaction rate for the depleting reaction.

An approximation to the slope of the product ion spectrum can be obtained by making certain assumptions. As noted in the report by Snuggs, et al.,<sup>34</sup> if the difference in drift distances,  $(v_{dA}t - v_{dB}t)$ , traveled by the two ion species in a time  $t$ , is large compared to the square root of the sum of the diffusion areas,  $(4D_{LA}t + 4D_{LB}t)^{\frac{1}{2}}$ , for the same time  $t$ , the following inequality holds:

$$(v_{dA} - v_{dB})^2 t^2 \gg r_L^2 \quad (3-55)$$

where  $r_L$  is defined in equation (3-23b). With this inequality holding, the following approximation can be made:

$$(\pi r_L^2)^{-\frac{1}{2}} \exp\left[-(z - r_d)^2 / r_L^2\right] = \frac{1}{|v_{dA} - v_{dB}|} \delta(u - u_1) \quad (3-56)$$

where

$$u_1 = \frac{v_{dA} t - z}{v_{dA} - v_{dB}} . \quad (3-57)$$

Equation (3-56) represents the physical situation where, under the assumed conditions expressed by equation (3-55), the factor representing a gaussian in  $z$  dominates the integral in  $u$  and that the value of  $u$  which maximizes this gaussian can be used to replace  $u$  wherever else it appears in the integrand.

If we also define the parameter  $\tau$  in the following way:

$$\tau = \frac{2t - (t_A + t_B)}{t_A - t_B} \quad (3-58)$$

with  $t_A = z/v_{dA}$  and  $t_B = z/v_{dB}$ , then we can make the following definitions:

$$r_{T1}^2 = 4D_{TA}(t - u_1) + 4D_{TB}u_1 = r_0^2(\varphi_+ + \varphi_- \tau) = r_0^2 \varphi_1 \quad (3-59a)$$

$$\gamma_1 = \alpha_A(t - u_1) + \alpha_B u_1 = \gamma_+ + \gamma_- \tau \quad (3-59b)$$

$$\eta_1 = [4\alpha_{AB}\alpha_{BA}u_1(t - u_1)]^{\frac{1}{2}} = [4\alpha_{AB}t_B\alpha_{BA}t_A(1 - \tau^2)]^{\frac{1}{2}}$$

where

$$\varphi_{\pm} = (4D_{TA}t_A \pm 4D_{TB}t_B)/(2r_0^2) \quad (3-60a)$$

$$\gamma_{\pm} = (\alpha_A t_A \pm \alpha_B t_B)/2. \quad (3-60b)$$

If we apply Equation (3-56) in Equation (3-39), with  $f_B$  equal to zero, we obtain:

$$\Phi_B(0, z, t) = \frac{asv_{dB} \alpha_{BA}}{|v_{dA} - v_{dB}|} \left[ 1 - \exp(-1/\varphi_1) \right] \exp(-\gamma_1) I_0(\eta_1). \quad (3-61)$$

If we take the logarithm of Equation (3-61) and then differentiate with respect to  $\tau$ , we obtain:

$$\frac{\partial \ln(\Phi_B)}{\partial \tau} = \frac{-(\varphi_-/\varphi_1^2)}{[\exp(1/\varphi_1) - 1]} - \gamma_- - \frac{\partial I_0(\eta_1)/\partial \tau}{I_0(\eta_1)}. \quad (3-62)$$

Since we are considering the case of only a depleting reaction,  $\alpha_{AB}$  is zero, and therefore  $\eta_1$  is also zero. In this case, Equation (3-62) reduces to:

$$\frac{\partial \ln(\Phi_B)}{\partial \tau} = -\gamma_- - \frac{(\varphi_-/\varphi_1^2)}{\exp(1/\varphi_1) - 1}. \quad (3-63)$$

Typically the region of the product ion profile where the slope is the easiest to measure is near the midpoint, i.e., for time near  $t_c = (t_A - t_B)/2$ . At  $t = t_c$ ,  $\tau$  equals zero and Equation (3-36) reduces to:

$$\left. \frac{\partial \ln(\Phi_B)}{\partial \tau} \right|_{\tau=0} = -\gamma_- - \frac{(\varphi_-/\varphi_+^2)}{\exp(1/\varphi_+) - 1}. \quad (3-64)$$

One should note that, if  $D_{TA}/v_{dA} = D_{TB}/v_{dB}$ , then  $\varphi_-$  is equal to zero and Equations (3-63) and (3-64) are simplified. At low  $E/N$  where the Einstein equation holds, this condition is met and the reaction rate determination is considerably simplified.

Equation (3-63) can be used as an approximation to the slope of the product ion spectra. The slope depends on the transverse diffusion



coefficient of both the parent and product ion species, as well as the forward reaction rate. Because of the form of  $\varphi_{-}$ , the two transverse diffusion coefficients vary the slope in opposite ways. An increase in  $D_T$  of the parent ion causes the parent ion intensity on the axis to undergo more attenuation, and the product ion spectrum will have a slope that is larger in magnitude. An increase in  $D_T$  of the product ion causes the product ion intensity on axis to undergo more attenuation, which causes the product ion spectrum to have a slope that is smaller in magnitude. In the case where the product ion  $D_T$  is quite large, its effect can become greater than that of both the depleting reaction rate and the parent ion  $D_T$ , and can cause the slope of the product ion spectrum to be opposite to that expected. The influence of one ionic species' transverse diffusion cannot be separated from the influence of the other species' transverse diffusion because both have the same dependence on pressure. However, the influence of the reaction rate on the product ion spectrum can be determined, since it varies with pressure in the opposite direction than does diffusion.

The separation procedure is iterative in nature, as all separations between  $D_T$  and  $\alpha$  are. One takes product ion spectra for two values of pressure that are as widely apart as possible. The values of  $E/N$  and  $z$  are kept fixed. For the low value of pressure, where the spectrum shape is "diffusion dominated," one estimates the value of  $\alpha$  and fits the analytical curve or numerical estimate of the slope by varying either or both

of the  $D_T$ 's. At high pressure, the product ion spectrum is "reaction dominated" and with these newly calculated values of transverse diffusion being used, the value of  $\alpha$  is varied until the value of the slope matches that of the experimental data. This value of  $\alpha$  is used at the low pressures to improve the values of  $D_T$  and the process is repeated until satisfactory agreement is obtained over the entire range of pressure. Normally, Equation (3-63) is used only to give initial estimates of the values of  $D_T$  and  $\alpha$ , and the analytical expression for the product ion flux, Equation (3-54), is compared to the experimental profiles to make final, accurate determinations of the reaction rate.

#### Forward-Backward Reactions

In the study of forward-backward reactions, the shape of both the parent and product ion arrival-time spectra can be used to determine the reaction rates. The study is more complicated than the study of depleting reactions for the obvious reason that there is one more variable that must be determined.

The analytical solutions for the transport equation with both forward and backward reactions are

$$\begin{aligned} \Phi_A(0, z, t) = & as \int_0^t du \left[ f_A \{ \delta(u) + \alpha_{AB} \alpha_{BA} (t-u) 2I_1(\eta)/\eta \} + f_B \alpha_{AB} I_0(\eta) \right] (3-38) \\ & \times \left[ v_{dA} + \left\{ \frac{2D_{LA}(z-r_d)}{r_L^2} \right\} \right] \exp \left[ -\gamma - (z-r_d)^2/r_L^2 \right] \\ & \times \left[ 1 - \exp \left( \frac{-r_0^2}{r_T^2} \right) \right] (\pi r_L^2)^{-\frac{1}{2}} \end{aligned}$$

and

$$\begin{aligned}
\Phi_B(0, z, t) = & \text{as} \int_0^t du \left[ f_B \{ \delta(t-u) + \alpha_{AB} \alpha_{BA}^u 2I_1(\eta) / \eta \} + f_A \alpha_{BA} I_0(\eta) \right] \quad (3-39) \\
& \times \left[ v_{dB} + \left\{ \frac{2D_{LB}(z-r_d)}{r_L^2} \right\} \right] \exp \left[ -\gamma - (z-r_d)^2 / r_L^2 \right] \\
& \times \left[ 1 - \exp \left\{ -\frac{r_0^2}{r_T^2} \right\} \right] (\pi r_L^2)^{-\frac{1}{2}}.
\end{aligned}$$

The ultimate test for the two reaction rates is to use the assumed reaction frequencies, along with the drift velocities, diffusion coefficients, and source fractions, in these two transport equations and verify that the experimental arrival-time spectra are closely matched. In practice, this method is impractical because of the many variables that must be determined. Two approximate techniques for arriving at values for the two reaction rates will be presented here, the first involving the use of the product ion arrival-time profile and the second involving the use of the parent ion arrival-time profile.

As in the last section, we can construct an approximate solution for the slope of the logarithm of the product ion spectrum versus time. The basic assumption requires that the difference in drift distances at a given time be large compared with the square root of the sum of the diffusion areas at that time. If this is true we arrive at equation (3-62):

$$\frac{\partial \ln(\Phi_B)}{\partial \tau} = \frac{-(\varphi_- / \varphi_1^2)}{\exp(1/\varphi_1) - 1} - \gamma_- - \frac{\partial I_0(\eta_1) / \partial \tau}{I_0(\eta_1)}. \quad (3-62)$$

If we consider the slope at the midpoint of the spectrum, that is at  $t = t_c = (t_A - t_B) / 2$ , then the derivative of  $I_0(\eta_1)$  will become zero and Equa-

tion (3-62) becomes:

$$\left. \frac{\partial \ln(\Phi_B)}{\partial \tau} \right|_{\tau=0} = -\gamma_- - \frac{(\varphi_-/\varphi_+^2)}{\exp(1/\varphi_+) - 1} \cdot \quad (3-65)$$

In this equation there are three sets of parameters that must be determined from the product ion spectra;  $\alpha_{AB}$  (which is assumed equal to  $\alpha_B$ ),  $\alpha_{BA}$  (which is assumed equal to  $\alpha_A$ ), and the pair of transverse diffusion coefficients,  $D_{TA}$  and  $D_{TB}$ . If  $\alpha_{AB}$  and  $\alpha_{BA}$  have different dependence on  $N$ , as is frequently the case with the forward (formation) reactions being three-body reactions and the backward (breakup) reactions being two-body reactions, it may be possible to separate out the dependence of  $\alpha_{AB}$ ,  $\alpha_{BA}$ , and the  $D_T$ 's.

Determination of forward and backward reaction rates can also be obtained by looking at the parent ion arrival-time spectrum. If the drift velocities of the parent and product ions are sufficiently different, the ions that spend part of their drift time as the product species will be displaced in time from those ions that spend all their drift as the parent species. If the product ion drifts faster, these parent ions will add a "foot" to the parent ion spectrum, whereas if the product ion drifts slower, they will add a "tail" to the spectrum.

In the report by Snuggs, et al.,<sup>34</sup> an analysis is presented that uses the ion density of reaction-influenced parent ions as a measure of reaction rates. If we apply the approximation expressed in Equation (3-56) to Equation (3-38), with  $f_B$  set equal to zero, we obtain:

$$\begin{aligned}
\Phi_A(0, z, t) &= \frac{as v_{dA}}{(\pi r_{LO}^2)^{\frac{1}{2}}} \left[ 1 - \exp\left(-\frac{r_0^2}{r_T^2}\right) \right] \exp\left[-\gamma_0 - (z - r_{d0})^2 / r_{LO}^2\right] \quad (3-66) \\
&+ \frac{as v_{dA}}{|v_{dA} - v_{dB}|} \left[ 1 - \exp(-1/\varphi_1) \right] \exp(-\gamma_1) t_A^{\alpha_{BA}} \alpha_{AB}^{(1-\tau)} \\
&\times \frac{I_1(\eta_1)}{\eta_1}
\end{aligned}$$

where

$$r_{TO}^2 = 4D_{TA}t \quad (3-67a)$$

$$r_{LO}^2 = 4D_{LA}t \quad (3-67b)$$

$$r_{d0} = v_{dA}t \quad (3-67c)$$

$$\gamma_0 = \alpha_A t \quad (3-67d)$$

Equation (3-66) has two principal terms, the first term representing the source-produced ions that have never reacted to form species B. This term will be denoted by  $\Phi_{AS}$ . The second term represents the ions that are detected as species A but have spent varying portions of their drift as species B due to the coupling reaction. The second term will be represented by  $\Phi_{AR}$ . In order to obtain an approximation to the total number of ions detected as  $\Phi_{AS}$ , we assume that

$$\frac{v_{dA}}{(\pi r_{LO}^2)^{\frac{1}{2}}} \exp\left[-(z - r_{d0})^2 / r_{LO}^2\right] = \delta(t - t_A) \quad (3-68)$$

Then the total number of ions detected as  $\Phi_{AS}$ , denoted by I, is given by:

$$\begin{aligned} I &= \text{as } [1 - \exp(-r_0^2/4D_{TA}t_A)] \exp(-\alpha_A t_A) & (3-69) \\ &= \text{as } [1 - \exp(-1/\{\varphi_+ + \varphi_-\})] \exp(-\{\gamma_+ + \gamma_-\}). \end{aligned}$$

Equation (3-69) is only an approximate measure of the ion current because of assumption (3-68). However, for typical values of  $v_d$ ,  $D_L$ ,  $D_T$ , and  $r_0$ , Equation (3-69) differs from equation (3-51) by less than one part in 1000.<sup>34</sup> Experimentally, the spectrum for  $\Phi_A$  will have a large peak and the area under this peak will be taken as an approximate experimental measure of I.

If I is inserted into the equation for  $\Phi_{AR}$  in order to eliminate the unknown source density s, one obtains:

$$\Phi_{AR} = \frac{I z \alpha_{AB} \alpha_{BA} (1+\tau)}{|v_{dA} - v_{dB}|} \frac{I_1(\eta_1)}{\eta_1} \frac{1 - \exp(-1/\varphi_1)}{1 - \exp(-1/\{\varphi_+ + \varphi_-\})} \frac{\exp(-\gamma_1)}{\exp(-\{\gamma_+ + \gamma_-\})}. \quad (3-70)$$

We assume that, because  $\alpha_{BA} \alpha_{AB}$  is small,  $\eta_1$  is much less than one and that  $I_1(\eta_1)/\eta_1$  is nearly its limit of 1/2. If one defines the third factor in Equation (3-70) as F and expands F in a Taylor series with respect to  $\tau$  about the point  $\tau = 1$ , one obtains:

$$F(\tau) \approx F(1) + (\tau-1) \partial F(1)/\partial \tau \quad (3-71)$$

$$\approx 1 + (1-\tau) \frac{\varphi_- / \{\varphi_+ + \varphi_-\}^2}{\exp(1/\{\varphi_+ + \varphi_-\}) - 1}.$$

Assuming that  $\varphi_-$  is small compared with  $\varphi_+$ , which is valid in most instances since it involves a difference of two similar terms compared to the sum of two terms, we can reduce Equation (3-71) to:

$$F(\tau) \approx \exp\left[\frac{(1-\tau)(\varphi_-/\varphi_+^2)}{\exp(1/\varphi_+)-1}\right] \quad (3-72)$$

The analysis of the fourth factor in Equation (3-70) is straightforward:

$$\frac{\exp(-\gamma_1)}{\exp(-\{\gamma_+ + \gamma_-\})} = \exp(-\gamma_+ - \gamma_- \tau + \gamma_+ + \gamma_-) = \exp(\gamma_- \{1 - \tau\}). \quad (3-73)$$

Combining Equations (3-70), (3-72), and (3-73) one obtains:

$$\bar{\Phi}_{AR} = \frac{I z \alpha_{AB} \alpha_{BA} (1+\tau)}{2 |v_{dA} - v_{dB}|} \exp\left[(1-\tau) \left\{ \frac{\varphi_-/\varphi_+^2}{\exp(1/\varphi_+)-1} \right\}\right] \exp[(1-\tau)\gamma_-]. \quad (3-74)$$

By rewriting Equation (3-74) and taking the logarithm, we get:

$$\ln \frac{\bar{\Phi}_{AR}}{(1+\tau)} = \ln \left[ \frac{I z \alpha_{AB} \alpha_{BA}}{2 |v_{dA} - v_{dB}|} \right] + (1-\tau) \left[ \gamma_- + \frac{\varphi_-/\varphi_+^2}{\exp(1/\varphi_+)-1} \right]. \quad (3-75)$$

Since the coefficient of the second term of Equation (3-75) can be measured by using the product ion spectrum via Equation (3-65), it is possible to measure the product of the forward and backward reaction frequencies from Equation (3-73). Determination of  $\gamma_-$  gives basically the difference in reaction frequencies, but if one frequency is small compared with the other, and this is frequently the case,  $\gamma_-$  may not determine the small reaction frequency accurately. From equation (3-75), this small  $\alpha$  may be determined accurately.

## CHAPTER IV

## MOBILITIES

Production of Ions

In this section the production of ions will be considered. The ions produced directly by electron impact or thermionic emission are true primary ions. In addition, under some conditions of this experiment, ions formed by secondary processes are produced almost solely in the ion source. These ions will be designated source-produced to distinguish them from the primary ions. However, for the considerations of this research there is no significant difference between source-produced and true primary ions.

Until a few years ago, little importance was attached to the mode of formation of the ions. It was considered sufficient merely to mass analyze the ions of beam and swarm experiments to describe the collision properties of the ions. The inadequacy of this procedure has been demonstrated in a number of beam and swarm experiments wherein the collisional properties of ions of a given chemical type are observed to depend on the nature and mode of operation of the ion source. In the case of an electron bombardment ion source, many beam and swarm experiments<sup>35,36</sup> have indicated that the rates of the reactions being investigated are extremely sensitive to the energy of the ionizing electrons. Therefore, the full description of a collision requires not only that the identity of the participants be known, but also their state of excitation be determined.



Unfortunately, the present experiment cannot determine the ionic excitation state, and the possibility of various states of excitation of the ions will have to be considered.

### CO<sup>+</sup>

The initial formation of CO<sup>+</sup> is by simple ionization:



The ionization potential<sup>37</sup> of CO is 14.0 eV and to the accuracy of our knowledge of our acceleration potential, this is where production of CO<sup>+</sup> begins in our ion source. The principal inaccuracy in our accelerating potential calculation is the drop in potential of about three volts across the resistance-heated cathode.

### C<sup>+</sup>

The formation of C<sup>+</sup> is believed to come from either of two processes, dissociative ionization:



or ion pair formation:



The appearance potential of the dissociative ionization process has been measured by several observers<sup>38-44</sup> to be about 22.7 eV whereas the ion pair formation was measured to be about 20.9 eV.<sup>40-44</sup>

### O<sup>+</sup>

The formation of O<sup>+</sup> is also believed to come from two processes,

either dissociative ionization:



or by ion pair formation:



In the case of  $\text{O}^+$ , the dissociative ionization appears at about 24.8 eV<sup>38,44</sup> whereas the ion pair formation appears at about 23.6 eV.<sup>43,44</sup>

In the ionization of CO, the processes that form  $\text{C}^+$  occur more frequently than do those that form  $\text{O}^+$ . This fact can be easily understood when one notes that the ionization potential of C is 11.3 eV<sup>45</sup> whereas the ionization potential of O is 13.6 eV.<sup>45</sup> Since the oxygen atom binds its outer electrons more strongly, one would expect that  $\text{C}^+$  would be formed from CO more often than would  $\text{O}^+$ . The  $\text{O}^+$  ion was not produced in sufficient quantity to allow measurements to be made on its transport properties.

#### $\text{CO}^+ \cdot \text{CO}$

The formation of  $\text{CO}^+ \cdot \text{CO}$  is due to the three-body attachment process:



The evidence that this reaction proceeds by a three-body reaction will be presented in Chapter VI, where the pressure dependence of the reaction frequency is shown to be  $N^2$ . The production of the dimer ion,  $\text{CO}^+ \cdot \text{CO}$ , decreased to vanishingly small rates when the pressure was reduced and the electric field strength increased. From this observation, substantial production of the dimer ion by direct processes with our ion source was

not indicated. Munson, et al.<sup>46</sup> reported the chemi-ionization reaction:



The appearance potential of this reaction was determined to be  $12.8 \pm 0.3$  eV. It is believed that while this reaction may have occurred in this experiment, it did not significantly contribute to the  $\text{CO}^+ \cdot \text{CO}$  ion flux.

If the pressure of the gas is made quite large and the E/N kept reasonably low, the clustering reaction, Equation (4-6), can be driven quite close to completion within the source. For these cases the dimer ion can be considered source produced. At higher values of E/N, data were taken at pressures where the dimer production went to completion outside the source, but early in the drift. In this case, the dimer ions cannot be considered completely source produced. Checks were made to insure that there was only an insignificant amount of the parent ion,  $\text{CO}^+$ , left at the shortest arrival time used in mobility studies.

### K<sup>+</sup>

Potassium ions were generated by thermionic emission from a platinum gauze covered with Kingsman Felspar. These ions are singly charged and in their electronic ground state.

### Other Trace Ions

At high pressures, greater than 0.5 Torr, and at very low E/N, several ions in trace quantities were seen.  $\text{C}_3\text{O}_2^+$ ,  $\text{C}_2\text{O}_3^+$ ,  $\text{C}_3\text{O}_3^+$  and occasionally higher masses were observed. All of these ions are presumed to be produced by multiple reaction processes, while the ions drift down the drift tube. None of these heavier ions were present in sufficient abundance to enable us to accomplish any kind of study of their transport

properties.

### Impurity Ions

As has been the case with the last two gases studied on the present apparatus, impurity ions were present under certain conditions, and great efforts had to be made to eliminate their effect in any of the studies we attempted. With CO, the principal impurities were located in the mass range of 41 to 47. The Refrigerated Vapor Bath eliminated these impurities when it was clean and had been in operation for several days. The effect of these impurities on any data that were used was negligible.

### Method of Data Analysis

Drift velocities were obtained from the experimental arrival-time spectra by using the mean arrival time  $\bar{t}$  of the spectra and the known drift distance  $z$ . In order to eliminate end effects and the first order diffusion correction to the drift velocity, a differencing technique was used and the drift velocity was calculated from:

$$v_d = \frac{z_i - z_j}{\bar{t}_i - \bar{t}_j} \quad (4-8)$$

where  $z_i$  and  $\bar{t}_i$  are, respectively, the drift distance and the observed mean arrival time for the  $i^{\text{th}}$  position of the moveable ion source. When more than two drift distances were used, a straight line of best fit (in the least squares sense) was constructed through the  $(z_i, \bar{t}_i)$  points and the slope of this line was used to determine  $v_d$ . The mobility  $K$  was calculated using the relation:

$$K = \frac{v_d}{E} . \quad (1-1)$$

This mobility was reduced to standard conditions of temperature and pressure by using Equation (1-2) and the data are presented as the reduced mobility versus  $E/N$ . From these data, a zero-field mobility is determined whenever possible.

This procedure has been justified analytically in Chapter III under the assumption of (1) a delta-function input pulse of ions, and (2) no reactions occurring in the drift region which lead to the creation of the ion species under consideration. The first of these assumptions is closely approximated in this experiment since the Tyndall shutter is left open for only a time of the order of one microsecond while the total drift time of the ions is of the order of several hundred microseconds. The second assumption can be fulfilled to a good approximation for most of the ions detected in CO.  $C^+$  and  $K^+$  are true primary ions and no reaction scheme was detected that produces these ions in the drift tube.  $CO^+$  and  $CO^+ \cdot CO$  are involved in a forward-backward reaction. By operating at high pressure and low electric field strength the reaction converting  $CO^+$  into the dimer could be driven to completion within the ion source or at least very early in the drift. Although the production of dimer ions within the drift tube violates assumption (2) of the analysis, it is clear that if no ions are produced after the ion swarm reaches the shortest drift distance used in the differencing scheme, the difference in average drift times will still represent the time taken by dimer ions to drift the distance involved.<sup>47</sup>

If gas pressures are kept low, and the drift time is kept reasonably

short, very little conversion of  $\text{CO}^+$  to the dimer will take place. The reaction rate converting the dimer back into  $\text{CO}^+$  is quite small, and by keeping the number of dimer ions low, a negligible number of  $\text{CO}^+$  ions are created in the drift tube.

### Experimental Procedures

#### Preparation of the System

In order to achieve low base pressure and thus minimize impurities in the drift region, the system is baked at an average temperature of about  $300^\circ\text{C}$  for 24 to 36 hours. Cooling requires several days because many of the rather massive internal components must cool mainly by radiation. The base pressure at the end of such a bake cycle is about  $2 \times 10^{-9}$  Torr as read by Bayard-Alpert ionization gauges located at the top of the drift tube, at the bottom of the outer vacuum chamber, and in the analysis region. The pressure in the drift tube with the isolation valve closed (see Figure 1) does not rise above  $7 \times 10^{-8}$  Torr.

The gas feedline and the Refrigerated Vapor Bath (RVB) cold trap are baked out at the same time as the main system. In contrast to the main system, however, the feedline and RVB must be periodically rebaked to remove impurities that collect in the RVB. To keep the clean drift chamber free from these impurities, the gas servo valve is kept closed, and the gas feed system is pumped externally. The feedline and RVB bake-out achieves approximately  $300^\circ\text{C}$  temperatures and lasts about 24 hours. Unlike the main system, there are no internal components to cool and the system returns to room temperature in about six hours.

Once the system and feedline have cooled to room temperature, carbon

monoxide is admitted to the feedline. Because gas regulators tend to introduce impurities into the gas, no regulators are used at the present time. Gas at tank pressure is introduced into a small volume closed off by a Granville-Phillips leak valve. The tank valve is closed, and this small volume of gas at high pressure is leaked into a larger volume containing the RVB. The pressure is thereby reduced sufficiently for proper operation of the gas servo valve. Because many of the gas impurities condense out rather slowly in the RVB, normally the trap is allowed to "pump" on the impurities for about 24 hours before the gas is introduced into the drift chamber.

With the isolation valve closed, the drift tube is pressurized with the sample gas by manually opening the servo-controlled valve until the desired pressure is reached. Control of the servo-valve is then transferred to the capacitance manometer-automatic pressure controller system, which maintains the desired pressure. The heating current to the electron filament or the alkali filament, which are kept on continuously at a low current value, is turned up and the temperature of the filament is allowed to stabilize. The desired electric field is established by applying a corresponding potential to the external resistor string which supplies the drift field electrode potentials.

#### Ion Source Parameters

The ion source may be operated in several different modes. If the Tyndall shutter located on the front plate of the ion source (refer to Figure 3) is left open and the electron beam is allowed to cross the ionization gap continuously, a dc mode of operation is obtained. This

mode of operation was used to give maximum ionic flux when determining what ion masses were present, i.e. when obtaining a mass scan. Another mode is to operate the electron beam dc but pulse the Tyndall shutter. This mode of operation is not used frequently in practice because the Tyndall shutter, while quite efficient, does let through a small fraction of the ions incident on it even when it is closed. Thus a small constant background of ions is observed in this mode. A third mode of operation is to pulse the electron beam and, at some later time, pulse the Tyndall shutter. Operation in this manner allows the best control over the ion swarm entering the drift tube. In addition, this mode of operation permits the technique of holding the swarm in the source for a short time to allow a reaction to go to completion before gating the swarm into the drift tube. Still another mode of operation is to pulse the electron beam but leave the Tyndall shutter open at all times. Since for a given number of ions created in the source, fewer ions will enter the drift region when the Tyndall shutter is pulsed than when it is simply left open, it is occasionally desirable to operate in this manner. This is particularly true during operation at low E/N, when very few ions reach the detector.

The typical mode of operation is to pulse both the electron beam control grid and the Tyndall shutter. The electron beam pulse width is typically 4.0 microseconds. The Tyndall shutter pulse width is typically 2.0 microseconds. The timing of the Tyndall shutter is adjusted so that, for a given pulse width, a maximum number of ions of the species under consideration exits the source. The interval of time between the pulsing of the electron beam and the pulsing of the Tyndall shutter will correspond



to the 1.5 centimeter distance between the center of the electron beam and the entrance aperture plate divided by the drift velocity of the ions. The timing of the Tyndall shutter pulse can be adjusted within reasonably wide limits ( $\pm 50$  percent) about this optimum time while allowing a usable number of ions to exit the source. The timing of the Tyndall shutter pulse can be adjusted to discriminate against one ion species in favor of another if their drift velocities are quite different.

The three grids in the alkali-source are shown in Figure 3. The first grid, called the "extraction" or "drawout" grid, draws the ions away from the filament and is normally adjusted to be 15 to 30 volts negative with respect to the filament. The second grid, referred to as the "pulse" grid, is biased positive with respect to the extraction grid and is adjusted to barely keep the alkali ions from passing through the grid, that is, to "bias off" the ion current. The application of a negative pulse of about one microsecond in duration to the pulse grid allows a short burst of alkali ions to pass through it and the third grid. The third grid is maintained at the potential of the repeller plate and through it the alkali ions enter the main part of the ion source. In the space between the repeller plate and the entrance aperture plate the ions thermalize and are then gated into the drift region by the Tyndall shutter.

#### Analysis Region Parameters

Once it has been ascertained that the application of a small attractive potential to the skimmer does not result in any dissociation in the differential pumping region for any of the ions under consideration, a potential of 3 or 4 volts is usually applied. This potential increases

the ion intensity at the detector by more than a factor of 10. The potentials of the two focusing tubes between the skimmer and the quadrupole are adjusted for maximum detected intensity. Typically they were set at about 60 volts. These potentials were checked to insure that no dissociation occurred in this portion of the analysis region. The ions were then decelerated to about 10 eV before entering the quadrupole in order to obtain good resolution in the spectrometer.

The quadrupole mass spectrometer was set on the  $e/m$  value corresponding to the ion species desired and usually remained on this setting several hours while other parameters were varied.

The high voltage to the channeltron was set to approximately three kilovolts and the input attenuator of the TMC time-of-flight analyzer was adjusted to permit counting of most of the ion signal pulses while excluding noise pulses. This was generally quite easy to do, due to the large signal pulses obtained from the channeltron. Normally the noise level amounted to less than three or four counts per channel during the accumulation of a spectrum with several thousand counts in its peak channel.

#### Data Accumulation Procedures

After the preceding adjustments had been made, data accumulation could begin. The normal operating procedure was to remain at a fixed pressure and investigate the  $E/N$  variation of  $v_d$  and  $D_L$  for a particular ion species by varying the electric field.

With the addition of the Preset Counter, several new steps in the data accumulation procedures were introduced. The Preset Counter allows

a variable delay (in one microsecond increments) between the electron beam gate pulse and the Tyndall shutter pulse, between the Tyndall shutter pulse and the triggering of the multi-channel analyzer, and between one set of pulses and the next set. The Preset Counter has four presettable controls: the time increment (usually set to one microsecond), the reset value, the lower limit set point, and the upper limit set point. It also has four control lines: one triggered by the displayed scaler overflowing, one triggered by the instantaneous count being less than the lower limit (the LO line), one triggered by the count being greater than or equal to the lower limit and less than the upper limit (the IN line), and one triggered by the count being greater than or equal to the upper limit (the HI line).

The settings on the reset, lower limit, and upper limit controls were determined as follows: the reset control was set to the number of microseconds comprising the delay between the electron beam pulse and the Tyndall shutter pulse subtracted from the scaler overflow value of 100 000. The lower limit set point was set to the number of microseconds comprising the delay between the opening of the Tyndall shutter and the triggering of the multichannel analyzer. The upper limit set point was set to the number of microseconds that are to elapse between the Tyndall shutter opening and the resetting of the counter.

The sequence of operations goes as follows: (1) when the counter resets, the LO control line drops to zero volts, triggering the electron beam gate pulser to open the electron beam control grid, (2) the counter counts up in one microsecond units until it overflows, dropping the over-

flow control line to zero volts and triggering the Tyndall shutter pulser to open the Tyndall shutter, (3) the counter counts in one microsecond units up to the low set point, where the IO control line resets to five volts and triggers the multichannel analyzer to start analyzing the incoming ion pulses, and (4) the counter counts up to the high set point, where the counter resets to the reset value.

One of the most valuable features of the use of the Preset Counter is the ability to multipulse, that is, to put into the drift tube several ion swarms at one time. If the delay between the time the ions are admitted to the drift tube and the time that the multi-channel analyzer is triggered is greater than the time the analyzer takes to count through all 256 channels, then at least one additional ion swarm can be admitted to the drift tube. By accurately spacing the two ion swarms apart in time, the wait that normally occurs while the second ion swarm is drifting toward the exit aperture of the drift tube can be used to analyze the drift times of the first ion swarm. In actual practice, up to seven ion swarms have been placed into the drift tube at one time.

The apparatus is initially set up as if only one swarm was going to be admitted to the drift tube at one time. The proper delay is determined so that the analyzer is triggered at the proper time to place the peak of the arrival-time spectrum in the center of the analyzer channels and the proper channel width is determined so that all ion arrivals are recorded in some channel. The delay and the channel width are recorded for use in the computer analysis program. The desired counter cycle time is determined by slightly overestimating the time it takes the multichannel

analyzer to count through all 256 channels. The delay between the electron beam gate pulse and the Tyndall shutter pulse is subtracted from the counter cycle time to determine the high set point value. The delay is reduced by increments of the cycle time until it falls between the values of the upper set point and the reset control. The multipulsing technique is especially beneficial at low E/N and high pressure, because at low E/N the ions will drift slowly and at high pressure diffusion will not spread the ion swarm very much in time.

During the counting periods for each of the chosen ion source positions, the temperatures at three points in the drift tube were measured by chromel-alumel thermocouples attached to the drift tube guard rings. Pertinent information about the run, such as the pressure, electric field, drift distances, ion source parameters, time analyzer parameters and the temperatures were recorded for later transfer to punched cards for the computer. Other observations, often qualitative, were recorded on a comment sheet. When the counting period ended, the spectrum was punched onto paper tape which could be read by the computer. The process of obtaining data from three or four positions to yield one mobility value at a particular value of E/N and pressure required from a minimum of 20 minutes up to about two hours, depending on the ion intensity at the field and pressures used.

After a period of data accumulation, the punched paper tape and the punched cards containing the run information were read into the computer and the data analyzed. The computer program which determines the mobility is similar to the one discussed in detail by Albritton, et al.<sup>48</sup>

The present program is written in Fortran V to run on the Univac 1108 computer. All of the mobility and drift velocity data and the information associated with the experimental data run are stored permanently on magnetic tape and printed out as computer output.

### Experimental Results

The experimental mobility results will be presented in this section. These results, along with other pertinent information, are given in tabular form in Appendix I.

#### CO<sup>+</sup>

Figure 7 presents the mobility data for CO<sup>+</sup> ions in carbon monoxide in graphical form. The symbols are coded according to the pressure at which the data were taken. Note that the data were taken at low pressure, from 0.026 to 0.106 Torr. Low pressures were used to reduce the frequency of the conversion of CO<sup>+</sup> into CO<sup>+</sup>·CO. Although the presence of a moderate degree of depletion reaction will not affect the determination of the mobility, if the reaction becomes too strong the correction term, Equation (3-46) of Chapter III:

$$v_d \approx v_d' \left[ 1 - \frac{2\alpha D_L}{v_d} \right] \quad (3-46)$$

will become appreciable. For the worst case, the data point at an E/N of 13.4 Td, the correction amounts to approximately 1.6 percent. As the drift velocity increases with increasing E/N the correction quickly becomes negligible. The reaction rate was estimated to be constant at  $1.1 \times 10^{-28} \text{ cm}^6/\text{sec}$  for the determination of this correction. All of the

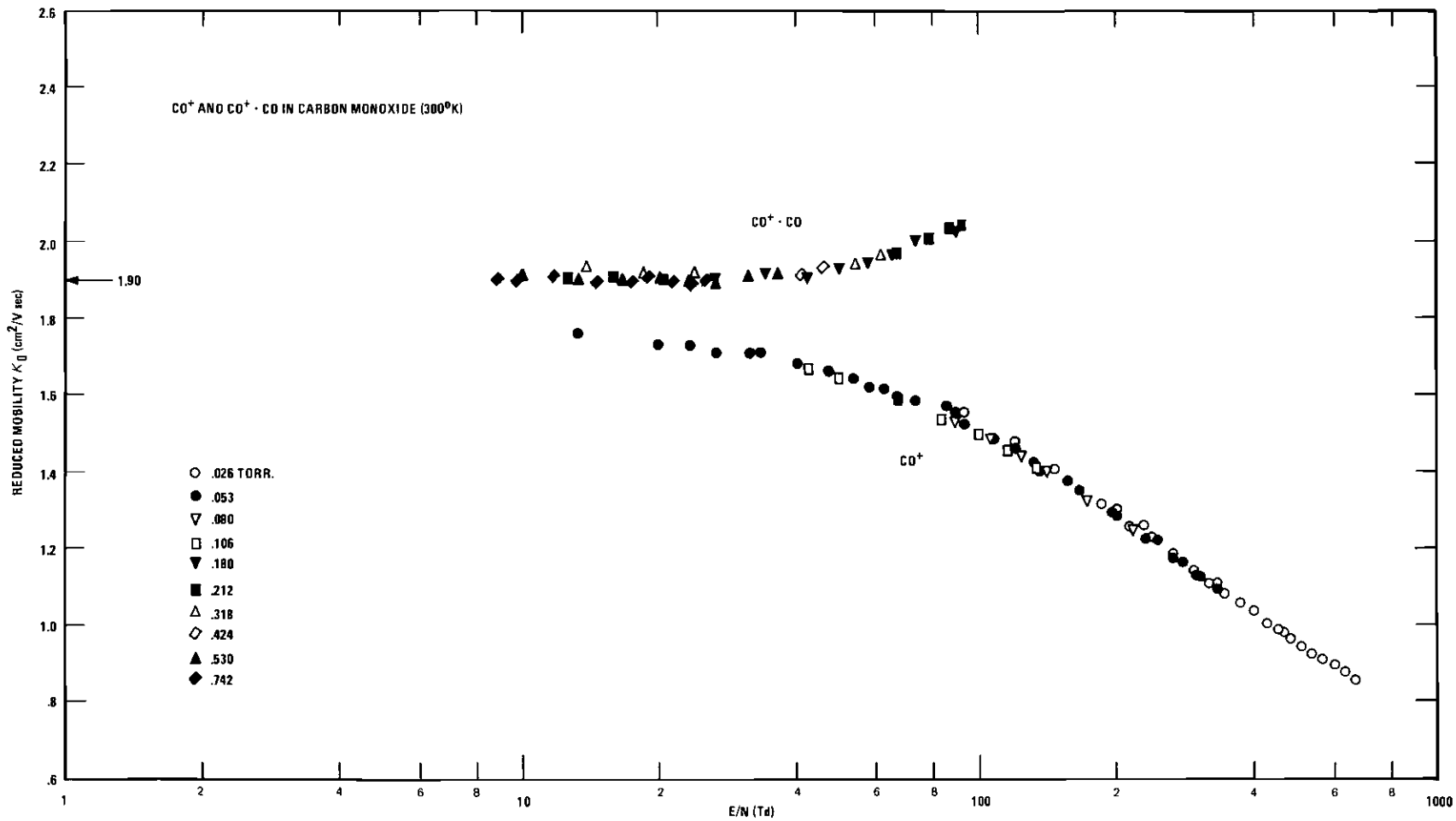


Figure 7. Mobility Results for CO<sup>+</sup> and CO<sup>+</sup>·CO in Carbon Monoxide

$\text{CO}^+$  data reported both in Figure 7 and in Appendix I have been corrected for the effects of the depletion reaction. In order to maintain a sufficient count rate of  $\text{CO}^+$  ions, only the three shortest drift distances were used when obtaining the low E/N data.

Even with the pressure held to 0.053 Torr, the increase in the reaction correction to the drift velocity calculation with decreasing E/N prevented data from being taken for values of E/N under 13 Td. The pressure could not be further decreased because at this value of E/N the electric field strength would have become so small that space charge and contact potentials could interfere with the measurement.<sup>49</sup> Because the E/N range covered is so restricted at low E/N, no zero-field mobility was determined. The mobility curve does flatten somewhat as it nears an E/N of 20 Td, and since all data taken in this and previous mobility measurements show little change in mobility below an E/N of 20 Td, an estimate of the zero-field mobility would be  $1.8 \text{ cm}^2/\text{V-sec}$ . From a value of  $1.76 \text{ cm}^2/\text{V-sec}$  at an E/N of 13.4 Td, the reduced mobility falls with increasing E/N. At the highest E/N measured, 667 Td, the mobility had decreased to a value of  $0.86 \text{ cm}^2/\text{V-sec}$ .

#### $\text{CO}^+\cdot\text{CO}$

Figure 7 also includes the reduced mobility data for  $\text{CO}^+\cdot\text{CO}$  ions in carbon monoxide. The  $\text{CO}^+\cdot\text{CO}$  data were taken at relatively high pressure, from 0.180 to 0.742 Torr. High pressures were used to force the reaction converting  $\text{CO}^+$  into the dimer toward completion. Keeping the



pressure above 0.175 Torr, the highest E/N we could obtain was about 92 Td. In order to reach higher values of E/N without decreasing the pressure, we would have had to pass the safety limit set on the voltage applied across the guard rings.

Because of the use of higher pressures for the  $\text{CO}^+\cdot\text{CO}$  mobility measurements, the reduced mobility was measured at values of E/N down to 8.9 Td. Below an E/N of 25 Td, the reduced mobility becomes constant, enabling an evaluation of the zero-field mobility. The zero-field mobility has a value of  $1.90 \text{ cm}^2/\text{V}\cdot\text{sec}$ . From the zero-field value, the mobility increases slightly as the E/N is increased. At the highest E/N of 92.1 Td, the reduced mobility had increased to  $2.04 \text{ cm}^2/\text{V}\cdot\text{sec}$ . At pressures below 0.180 Torr, we could not insure that the reaction had gone to completion even for the longest drift distance used.

In the work done to determine the ion-molecule reaction rate between  $\text{CO}^+$  and  $\text{CO}^+\cdot\text{CO}$ , rough estimates of the mobility of the dimer ion were made for values of E/N up to 150 Td. These estimates were made by examining the width of the arrival-time spectra which were strongly influenced by reactions. These data are reported in Chapter VI.

### $\text{C}^+$

Figure 8 displays the mobility results for the drift of  $\text{C}^+$  in carbon monoxide. The mobility values were obtained over an E/N range from 14 to 745 Td. The  $\text{C}^+$  mobility data could not be obtained with the same degree of accuracy achieved with the other ions. The production of  $\text{C}^+$  in the source was several orders of magnitude smaller than that of  $\text{CO}^+$ . In order to obtain a sufficiently large count rate to achieve adequate statistics, the space charge effects due to the overwhelming abundance of  $\text{CO}^+$  would

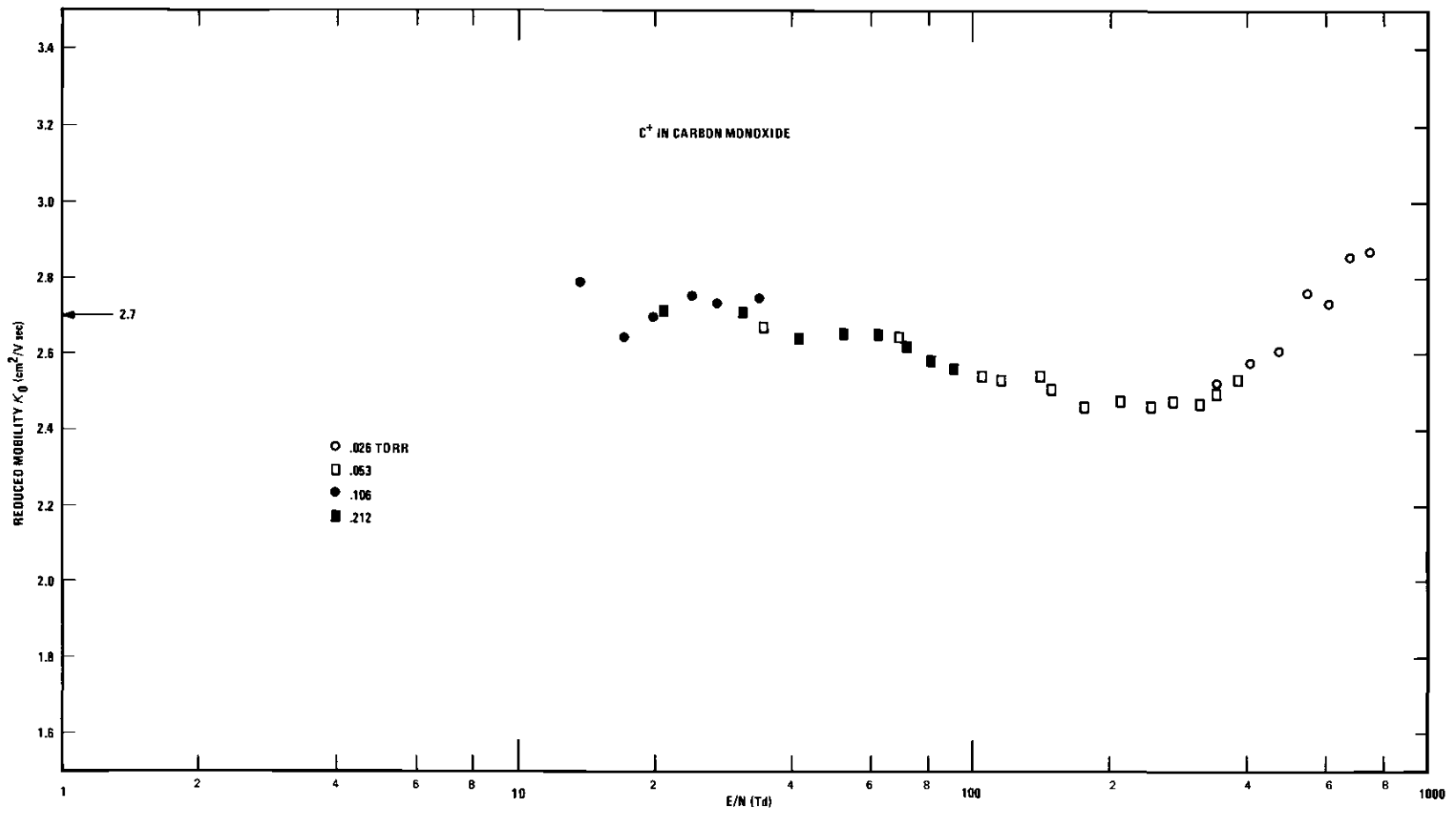


Figure 8. Mobility Results for  $\text{C}^+$  in Carbon Monoxide

have become evident. There was evidence in the work of Albritton, et al.<sup>50</sup> that the mobility of a minority ion species could be affected by the space charge produced by the dominant ion species. To avoid this problem, the total ion flux had to be reduced so that space charge could not distort the electric field even within the  $\text{CO}^+$  ion swarm. At this total ion flux, the count rate of the  $\text{C}^+$  ions was much lower than normal for mobility data and therefore the total number of  $\text{C}^+$  ions detected was small. The random error in the average arrival time is therefore increased and the mobility data points reflect this scatter.

Below an  $E/N$  of 35 Td, the reduced mobility of  $\text{C}^+$  appears constant, within the scatter of the data. The zero-field mobility is determined to be  $2.7 \text{ cm}^2/\text{V-sec}$ . From the zero-field value, the reduced mobility first decreases, reaching a minimum of  $2.46 \text{ cm}^2/\text{V-sec}$  around a value of  $E/N$  of 250 Td, and then increases for higher values of  $E/N$ . At the highest  $E/N$  we measured, 745 Td, the reduced mobility had risen to a value of  $2.85 \text{ cm}^2/\text{V-sec}$ .

### $\text{K}^+$

The mobility values for potassium ions in carbon monoxide are given in Figure 9. The data represent the reduced mobility over a range of  $E/N$  from 4 to 640 Td. The data were obtained over a pressure range of 0.026 to 0.795 Torr. Below an  $E/N$  of 20 Td, the mobility was constant and the zero-field mobility is  $2.30 \text{ cm}^2/\text{V-sec}$ . The  $\text{K}^+$  reduced mobility curve shows the characteristic "hump" exhibited by  $\text{K}^+$  in  $\text{H}_2$ ,  $\text{D}_2$ ,  $\text{N}_2$ ,  $\text{O}_2$  and  $\text{NO}$ . In this case, the mobility increased with increasing  $E/N$  from its zero-field value to  $2.75 \text{ cm}^2/\text{V-sec}$  at an  $E/N$  of 250 Td and then declined with

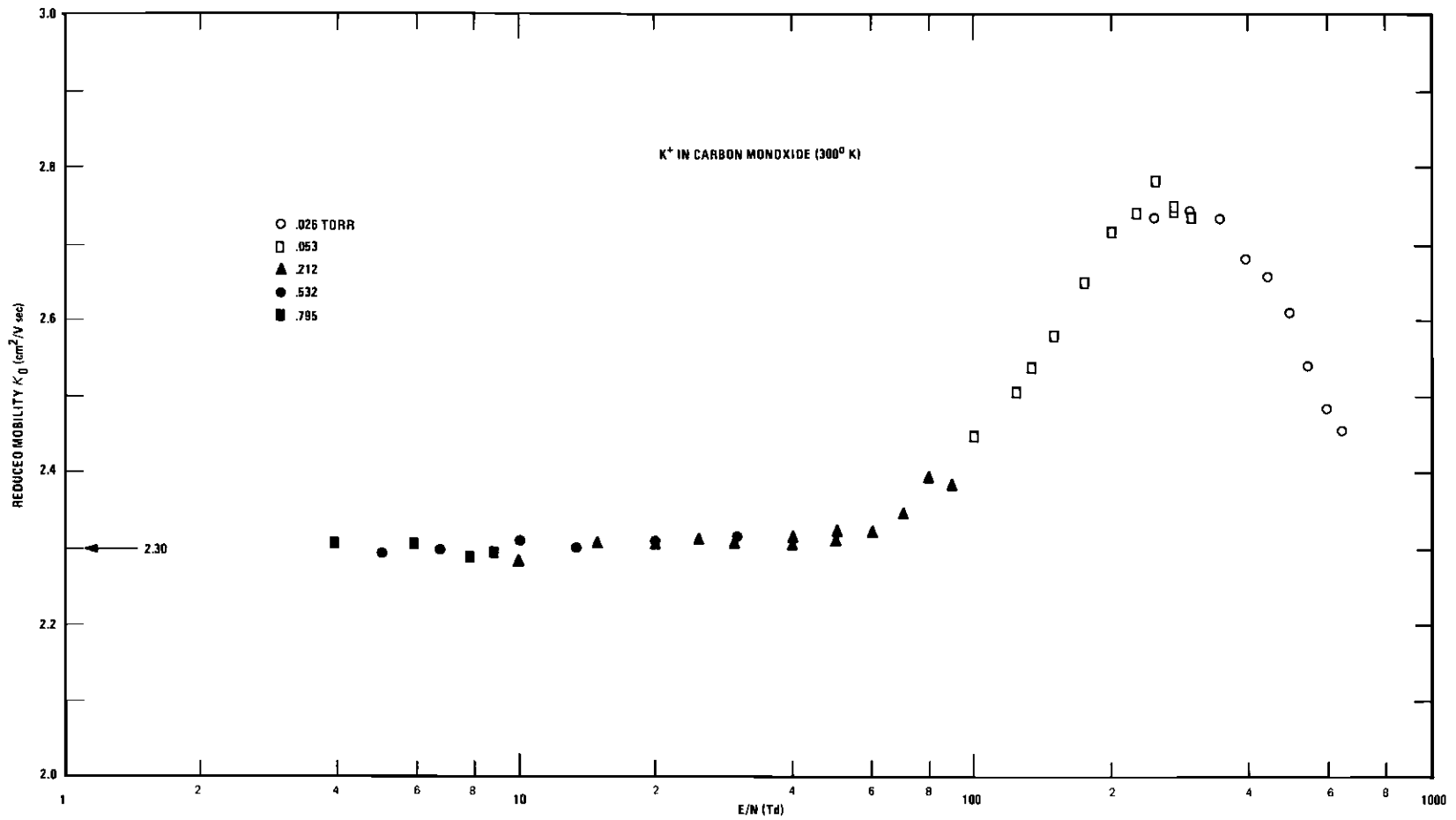


Figure 9. Mobility Results for K<sup>+</sup> in Carbon Monoxide

increasing E/N. At the maximum value of E/N recorded, 640 Td, the  $K^+$  mobility had decreased to  $2.45 \text{ cm}^2/\text{V-sec}$ .

### Error Analysis

Determination of the drift velocity from a pair of experimental spectra requires that the difference in the drift distances,  $\Delta z = z_i - z_j$ , and the difference in mean arrival times,  $\Delta \bar{t} = \bar{t}_i - \bar{t}_j$ , be measured. Conversion of this drift velocity into a reduced mobility requires knowledge of the electric field strength E, the pressure p, and the temperature T. The reduced mobility can be expressed in terms of these experimental quantities by

$$K_o = (\Delta z / E \Delta \bar{t}) (p / 760 \text{ Torr}) (273.16^\circ \text{K} / T) . \quad (4-9)$$

Each of the quantities in Equation (4-9) will be discussed in turn.

#### Distance

The absolute measurements of the drift distances are accurate to  $\pm 0.005 \text{ cm}$  and the ion source can be positioned at any of these distances with a reproducibility of  $\pm 0.003 \text{ cm}$ . Hence, for the shortest  $\Delta z$  normally used, 6.25 centimeters, the maximum systematic error is  $\pm 0.16$  percent and the maximum random error is  $\pm 0.10$  percent. Should the absolute drift distances be in error due to disassembly and reassembly of the ion source (although they are not believed to be), the relative drift distances would not change and the accuracy of the  $\Delta z$  measurements would not be affected.

#### Electric Field

The possible error in the electric field arises mainly from the possible error in the drift potential V applied across the external

electrode resistor string and in the drift length  $z_i$ . The error in the drift potential  $V$  is associated with the systematic  $\pm 0.1$  percent possible error in the resistors of the voltage divider plus the systematic  $\pm 0.01$  percent possible error in the total voltage measurement. For a drift length of 6.25 centimeters, the random error in  $z_i$  is  $\pm 0.05$  percent and the systematic error is  $\pm 0.08$  percent. Since the errors in  $z_i$  and  $V$  are independent, the two systematic errors are combined by taking the square root of the sum of their squares, resulting in a possible systematic error in  $E$  of  $\pm 0.13$  percent. The total possible random error is  $\pm 0.05$  percent.

#### Temperature

The temperature for a given mobility value is obtained from the average of at least nine thermocouple readings, one reading of each of the three drift tube thermocouples for each of at least three drift distances. This average value is believed to represent the true gas temperature with a possible systematic error of  $\pm 0.5$  percent. In addition, the ion source heating effects can cause a temperature gradient of up to about  $3.0^\circ\text{C}$  in the drift tube. A random error of  $\pm 0.5$  percent is used to include the possible temperature gradient.

#### Pressure

Random error in the pressure measurement arises from the zero drift of the capacitance manometer. During the intervals between the pumping out of the drift tube and the checking of this zero, the drift is always less than  $\pm 2 \times 10^{-4}$  Torr. At 0.1 Torr this represents a possible error of  $\pm 0.5$  percent. For pressures below 0.1 Torr, care is taken to

check the zero drift more often and the same  $\pm 0.5$  percent error limit holds.

During the work of Moseley, a calibration of the MKS Baratron was made, using a McLeod gauge. The details of the calibration can be found in the report by Moseley, et al.<sup>51</sup> The result of the calibration was determined to be accurate to within  $\pm 2.0$  percent. Since his work, another method of calibrating the Baratron was developed, involving the use of the mobility of potassium ions in nitrogen gas.<sup>30</sup> Calibration by this means was performed both during the initial and final stages of this research. Inspection of the mobility values for  $K^+$  in  $N_2$  showed that the pressure calibration had shifted further than that reported by Moseley. The pressure calibration factor was increased from 1.045 to 1.06. The results can be seen in Figure 10. The solid dots represent data taken before the research on carbon monoxide was performed, while the open circles represent data taken after most of the data on carbon monoxide had been obtained. Since the mean of both sets of data correspond to a mobility of  $2.550 \text{ cm}^2/\text{V-sec}$ , in excellent agreement with the established value of  $2.54 \text{ cm}^2/\text{V-sec}$ ,<sup>30</sup> and the standard deviation of the data is 0.5 percent, a systematic error limit of  $\pm 1.0$  percent is assigned to the determination of  $p$ .

### Time

Systematic errors in the measurement of  $\bar{t}$  due to diffusion and reaction are discussed in Chapter III. The diffusion error for differenced mean arrival times  $\Delta\bar{t}$  should yield drift velocities differing from the true drift velocities by no more than  $\pm 0.1$  percent. The error to the

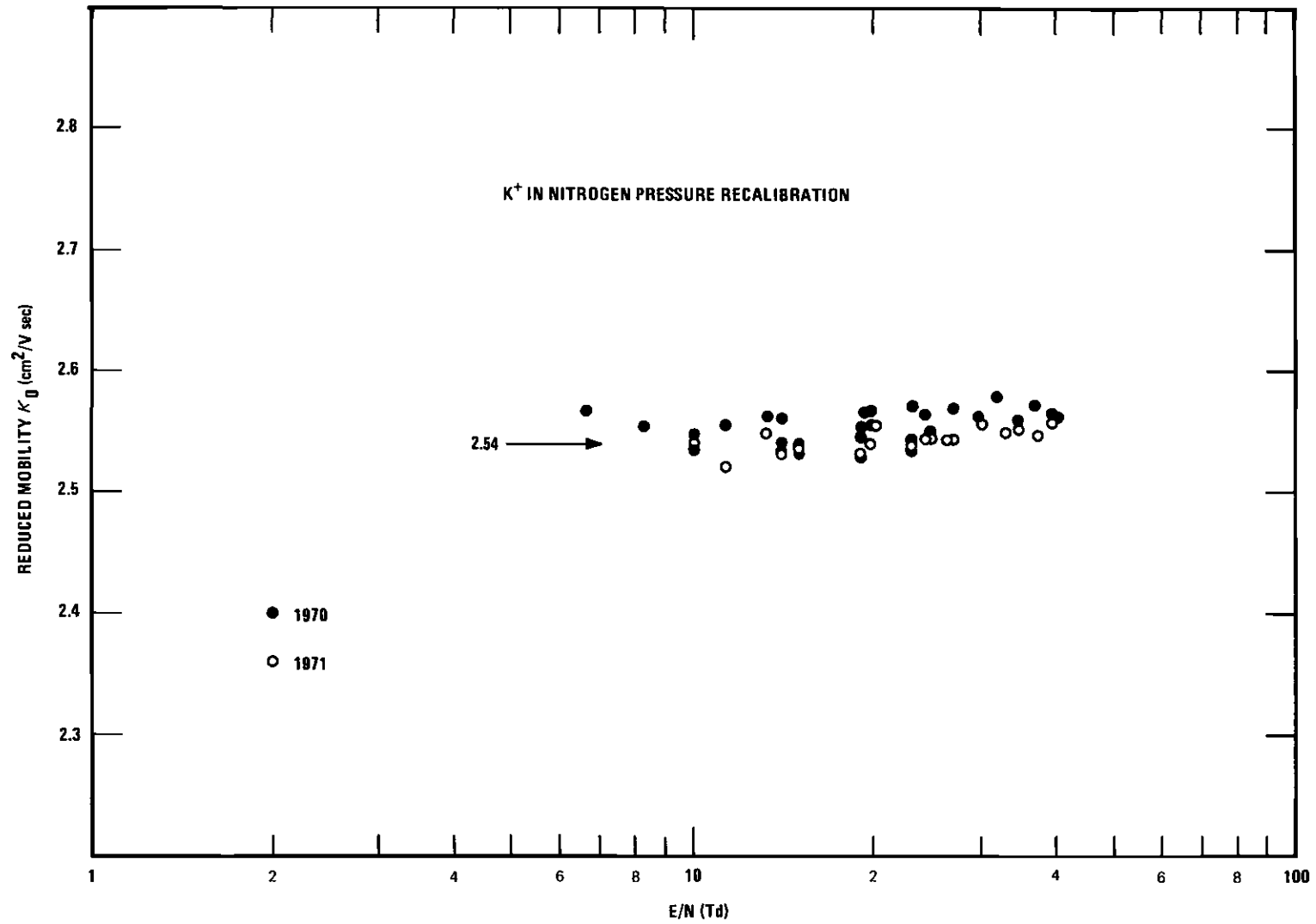


Figure 10. Pressure Recalibration Data; Mobility of  $\text{K}^+$  in Nitrogen Gas



mobility values due to the presence of a reaction depends on the reaction frequency,  $\alpha$ , if the ionic species being measured is involved in only a depletion type reaction. The ion that is affected the most by a depletion reaction is  $\text{CO}^+$ . At the lowest values of  $E/N$  used, the reaction correction term is about 1.5 percent. The data were corrected to account for this effect, but error limits of  $\pm 0.5$  percent are assigned. At higher values of  $E/N$  the reaction effect quickly becomes negligible, due to the increase in drift velocity, so the errors are reduced.

For  $\text{CO}^+ \cdot \text{CO}$ , the depletion or backward reaction into  $\text{CO}^+$  is very small, even at high pressures. A systematic error limit due to the effect of depleting reactions of  $\pm 0.2$  percent is assigned. Because no data were taken when the forward reaction had not been driven to completion by the shortest drift distance used, no error is introduced by the forward reaction.

For  $\text{C}^+$ , again the depletion reaction frequency was very small, apparently caused by a very weak reaction forming  $\text{CO}^+$ . An error limit of  $\pm 0.2$  percent was assigned.

For  $\text{K}^+$ , no reaction products were detectable except at the highest pressures, and then they were present in such a small concentration that no effect from the reaction could be detectable.

A measure of the random experimental error is obtained by examining the differences between the mean arrival time for each of the positions measured and the least squares fit to a straight line. The standard deviation for only a few points exceeded 0.5 percent. Thus, for these ions, a random error limit of  $\pm 0.5$  percent is assigned. For  $\text{C}^+$ , the random scatter was much larger, and here a random error of  $\pm 3.0$  percent is

assigned.

### Total Error

Since the random errors are independent of the systematic errors, the square root of the sum of the squares of the possible random and systematic errors will yield a bound on the error of our mobility results.

Table 1 gives the sums of these errors.

Table 1. Summary of the Errors Involved in the Mobility Measurements

Type of Error		$\text{CO}^+$	$\text{CO}^+ \cdot \text{CO}$	$\text{C}^+$	$\text{K}^+$
Distance	random	0.10	0.10	0.10	0.10
	systematic	0.16	0.16	0.16	0.16
Electric Field	random	0.05	0.05	0.05	0.05
	systematic	0.13	0.13	0.13	0.13
Temperature	random	0.5	0.5	0.5	0.5
	systematic	0.5	0.5	0.5	0.5
Pressure	random	0.5	0.5	0.5	0.5
	systematic	1.0	1.0	1.0	1.0
Time	random	0.5	0.5	3.0	0.5
	systematic	0.51	0.22	0.22	0.1
Root Mean Square Total of Random and Systematic Errors		1.53	1.46	3.30	1.45

The bounds on the amount by which a recorded value of  $K_0$  may be in error are, in percentage, as follows:  $\text{CO}^+$ ,  $\pm 1.5$ ;  $\text{CO}^+ \cdot \text{CO}$ ,  $\pm 1.5$ ;  $\text{C}^+$ ,  $\pm 3.3$ ; and  $\text{K}^+$ ,  $\pm 1.5$ .

Comparison With Existing Data

Mobility values for ions in carbon monoxide as a function of E/N have been determined by two other researchers, R. N. Varney and M. Saporoschenko. The mass-analyzed data of Saporoschenko<sup>5</sup> give mobility values for CO<sup>+</sup> that are approximately 20 percent higher than ours over an E/N range of about 100 to 475 Td. The mobility values for CO<sup>+</sup>·CO agree to within 5 percent with the results of this research in the E/N range of 40 to 95 Td. Below this range, Saporoschenko has no data, leading him to an erroneously low value for the zero-field mobility. Above this range, he appears to enter the regime where the ions analyzed as CO<sup>+</sup>·CO have not drifted as that species throughout the entire drift region, and the values reported would refer to an "apparent" mobility.

The non-mass analyzed data of Varney<sup>4</sup> reveal the existence of two ion species. The slower drifting species gives a mobility curve similar to Saporoschenko's "apparent" mobility of CO<sup>+</sup>·CO at high E/N. The faster ion was suspected of being C<sup>+</sup>, but the agreement between his mobility data and that of this research is poor.

A value for the zero-field mobility for K<sup>+</sup> in CO was obtained by Mitchell<sup>3</sup> in 1934. His value of 2.18 cm<sup>2</sup>/V-sec for the reduced mobility agrees fairly well with our value of 2.30 cm<sup>2</sup>/V-sec.

Comparison between the predictions of a pure polarization force law and the data of this research can be obtained. If one calculates the reduced mobility for the pure polarization force,

$$f_p = 2\alpha e^2 / r^5 \quad (4-10)$$

where  $\alpha$  is the mean polarizability of the neutral molecules, the formula becomes<sup>52</sup>

$$K_{oP} = \frac{13.876}{(\alpha\mu)^{\frac{1}{2}}} \text{ cm}^2/\text{V-sec} \quad (4-11)$$

where  $\mu$  is the reduced mass in gm/mole. Taking  $1.95 \text{ \AA}^3$  for the polarizability of carbon monoxide,<sup>53</sup> one obtains the values indicated in Table 2.

Table 2. Pure Polarization Force Mobilities versus Experimental Data

Ion	$K_{oP}$	$K_o$	Deviation
$C^+$	3.43	2.7	27%
$K^+$	2.46	2.30	7%
$CO^+ \cdot CO$	2.30	1.90	21%

Another valuable comparison with the values of the mobility of  $K^+$  in CO as a function of  $E/N$  is with the data for  $K^+$  in  $N_2$ . Carbon monoxide is isoelectronic with nitrogen and the principal difference is in the permanent dipole moment of CO. The reduced mobility of  $K^+$  in CO and  $N_2$  are compared in Figure 11. The data for  $K^+$  in  $N_2$  was recently obtained by G. M. Thomson of this laboratory. These mobility values were measured

in the process of obtaining improved measurements on  $ND_L$  of  $K^+$  in nitrogen.<sup>54</sup>

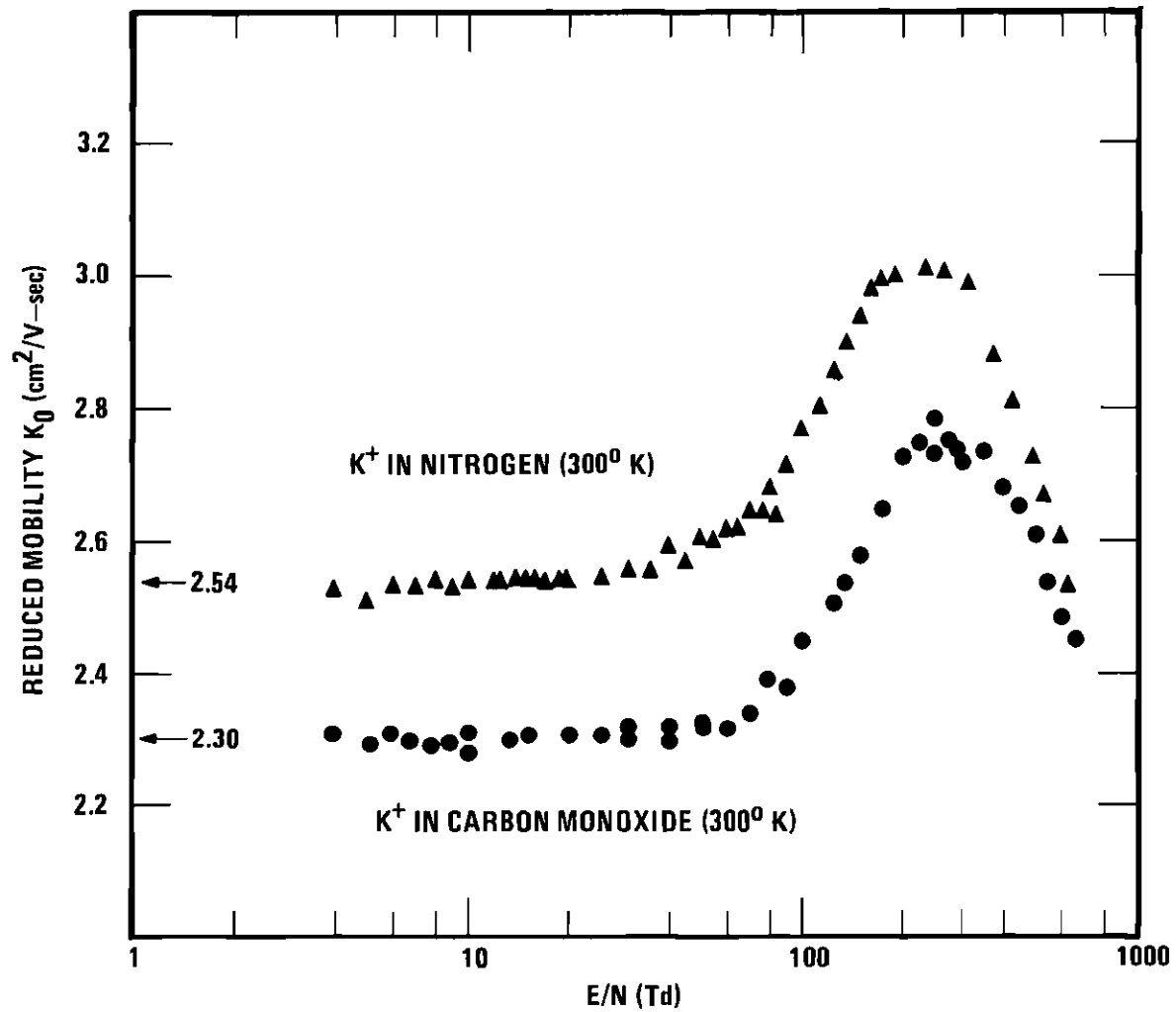


Figure 11. Mobility Comparison for Potassium Ions Drifting in Carbon Monoxide and Nitrogen

## CHAPTER V

## LONGITUDINAL DIFFUSION COEFFICIENTS

Method

As discussed in Chapter III, the width of the experimental arrival-time spectrum of source-produced ions is basically a function of the longitudinal diffusion coefficient. The overall magnitude of the arrival-time spectrum depends on the transverse diffusion coefficient and the reaction frequency, but these two parameters have little effect on the overall shape. Moseley, et al.<sup>55</sup> showed that the transverse diffusion coefficient,  $D_T$ , could be varied from  $0.01 D_L$  to  $10 D_L$ , and the reaction frequency,  $\alpha$ , could be varied from zero up to  $10^6 \text{ sec}^{-1}$  without appreciably distorting the shape of the arrival-time spectrum. Therefore, even when only estimates of the transverse diffusion coefficient and the reaction frequency are available,  $D_L$  can be determined from the shape of the experimental profiles of source-produced ions.

The technique used to determine  $D_L$  was to assume a value for  $D_L$  in the analytical expression for source-produced flux, Equation (3-38):

$$\Phi(0, z, t) = \frac{a s e^{-\alpha t}}{4(\pi D_L t)^{\frac{3}{2}}} \left( v_d + \frac{z}{t} \right) \left[ 1 - \exp\left(-\frac{r_o^2}{4D_T t}\right) \right] \exp\left[-\frac{(z - v_d t)^2}{4D_L t}\right] \quad (5-1)$$

and vary this value until the analytical profile and the experimental data agree best when normalized with respect to intensity and analysis time.

As described in Chapter III, this is done by an iterative scheme on the computer at the same time the mobility analysis is performed. The computer program uses the drift velocity from previous calculations, assumes the transverse diffusion coefficient is equal to the longitudinal diffusion coefficient, and sets the reaction frequency to zero.

Figure 12 shows a computer fit to one experimental arrival-time spectrum. The histogram represents the experimental data and the smooth curve represents the curve-fitted analytical curve. The values indicated on the figure are those used by the computer program except for the longitudinal diffusion coefficient which is determined by the curve-fitting procedure. The agreement is seen to be quite good.

#### Experimental Procedures

The computer determines a longitudinal diffusion coefficient for every experimental spectrum which is accepted for mobility analysis. However, not all of these  $D_L$  values are acceptable. The differencing technique used in the analysis of mobilities cannot be applied in the determination of a value of  $D_L$  for each spectrum. More stringent conditions than those acceptable for use in mobility measurements must be observed when obtaining arrival-time spectra that are expected to yield accurate longitudinal diffusion coefficients. The following additional restrictions must be placed on the spectra:

1. The use of the Tyndall shutter to gate the ions into the drift region at a precisely known time under precisely determined conditions is a necessity.

2. The initial ionic density in the ion swarm must be low, so that no detectable space charge broadening of the ion swarm occurs.



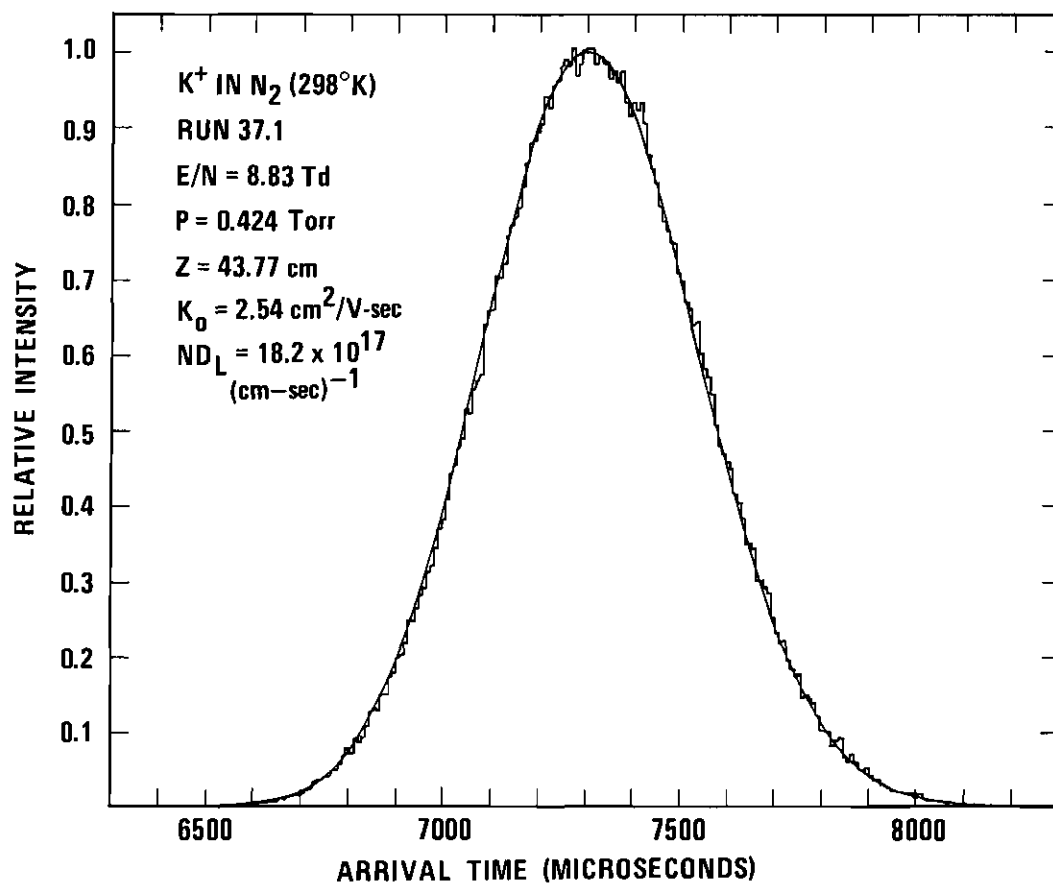


Figure 12. Sample Experimental Arrival-Time Spectrum Showing Fit to Computer-Generated Analytical Profile

3. The ions composing an experimental spectrum must have been formed in the ion source. The condition that a reaction go to completion before the ion swarm has drifted the shortest drift distance used is not sufficient for spectra used in the determination of  $D_L$ . No spectra that have been substantially affected by ion production in the drift region are used in the final  $D_L$  determination.

Since one run at a given pressure and  $E/N$  generally includes spectra taken at four different drift distances, comparisons such as that shown in Figure 12 are made for each distance. The resulting values of  $D_L$  are then averaged to determine the longitudinal diffusion coefficient. For a set of data which met the conditions discussed above, the values of  $D_L$  would generally not differ by more than 7 or 8 percent from position to position.

#### Experimental Results

Longitudinal diffusion coefficients were determined for  $CO^+$  and  $K^+$  ions in carbon monoxide over a wide range of drift distances and values of  $E/N$ . The results for these two ion species are shown in Figure 13. Since  $D_L$  varies as  $1/N$ , the results are expressed as the value of  $ND_L$  versus  $E/N$ . Note that for both ions the value of  $ND_L$  appears to approach a limiting value as the value of  $E/N$  decreases toward zero. This observation is in agreement with the prediction of the Einstein equation.

#### $CO^+$

The range of  $E/N$  values for the  $D_L$  determination of  $CO^+$  was limited to 13 Td and above. At lower values of  $E/N$  the ion-molecule reaction

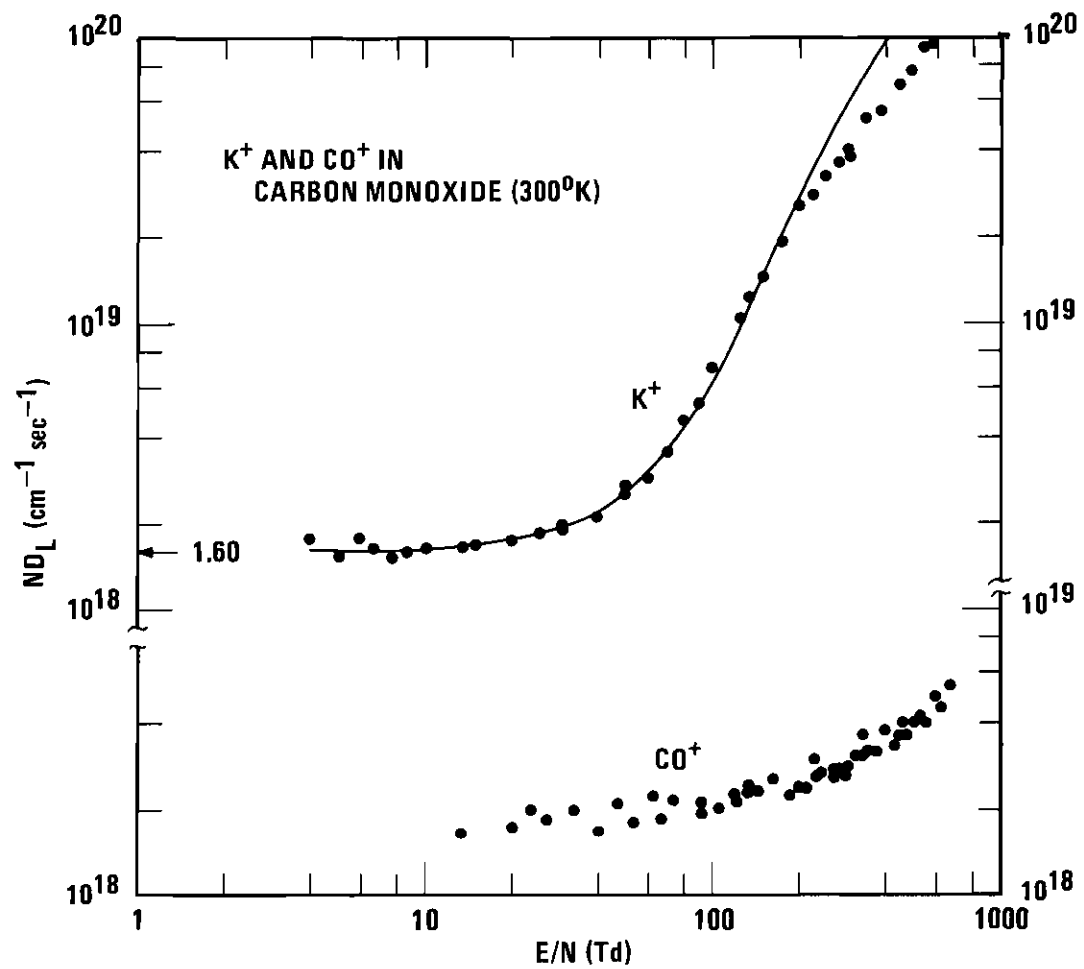


Figure 13. Longitudinal Diffusion Coefficient Results for  $K^+$  and  $CO^+$  in Carbon Monoxide

converting  $\text{CO}^+$  into  $\text{CO}^+\cdot\text{CO}$  kept the count rate of the  $\text{CO}^+$  ions so low that accurate determination of  $D_L$  was not possible. In addition, the reaction effect that distorts the mobility results at low values of  $E/N$  (see Equation 3-48) could have likewise distorted the  $D_L$  values unless the reaction rate was accurately known and included in the curve-fitting procedure.

Since the zero-field reduced mobility could not be determined, no zero-field longitudinal diffusion coefficient could be calculated from the Einstein equation. The most significant feature of the  $\text{CO}^+$  longitudinal diffusion coefficient results is the slow increase in  $ND_L$  as the value of  $E/N$  is increased, as compared with the results for  $\text{K}^+$ . This behavior is similar to that seen in  $\text{N}_2$ ,  $\text{O}_2$ , and  $\text{NO}$ .<sup>56-58</sup> A relatively slow increase in  $ND_L$  versus  $E/N$  for  $\text{N}_2^+$  in  $\text{N}_2$ ,  $\text{O}_2^+$  and  $\text{O}_2^-$  in  $\text{O}_2$ , and  $\text{NO}^+$  in  $\text{NO}$  has been observed when compared with the values of  $ND_L$  for all other ions in these gases. The slower increase in  $ND_L$  for these cases may be attributed to the role that resonant charge exchange plays in the total scattering interaction for these ions.

### $\text{K}^+$

Longitudinal diffusion coefficients for  $\text{K}^+$  in carbon monoxide were obtained for values of  $E/N$  from 4 to nearly 600 Td. The values of  $ND_L$  range from  $1.63 \times 10^{18} \text{ (cm-sec)}^{-1}$  at low values of  $E/N$  (less than 11 Td) to nearly  $10^{20} \text{ (cm-sec)}^{-1}$  at high values of  $E/N$ . The value of  $ND_L$  predicted by the Einstein equation from the zero-field reduced mobility is  $1.60 \times 10^{18} \text{ (cm-sec)}^{-1}$ , in excellent agreement with the low  $E/N$  value of  $ND_L$  as measured in this experiment. In past research by this laboratory on  $\text{N}_2$ ,  $\text{O}_2$ , and  $\text{NO}$ , there has been difficulty in obtaining values of  $ND_L$

that agree closely with the values predicted by using the Einstein equation along with the value of the zero-field reduced mobility. In all the measurements made on  $ND_L$  in these gases, the diffusion coefficient was larger than predicted for positive ions and smaller than predicted for negative ions. Since the previous measurements were made, advances in the methods of analyzing arrival-time spectra have been made. In addition, the fringing field from the source magnet has been eliminated by removing the magnet. Excellent agreement, well within the error bars, between the value of  $ND_L$  measured at low  $E/N$  and the value predicted from the Einstein equation and the zero-field reduced mobility has been obtained for  $K^+$  in CO and for recent work on  $K^+$  in  $N_2$ .<sup>54</sup> It is believed that either errors in determining the proper value of  $D_L$  from the arrival-time spectra or errors due to instrumental effects, such as the magnetic field near the source, were the sole cause of the earlier discrepancy between theory and experiment.

Expressions for the longitudinal and transverse diffusion coefficients, in terms of the drift velocity, can be derived from theory developed by Wannier. These expressions were described in Chapter III, and are appropriate for all values of  $E/N$  so long as the polarization force is the dominant interaction between the ions and neutral molecules. Using the values of drift velocity derived from our previous calculations,  $ND_L$  was determined from the Wannier expressions and plotted as the solid curve on Figure 13. Below an  $E/N$  of 200 Td, the agreement with the experimental data for  $K^+$  is excellent. It needs to be pointed out that the value of the drift velocity, applicable to the particular value of  $E/N$  at

which the theoretical estimate is being made, was used in the  $D_L$  calculation. The pure polarization force theory predicts that the mobility will be constant, independent of  $E/N$ . It appears that the Wannier relation between  $D_L$  and the mobility is at least approximately correct even when the mobility deviates from its zero-field value.

The discrepancy between the experimental values of  $ND_L$  and the Wannier prediction above an  $E/N$  of 200 Td is believed to be a physical effect due to changes in the interaction between the ions and neutral molecules at large values of  $E/N$ .

#### $CO^+ \cdot CO$

Measurements of the longitudinal diffusion coefficient for  $CO^+ \cdot CO$  could be made only at low values of  $E/N$ . A strict requirement for accurate measurement of  $D_L$  is that all ions of the species detected must be source produced. Since  $CO^+ \cdot CO$  is produced by an ion-molecule reaction, only at very low values of  $E/N$  could this requirement be fulfilled by forcing the reaction to proceed to completion within the ion source. At low values of  $E/N$ ,  $D_L$  can be determined by using the Einstein equation and the zero-field reduced mobility. The experimental values of  $ND_L$  for  $CO^+ \cdot CO$  agree with the Einstein equation predictions within about 5 percent.

In the intermediate  $E/N$  region we could obtain accurate mobility values by relaxing the requirement that all ions must be created in the source, and only require that all ions must be produced before the shortest drift distance used is reached. These mobility studies do not produce arrival-time spectra that can be analyzed for accurate values of diffusion coefficients. The shape of the arrival-time spectrum, and therefore the

measured value of the longitudinal diffusion coefficient, depends on the drift parameters of the ions for the entire drift and all ions must be source produced if accurate values of  $D_L$  are to be obtained.

### C<sup>+</sup>

No values of  $D_L$  are reported for C<sup>+</sup> ions in carbon monoxide. The production of C<sup>+</sup> in the ion source was very small in comparison with CO<sup>+</sup> and even using long counting periods, the statistics were poor. The shape of the arrival-time spectrum is much more sensitive to counting statistics than is the average time-of-arrival, so although the mobility could be measured with reasonable error bounds, the random scatter in the  $D_L$  values rendered them almost useless. The only conclusion drawn from the arrival-time spectra was that the value of  $ND_L$  increases rapidly as the value of E/N is increased above the thermal range.

### Error Analysis

The possible errors in the determination of  $D_L$  can be put into four categories: the error in determining the drift velocity, the error in determining the "best" fit between the theoretical and experimental profiles, the possible error in the number density measurement, and any systematic errors that would prevent the experimental data from agreeing with an acceptable theoretical model.

The error in the determination of the drift velocity arises from two sources, the error in determining  $\overline{\Delta t}$ , and the error in determining  $\Delta z$ . From Table 1, the error is: for CO<sup>+</sup>,  $\pm 0.74$  percent, and for K<sup>+</sup>,  $\pm 0.54$  percent.

By the use of a computer simulation program, the percentage error in the measured value of  $D_L$  produced by an error in the drift velocity was calculated. Simulated arrival-time spectra were computed using given values of  $v_d$  and  $D_L$ . Values of  $v_d$  that were "in error" were given to the curve-fitting program used in calculating  $D_L$ . The values of  $D_L$  used to generate the arrival-time spectra were then compared to the  $D_L$  values calculated by the curve-fitting program. The error in  $D_L$  was found to be about three times the error in the drift velocity. For this reason, the error limits in the preceding paragraph must be multiplied by a factor of three.

The error in determining the "best" fit can be estimated by investigating the difference between values of  $D_L$  obtained by fitting the several spectra (usually four) taken at different drift distances, but otherwise under the same conditions. For  $CO^+$ , at values of  $E/N$  from 13 to 50 Td, the random error is about  $\pm 12$  percent, while for  $E/N$  greater than 50 Td, the random error is about  $\pm 5$  percent. The increase in the random error in curve-fitting at low  $E/N$  comes from two sources; first, the data contain poorer statistics due to many of the  $CO^+$  ions being converted into the dimer, and secondly, because of this depletion, only the first few source positions could be used. Any distortions caused by non-thermalization of the ions or by non-uniform source output are reduced by diffusion as the ion swarm drifts. If the first few source positions are used, these distortions are larger than if the last few source positions are used.

The "best" fit error for the  $K^+$  ions is uniformly  $\pm 5.0$  percent



since at all values of  $E/N$ , sufficiently good statistics could be obtained and the longer drift distances could be used.

The number density error does not enter until  $ND_L$  is calculated or a particular value of  $E/N$  is associated with a value of  $D_L$ . The possible error in  $N$  arising from errors in pressure and temperature is  $\pm 1.3$  percent for both  $CO^+$  ions and  $K^+$  ions.

The possible errors caused by effects that are not known, and therefore cannot be accounted for, are very difficult to assess. If one has a theory that predicts the experimental quantity that is to be measured, unknown effects should manifest themselves as discrepancies between theory and agreement. Because of the excellent agreement between the Wannier prediction for  $ND_L$  and the experimental data for the  $K^+$  ions at low and intermediate values of  $E/N$ , it is felt that no gross systematic errors have been neglected that were not also present in the drift velocity measurements.

The bounds on the amount by which a recorded value of  $ND_L$  may be in error are: for  $CO^+$ ,  $E/N$  from 13 to 50 Td,  $\pm 12.2$  percent,  $E/N$  greater than 50 Td,  $\pm 5.6$  percent; and for  $K^+$ ,  $\pm 5.4$  percent.

As stated in Chapter I, there are no published results on  $K^+$  in  $CO$  with which the values of  $ND_L$  obtained in this research can be compared. It is interesting, however, to compare the results for  $K^+$  in  $CO$  with the recent results for  $K^+$  in nitrogen.<sup>54</sup> Carbon monoxide is isoelectronic with nitrogen and the principal difference is in the permanent dipole moment of  $CO$ . The longitudinal diffusion coefficients for  $K^+$  in  $CO$  and  $N_2$  are compared in Figure 14. The data for  $K^+$  in  $N_2$  were recently

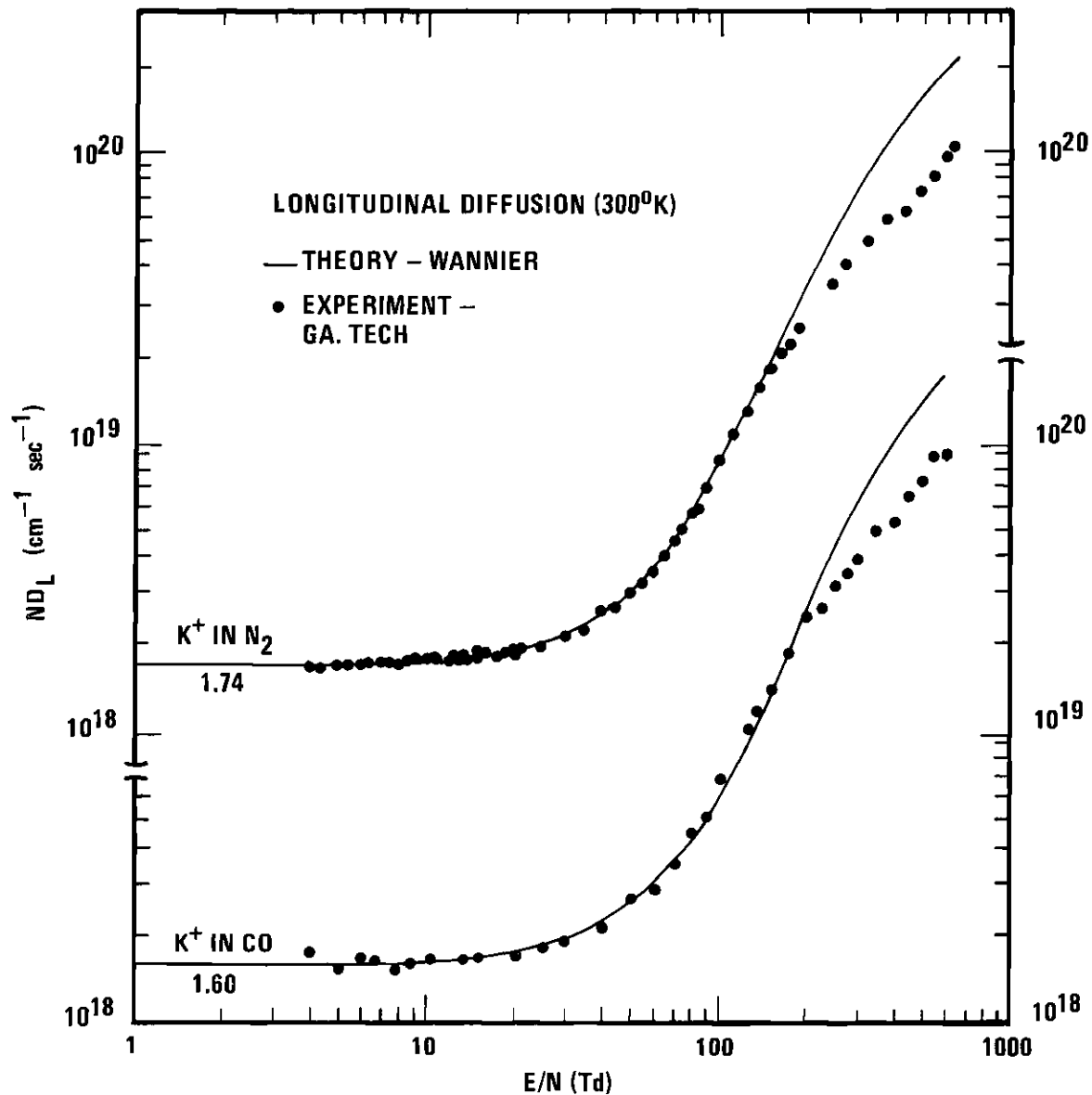


Figure 14. Longitudinal Diffusion Coefficient Results for  $K^+$  in Carbon Monoxide and Nitrogen. (The accuracy of the experimental data decreases as  $E/N$  is raised above 225 Td, but the drop below the Wannier prediction in both gases is believed to be real and pronounced.)

obtained by G. M. Thomson of this laboratory to replace values measured by Moseley, et al.<sup>56</sup> that appeared to be inaccurate, particularly at low E/N.

## CHAPTER VI

## ION-MOLECULE REACTIONS

In this chapter the results of the study of ion-molecule reactions occurring in carbon monoxide will be presented. In the pressure range of 0.026 to 0.795 Torr, the principal reaction was the clustering of a carbon monoxide molecule onto a  $\text{CO}^+$  ion. Through the study of this reaction the equation describing this reaction was found to be:



The pressure dependence of the reaction frequency established the three-body nature of the reaction. The emerging CO molecule must be present to carry away the energy released by the formation of the molecular bond in  $\text{CO}^+ \cdot \text{CO}$ .

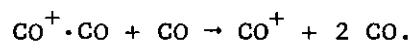
As the pressure was increased, the existence of this clustering reaction was evidenced by the rapid decrease in population of the source-produced  $\text{CO}^+$  ion species, by the rapid increase in the population of the dimer ion species,  $\text{CO}^+ \cdot \text{CO}$ , and by an analysis of the time-of-arrival spectrum of the dimer ion. The arrival times of  $\text{CO}^+ \cdot \text{CO}$  ions vary from those typical of the drift of pure  $\text{CO}^+$  to those attributed to the drift of pure  $\text{CO}^+ \cdot \text{CO}$ . The spread in arrival times, above that due to diffusion, is due to ions drifting through part of the drift tube as  $\text{CO}^+$ , reacting with the CO molecules composing the drift gas, and drifting the remainder of the drift distance as  $\text{CO}^+ \cdot \text{CO}$ .

Two other minor reactions were also detected. An apparent charge exchange reaction occurred between the source produced  $C^+$  ions and the CO gas:



The existence of this reaction was shown by the presence of a small number of  $CO^+$  ions arriving at the detector with abnormally short drift times. The fastest ion observed was  $C^+$  and the leading edge of the fast  $CO^+$  ion spectrum corresponded to the drift velocity of  $C^+$ . As with the clustering reaction, ions apparently drifted part of the drift distance as  $C^+$ , reacted with the CO gas molecules, and drifted the rest of the way as  $CO^+$ . This reaction was very weak and observable only at high pressure and moderate E/N. No reaction rate information could be obtained for this reaction.

The other minor reaction observed was the breakup of the  $CO^+ \cdot CO$  cluster:



The evidence for the existence of this reaction was the arrival of  $CO^+$  ions with the drift times corresponding to the dimer ions and not characteristic of  $CO^+$ . These fast  $CO^+$  ions did not have as short a drift time as ions spending their life as  $C^+$ , but formed a small peak about the drift time of  $CO^+ \cdot CO$ . The rate of this reaction could not be determined, since the number of  $CO^+$  ions detected as formed by the dissociation process was small and partially masked by the charge exchange reaction from  $C^+$ .

### Method

The method used to determine the reaction rate for the clustering reaction is known as "product ion curve fitting." As explained in Chapter III, product ion curve fitting involves the matching of experimental arrival-time spectra for the product ion species with the analytical expression appropriate to that species. Equation (3-54) describes the flux of product ions when there is no depletion of the product species back into the parent species:

$$\begin{aligned} \Phi_B(0, z, t) = & \text{as} \int_0^t du \left[ f_B \delta(t-u) + f_A \alpha_{BA} \right] (\pi r_L^2)^{-\frac{1}{2}} \\ & \times \left[ \frac{2D_{LB}(z-r_d)}{r_L^2} + v_{dB} \right] \exp \left[ -\gamma - \frac{(z-r_d)^2}{r_L^2} \right] \\ & \times \left[ 1 - \exp \left( -\frac{r_0^2}{r_T^2} \right) \right] \end{aligned} \quad (6-4)$$

where

$$r_T^2 = 4 D_{TA}(t-u) + 4D_{TB}u, \quad (6-5a)$$

$$r_L^2 = 4 D_{LA}(t-u) + 4 D_{LB}u, \quad (6-5b)$$

$$r_d = v_{dA}(t-u) + v_{dB}u, \quad (6-5c)$$

$$\gamma = \alpha_A(t-u) + \alpha_B u, \quad (6-5d)$$

$f_i$  is the fraction of ions of species  $i$  created in the source, and  $u$  is

the time the ions spend as species B.

If the difference in distances traveled in a time  $t$ ,  $(v_{dA}t - v_{dB}t)$ , is large compared to the square root of the sum of the diffusion areas,  $(4D_{LA}t + 4D_{LB}t)^{\frac{1}{2}}$  at this same time  $t$ , then several simplifying approximations can be made. As outlined in Chapter III, these approximations lead to an expression, Equation (3-63), relating the slope of the logarithm of the product ion current versus time to the reaction frequency and transverse diffusion coefficients. If the drift velocities of the parent and product ion species are sufficiently different, the use of this expression is convenient. If the drift velocities are different, but not greatly so, the best way to analyze the data is to use the full analytical expression for the product ion flux as a function of time and to actually fit the experimental arrival-time spectra to it. This was the scheme used in this research. In the curve-fitting procedure, the feature of the arrival-time spectrum that is most carefully matched is the broad sloping shoulder, for the slope of the shoulder is partially determined by the reaction frequency, and this is the quantity we wish to measure.

The first quantities that must be determined from the arrival-time spectrum are the drift velocities. Neglecting the transverse diffusion term in Equation (3-63), one can show that the calculated value of reaction frequency is directly dependent on both the difference in drift velocities and the absolute value of the product ion drift velocity used in the calculation. In the case of the  $CO^+$  clustering reaction, the drift velocity for the parent ion was well known from our mobility measurements. These mobility measurements were made at low pressure where the reaction

does not influence the mobility determination greatly. However, at some of the values of  $E/N$  where the reaction frequency was measured, it was not possible to obtain sufficiently high pressures to allow the reaction to go to completion early enough in the drift to allow valid mobility measurements to be made on the product ion species. In these cases the mobility measurement had to be made directly from the reaction-influenced arrival-time spectra. The width of the product ion arrival-time spectrum is a function of the difference in drift velocities, since the leading edge is determined by the drift time of the faster species while the trailing edge is a function of the drift time of the slower species. If the product ion spectra can be obtained at pressures where both the leading and trailing edges are reasonably sharp and well determined, then by using the known  $\text{CO}^+$  drift velocity, the  $\text{CO}^+\cdot\text{CO}$  drift velocity can be roughly calculated.

The equation for the product ion current, Equation (6-4), contains the longitudinal diffusion coefficients in the quantity  $r_L$ . Estimates of  $D_L$  are needed in order to evaluate the expression, but they do not play an important role in the overall shape of the spectrum. The estimate for the slope of the product ion profile, Equation (3-63), does not contain  $D_L$  for either ion species. The longitudinal diffusion coefficients are important only in determining the slope of the leading and trailing edges, not in determining the slope of the broad shoulder that is important in reaction frequency determinations.

Once the drift velocities are determined, and estimates for the longitudinal diffusion coefficients are found, the transverse diffusion



coefficients and the reaction frequency are determined. Both  $D_T$  and  $\alpha$  affect the product ion spectra in the same way; they determine the slope of the shoulder. To separate the effects of transverse diffusion and reaction, the differing effects of pressure on these two quantities are used. Transverse diffusion varies inversely with pressure, whereas for the three-body clustering reaction the reaction frequency increases as the square of the pressure. At low pressure, the slope of the product ion spectrum is influenced more strongly by diffusion than at high pressure. The effect of the reaction frequency is just opposite, being more influential at high pressure than at low pressure. The best values of transverse diffusion coefficients and reaction frequencies are arrived at by iteration. At low pressures, a guess is made for the value of the reaction frequency, and the transverse diffusion coefficients are varied to get a close fit between the experimental data taken at this pressure and the analytical profiles computed. Either or both of the transverse diffusion coefficients can be varied to arrive at the proper fit, for they have the same pressure dependence and their separate effects cannot be distinguished. Once good values of transverse diffusion have been determined, the high pressure experimental spectra are examined. The previously determined  $D_T$ 's are used and the value of the reaction frequency is varied to arrive at a good fit. The process is repeated until stationary values for both transverse diffusion coefficients and reaction frequency are found. The agreement at various pressures indicates that the proper value of reaction rate has been determined.

There is one more parameter that may have to be determined. The

reaction occurs within the source as well as in the drift tube. The fraction  $f_B$  represents the relative amount of  $\text{CO}^+\cdot\text{CO}$  that is produced within the source. Since the drift distance between the region where the  $\text{CO}^+$  ions are formed and the entrance aperture of the source is small compared with the total drift distance, relatively little source produced  $\text{CO}^+\cdot\text{CO}$  is present when reaction rate measurements are made. An estimate of  $f_B$ , and therefore  $f_A$ , can be made by determining the time taken by the  $\text{CO}^+$  ions to drift to the entrance aperture of the source and multiplying this by the appropriate reaction frequency.

Figures 15 and 16 demonstrate the resolution of the curve-fitting procedure. The values of mobility and  $\text{ND}_L$  for each species were determined as described earlier. The value of  $\text{ND}_T$  for the dimer ion was determined from the Wannier expression and was not found experimentally. By using the curve-fitting procedure, the value of the reaction rate at an  $E/N$  of 75 Td was determined to be  $1.35 \times 10^{-28} \text{ cm}^6/\text{sec}$ , with  $\text{ND}_T$  for  $\text{CO}^+$  set equal to  $17.1 \times 10^{17} (\text{cm}\cdot\text{sec})^{-1}$ . The reaction rate coefficient was then varied by  $\pm 10$  percent, and in each case, the value of  $\text{ND}_T$  for  $\text{CO}^+$  was adjusted so that at 0.133 Torr the theoretical profiles again agreed with the experimental data. These three identical curves are plotted as the dashed line in Figure 15.

Keeping the reaction rate coefficients and values of  $\text{ND}_T$  constant for these three curves, the reaction frequencies and values of  $D_T$  were computed for a pressure of 0.080 Torr. These values were used to compute the analytical curves displayed as the dashed curves in Figure 16. Because the reaction frequency varies as  $N^2$  and the diffusion coefficients

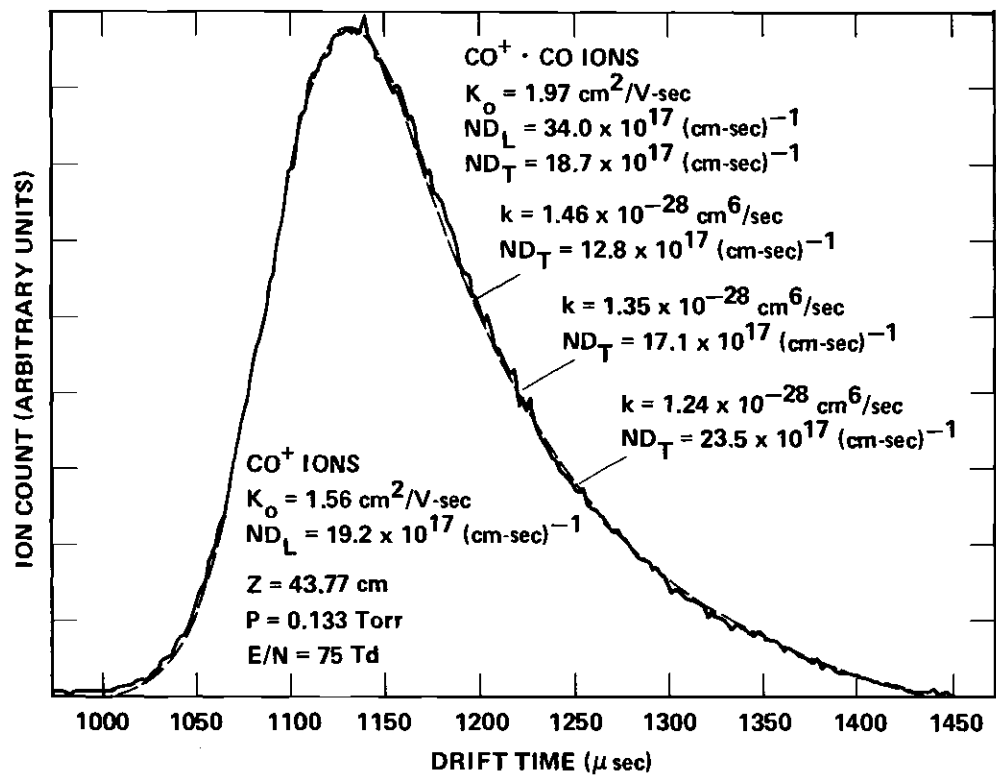


Figure 15. Product Ion Arrival-Time Spectrum At High Pressure

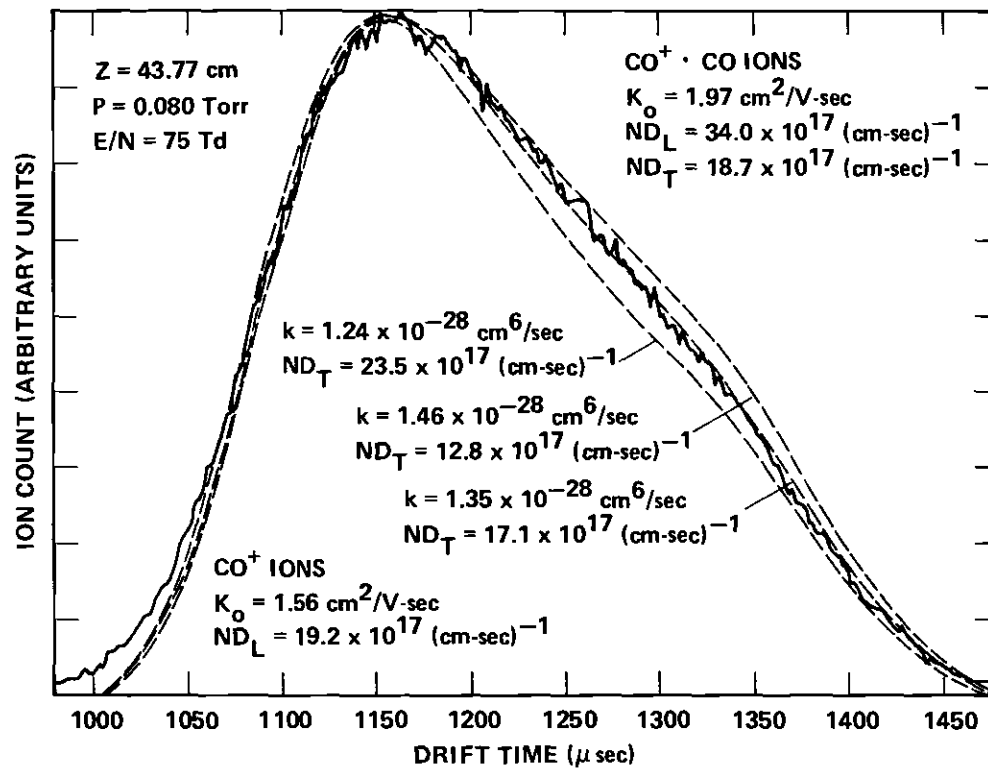


Figure 16. Product Ion Arrival-Time Spectrum At Low Pressure

vary as  $1/N$ , the three analytical curves are no longer identical and the match with the experimental arrival-time spectrum indicates the correctness of the determined rate constant. The value of  $ND_T$  for  $CO^+$  that is determined along with the reaction rate must be used with due caution. The value of  $ND_T$  for  $CO^+.CO$  predicted by the Wannier expression is assumed to be correct. Any error in this value will produce corresponding errors in the value of  $ND_T$  for  $CO^+$ , since both transverse diffusion coefficients have the same pressure dependence.

#### Experimental Procedures

The experimental procedures used to obtain product ion spectra are similar to those for mobility measurements, but with several important differences. Extra precautions must be taken to eliminate any impurity reactions, since they might interfere with the reaction studied. Only the longest drift distances are used in order to obtain the greatest possible separation in drift times between the two ion species. The use of the preset counter to introduce the proper delay in triggering the multi-channel analyzer is a necessity, since as much resolution as possible is needed in the spectra. As in the study of longitudinal diffusion, the Tyndall shutter must be used to gate the ions into the drift region at a precisely known time under precisely determined conditions, and the initial charge density in the ion swarm must be low so that no detectable space charge broadening occurs.

The first step in obtaining the product ion spectra is to determine what pressures are going to be used at a particular value of  $E/N$ . The study of the reaction at a particular  $E/N$  requires data at a variety

of pressures, some low enough so that the main effects are due to diffusion, and some high enough so that reaction effects are dominant. At pressures that are too high, the product ion profiles will begin to resemble spectra for source produced ions and will lose the information on how fast the reaction occurred. At too low a pressure, longitudinal diffusion will spread the drift times to the extent that differing drift times produced by ions spending various times as different ionic species will be hidden. There is normally a band of pressures where useful and accurate information can be obtained.

Next, the purity of the gas must be checked. Mass scans over a range of masses from 1 to over 200 amu were made to insure that no impurity reactions were present. Frequently the mass scans showed small amounts of impurities, and the Refrigerated Vapor Bath cold trap would have to be pumped and baked out in order to achieve the desired purity in the gas flow. Data were never taken when impurities were present that could affect the clustering reaction.

Once the desired value of pressure and  $E/N$  were determined and the system checked for impurities, the product ion profiles were determined. Both the electron beam gate and the Tyndall shutter were always used. The delay between the opening of the electron beam gate and the gating of the ions into the drift tube was made short to prevent substantial reaction from occurring within the source. The preset counter would be set to trigger the multichannel analyzer so that the arrival-time spectra would be spread over as many channels as possible. Because we were always using long drift distances, it was frequently possible to allow several

ion swarms to drift in the drift tube at one time and thereby increase the rate at which we could take data. Data were recorded until the peak channel accumulated from 8000 to 16 000 counts. The profiles were both recorded on paper tape for further computer analysis, and plotted with an X-Y recorder for visual analysis.

#### Effect of Source Magnet

As mentioned in Chapter II, the presence of the magnetic field from the source magnet affected the profiles of the product ion. When the electron bombardment ion source was designed, the addition of a small magnetic field in the direction of the electron beam was considered desirable to prevent the electrons from being scattered out of the beam due to collisions with gas molecules. For this purpose, the magnetic field worked well. It was also believed that magnetic fields might affect the drift and analysis of the low energy ions, so that the entire drift tube, including the ion source, was made out of non-magnetic materials, except for the source magnet, of course. Although the source magnetic field was kept reasonably low, about 100 gauss, it penetrated several centimeters into the drift region at levels up to several gauss.

When the initial work was being done on the analysis of the product ion profiles, an anomaly in the arrival-time spectra showed up. Those ions that were created by reaction early in the drift were disturbed by the magnetic field near the ion source. The product ion spectra, which normally reflected the decrease in intensity of the parent ion species from which they were created, showed an apparent increase in intensity for the first few centimeters of drift. Over the rest of the drift, the product ion spectra showed the normal decrease produced by transverse

diffusion and reaction. It is not known why the magnetic field affected the product ions in this manner.

Once the magnet was replaced by non-magnetized metal, and the magnetic field within the drift region thus removed, the product ion spectra assumed their expected shape. A large group of tests were run to check out the effect of the absence of the magnetic field on the various measurements made on the drift tube, but no changes in measured values were found. The ion source shows the effect of the absence of the magnetic field by an increase in the number of ions that are not blocked by the closed Tyndall shutter. However, the Tyndall shutter is still quite effective, and the small background that occurs is easily accounted for.

#### Experimental Results

Reaction rate coefficients were obtained over an  $E/N$  range of 75 to 150 Td. At each value of  $E/N$  where the reaction rate was measured, experimental data were taken at three or four pressures, from 0.078 to 0.159 Torr. Using reasonable values for the transverse diffusion coefficients, the values of the reaction frequency,  $\alpha$ , were clearly dependent on the number density to the second power, indicating that the reaction was definitely three-body. The measured values of the reaction rate coefficient varied from a high of  $1.35 \times 10^{-28} \text{ cm}^6/\text{sec}$  at an  $E/N$  of 75 Td to  $1.1 \times 10^{-28} \text{ cm}^6/\text{sec}$  for values of  $E/N$  between 110 and 150 Td.

No theoretical equation appears to be available for an accurate calculation of the average energy of the reacting  $\text{CO}^+$  ions in the intermediate range of  $E/N$  explored here. However, Fahr and Müller<sup>59</sup> have developed a theory applicable to the high- $E/N$  regime for the case where



resonant charge transfer collisions dominate the transport behavior of the ions, as is the case here. Their analysis gives the average energy of the ions derived from the electric field in excess of the thermal value as  $\pi m v_d^2/4$  where  $m$  is the mass of the ions.<sup>60</sup> In the absence of a more appropriate expression, we have used it to estimate the average "field energy" of the reacting  $\text{CO}^+$  ions above the thermal value in our intermediate range of  $E/N$ . The results are that the average "field energy" is estimated to be 60 percent of the thermal value at  $E/N = 75$  Td and 184 percent of the thermal value at  $E/N = 150$  Td.

The drift velocities measured from the width of the product ion curve are not nearly as accurate as those measured by the standard mobility technique. However, values of  $E/N$  can be reached with the product ion curve-fitting technique that are not accessible to the mobility measurements. The mobility of  $\text{CO}^+\cdot\text{CO}$  was measured by the curve-fitting method from an  $E/N$  of 75 Td to an  $E/N$  of 150 Td. As expected, the mobility increased steadily with increasing  $E/N$  to a value of  $2.3 \text{ cm}^2/\text{V}\cdot\text{sec}$  at an  $E/N$  of 150 Td.

#### Error Analysis

Systematic errors arise from using improper values of drift velocity, longitudinal diffusion coefficients, and in the case of the dimer ion, the depleting reaction rates. The drift velocity of  $\text{CO}^+$  is known to  $\pm 0.8$  percent from mobility measurements taken at low pressures. The drift velocity of the  $\text{CO}^+\cdot\text{CO}$  ion is determined from the width of the product-ion spectra. At values of  $E/N$  of 75 and 87.5 Td this drift velocity could be checked against mobility measurements and they agreed within

about  $\pm 3$  percent. Since the drift velocity measurement of  $\text{CO}^+\cdot\text{CO}$  involved the use of the difference in drift velocities, as does the reaction rate determination, the error in the drift velocities is set at  $\pm 4$  percent. The determination of reaction rates is very insensitive to the values of  $D_L$  used in the curve-fitting program. Any error due to inaccurate knowledge of the proper values of  $D_L$  would have to be less than  $\pm 1.0$  percent.

The depletion reaction rate for  $\text{CO}^+\cdot\text{CO}$  conversion into other ionic species is very hard to determine. Small amounts of ions representing larger clusters of carbon oxides were detected. Their intensity at the pressures where the reaction rate measurements were made were quite small and a  $\pm 3$  percent error is allowed for the reaction contribution to the error in the reaction rate. The breakup of  $\text{CO}^+\cdot\text{CO}$  back into  $\text{CO}^+$  was noticeable, but very small at the pressures used for reaction rate measurements. The effect of this breakup was easier to determine, since the parent-ion arrival-time spectra could be compared with the predictions of the transport equations for various values of backward reaction rate. There is, however, an interfering reaction due to the charge exchange between  $\text{C}^+$  and  $\text{CO}^+$ . Upper bounds on the amount of backward reaction taking place were obtainable, and they indicated that the reaction effect would produce an error in the forward reaction rate of less than one percent. Upper bounds on the backward reaction rate were of the order of  $10^{-14}$   $\text{cm}^3/\text{sec}$ .

The principal source of random error is in the determination of the values of  $\alpha$  and  $D_T$  that fit the experimental product-ion arrival-

time spectra. From examination of the curves, such as those illustrated in Figures 15 and 16, it was determined that the error involved in this selection process was less than 10 percent. The value of  $D_T$  for  $\text{CO}^+\cdot\text{CO}$  was usually kept constant, but any error from this estimate would be compensated for in the value of  $D_T$  that was used for  $\text{CO}^+$ . The values of  $D_T$  decided on for each spectrum were given no reliability, since it was not possible to determine uniquely the values for each separate  $D_T$ .

Combining the total  $\pm 5$  percent systematic error with the independent  $\pm 10$  percent random error in a root-mean-square sense, the total error is set at  $\pm 12$  percent.

#### Comparison with Existing Data

As stated in Chapter I, the only existing data on the ion-molecule reaction rate between  $\text{CO}^+$  and  $\text{CO}^+\cdot\text{CO}$  is presented in a paper by Chong and Franklin.<sup>6</sup> In this paper the forward reaction rate is determined to be  $1.43 \times 10^{-28} \text{ cm}^6/\text{sec}$ , in reasonable agreement with our data. At high pressures an equilibrium constant was determined and thereby a backward (detachment) reaction rate was obtained. This backward reaction rate is much larger than the upper limit set by the data presented here. In the determination of the equilibrium constant, no mention was made concerning the precautions taken (if any) in the evaluation of the mass discrimination factor or in the use of high potentials in the ion extraction region. Both of these factors could have serious effects on the validity of the equilibrium constant.

## CHAPTER VII

## CONCLUSIONS

Mobilities

The mobility of  $\text{CO}^+$  in CO was measured over an E/N range from 13 to 667 Td and over a pressure range of 0.026 to 0.106 Torr. The reduced mobility varied from a value of  $1.76 \pm 0.03 \text{ cm}^2/\text{V-sec}$  at an E/N of 13.4 Td to  $0.86 \pm 0.2 \text{ cm}^2/\text{V-sec}$  at an E/N of 667 Td. No zero-field mobility for  $\text{CO}^+$  was obtained due to the effect of an ion-molecule reaction with the CO molecules at low values of E/N.

The mobility of  $\text{CO}^+\cdot\text{CO}$  in CO was measured over an E/N range from 9 to 92 Td and over a pressure range from 0.180 to 0.742 Torr. The zero-field reduced mobility was determined to be  $1.90 \pm 0.03 \text{ cm}^2/\text{V-sec}$ , and the mobility increased with increasing E/N.

The mobility of  $\text{C}^+$  in CO was measured over an E/N range from 14 to 745 Td and over a pressure range from 0.026 to 0.212 Torr. The zero-field reduced mobility was found to be  $2.7 \pm 0.1 \text{ cm}^2/\text{V-sec}$ .

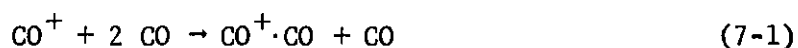
The mobility of  $\text{K}^+$  in CO was measured over an E/N range from 4 to 640 Td, and over a pressure range from 0.026 to 0.795 Torr. The zero-field reduced mobility was determined to be  $2.30 \pm 0.04 \text{ cm}^2/\text{V-sec}$ . The reduced mobility showed the characteristic "hump" of alkali ions drifting in molecular gases, with the "hump" peaking at a reduced mobility of  $2.75 \pm 0.04 \text{ cm}^2/\text{V-sec}$  for an E/N of 250 Td.

### Longitudinal Diffusion Coefficients

Longitudinal diffusion coefficients were measured for  $\text{CO}^+$  and  $\text{K}^+$  in carbon monoxide. For  $\text{CO}^+$ , values of  $D_L$  were obtained over the range of  $E/N$  from 13 to 667 Td and over a pressure range of 0.026 to 0.053 Torr. For  $\text{K}^+$ , values of  $D_L$  were obtained over the range of  $E/N$  from 4 to nearly 600 Td and over a pressure range from 0.026 to 0.795 Torr. The values of  $ND_L$  for  $\text{K}^+$  rose steeply, from a value of  $1.63 \pm 0.09 \times 10^{18} \text{ (cm-sec)}^{-1}$  at low  $E/N$  to nearly  $10^{20} \text{ (cm-sec)}^{-1}$  at our highest values of  $E/N$ . The measured values of  $ND_L$  for  $\text{CO}^+$  did not rise nearly as steeply, possibly due to the effect of resonant charge transfer in the interaction potential for  $\text{CO}^+$  ions in CO. The values of  $ND_L$  for  $\text{K}^+$  agreed very well with the predictions of the theory for polarization force interactions at values of  $E/N$  less than 200 Td.

### Ion-Molecule Reactions

The rate constant for the reaction

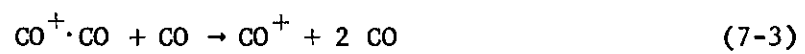


was measured over the  $E/N$  range from 75 to 150 Td and at pressures from 0.053 to 0.159 Torr. The rate coefficient was found to vary from  $1.35 \pm 0.16 \times 10^{-28} \text{ cm}^6/\text{sec}$  at an  $E/N$  of 75 Td to  $1.10 \pm 0.13 \times 10^{-28} \text{ cm}^6/\text{sec}$  for values of  $E/N$  between 110 and 150 Td. The data clearly indicate that this reaction is three-body over the  $E/N$  and pressure range of these measurements.

The reactions



and



were also observed, but no rate coefficients could be determined for their rates of reaction.

## APPENDIX I

## TABULATION OF THE MOBILITY RESULTS

The following pages list the results of the mobility determinations described in Chapter IV. The drift velocity and mobility results appear in order of increasing E/N for each ion species. E/N is in Townsends (Td). The reduced mobility is simply the value of the ratio  $v_d/E$ , reduced according to Equation (1-2) to 760 Torr at 0°C. The standard deviation is the standard deviation in percentage of the experimental points from the least squares fit straight line. The drift velocity is obtained from the least squares fit straight line except when only two positions were used. Then a simple difference was employed. The units are  $10^4$  cm/sec. Pressure is in Torr. Run number refers to an identification number assigned to each set of (usually) four experimental spectra.

Table 3. Mobility and Drift Velocity Results for CO<sup>+</sup> Ions  
in Carbon Monoxide

E/N (Td)	Reduced Mobility (cm <sup>2</sup> /V-sec)	Standard Deviation (Percent)	Drift Velocity (10 <sup>4</sup> cm/sec)	Pressure (Torr)	Run Number
13.37	1.76	0.0	0.631	0.053	224
20.04	1.73	0.5	0.933	0.053	223
23.37	1.73	0.4	1.09	0.053	238
26.71	1.71	0.2	1.23	0.053	222
31.62	1.71	0.1	1.45	0.053	46
33.37	1.71	0.5	1.53	0.053	221
40.12	1.68	0.1	1.82	0.053	211
42.61	1.67	0.3	1.91	0.106	17
46.74	1.66	0.1	2.08	0.053	220
49.88	1.64	0.4	2.19	0.106	14
53.46	1.64	0.1	2.35	0.053	210
58.10	1.62	0.2	2.53	0.053	45
62.67	1.62	0.4	2.72	0.053	225
66.79	1.59	0.1	2.86	0.053	209
66.96	1.59	0.1	2.86	0.106	4
73.19	1.58	0.0	3.12	0.053	226
83.76	1.54	0.2	3.46	0.106	5
85.32	1.57	0.3	3.60	0.053	18
89.77	1.55	0.0	3.74	0.053	1
89.80	1.53	0.2	3.69	0.080	39
93.35	1.52	0.1	3.82	0.053	207
93.61	1.56	0.4	3.91	0.026	199
94.12	1.52	0.1	3.84	0.053	206
100.5	1.50	0.0	4.04	0.106	3
106.6	1.49	0.3	4.26	0.080	38
107.4	1.49	0.0	4.29	0.053	205
117.4	1.45	0.0	4.58	0.106	6
120.3	1.48	0.1	4.77	0.026	198
120.7	1.46	0.2	4.73	0.053	204
124.3	1.44	0.1	4.80	0.080	37
134.0	1.42	0.0	5.13	0.053	203
134.2	1.41	0.2	5.07	0.106	2
134.5	1.40	0.1	5.07	0.053	159
142.0	1.40	0.0	5.34	0.080	36
147.0	1.40	0.2	5.55	0.026	197
157.6	1.37	0.1	5.82	0.053	27
167.5	1.35	0.2	6.09	0.053	202
173.0	1.33	0.0	6.17	0.080	35



Table 3. (Continued)

E/N (Td)	Reduced Mobility (cm <sup>2</sup> /V-sec)	Standard Deviation (Percent)	Drift Velocity (10 <sup>4</sup> cm/sec)	Pressure (Torr)	Run Number
187.2	1.32	0.2	6.61	0.026	188
196.7	1.29	0.2	6.83	0.053	28
199.8	1.29	0.1	6.91	0.053	161
200.2	1.30	0.1	6.99	0.026	167
213.8	1.26	0.1	7.23	0.026	187
217.3	1.25	0.3	7.31	0.080	34
227.6	1.26	0.4	7.71	0.026	195
233.1	1.22	0.0	7.68	0.053	162
240.6	1.23	0.2	7.94	0.026	186
246.0	1.22	0.2	8.07	0.053	29
266.6	1.18	0.1	8.43	0.053	163
267.2	1.18	0.1	8.50	0.026	185
281.8	1.16	0.1	8.80	0.053	201
293.7	1.14	0.1	9.01	0.026	184
300.0	1.13	0.2	9.11	0.053	164
308.4	1.12	0.0	9.32	0.053	200
320.2	1.11	0.1	9.55	0.026	183
333.6	1.09	0.1	9.81	0.053	165
333.7	1.11	0.2	9.95	0.026	169
346.8	1.08	0.1	10.10	0.026	182
374.2	1.06	0.3	10.65	0.026	181
400.6	1.04	0.2	11.17	0.026	170
427.4	1.00	0.2	11.53	0.026	180
454.6	0.986	0.1	12.04	0.026	179
467.4	0.982	0.2	12.34	0.026	171
481.0	0.965	0.1	12.47	0.026	178
507.3	0.945	0.2	12.89	0.026	177
534.4	0.925	0.0	13.28	0.026	172
566.8	0.911	0.0	13.87	0.026	176
600.7	0.896	0.3	14.46	0.026	173
633.3	0.875	0.1	14.89	0.026	175
667.5	0.857	0.2	15.37	0.026	174

Table 4. Mobility and Drift Velocity Results for  $\text{CO}^+\cdot\text{CO}$  Ions  
in Carbon Monoxide

E/N (Td)	Reduced Mobility ( $\text{cm}^2/\text{V}\cdot\text{sec}$ )	Standard Deviation (Percent)	Drift Velocity ( $10^4 \text{ cm/sec}$ )	Pressure (Torr)	Run Number
8.87	1.90	0.2	0.453	0.742	217
9.84	1.90	0.2	0.502	0.742	216
10.1	1.90	0.1	0.516	0.530	155
11.8	1.91	0.1	0.607	0.742	215
12.7	1.90	0.4	0.651	0.212	24
13.4	1.90	0.0	0.684	0.530	154
14.0	1.93	0.1	0.728	0.318	43
14.8	1.89	0.1	0.751	0.742	214
16.0	1.91	0.0	0.821	0.212	23
16.8	1.90	0.0	0.855	0.530	153
17.7	1.89	0.2	0.899	0.742	213
18.7	1.91	0.4	0.960	0.318	42
19.2	1.91	0.1	0.984	0.742	158
20.1	1.90	0.0	1.02	0.530	152
20.5	1.90	0.2	1.05	0.212	22
21.6	1.90	0.1	1.10	0.742	157
23.4	1.89	0.1	1.19	0.530	151
23.6	1.89	0.2	1.20	0.742	212
24.0	1.92	0.2	1.24	0.318	41
25.6	1.90	0.0	1.31	0.742	156
26.7	1.90	0.1	1.36	0.180	21
26.8	1.89	0.1	1.36	0.530	150
31.5	1.91	0.1	1.62	0.530	228
34.6	1.92	0.1	1.78	0.180	20
36.7	1.92	0.1	1.89	0.530	229
41.3	1.92	0.1	2.12	0.424	231
42.4	1.91	0.5	2.17	0.180	19
45.9	1.93	0.2	2.38	0.424	230
50.1	1.93	0.3	2.60	0.180	13
54.1	1.94	0.1	2.82	0.318	232
57.9	1.95	0.4	3.03	0.180	12
61.2	1.96	0.1	3.22	0.318	233
65.7	1.97	0.7	3.47	0.180	11
66.8	1.97	0.2	3.54	0.212	234
73.4	2.00	0.2	3.96	0.180	10
78.8	2.01	0.2	4.25	0.212	235
86.8	2.03	0.4	4.73	0.212	236
89.3	2.03	0.0	4.87	0.180	8
92.1	2.04	0.5	5.06	0.212	237

Table 5. Mobility and Drift Velocity Results for  $C^+$  Ions  
in Carbon Monoxide

E/N (Td)	Reduced Mobility ( $cm^2/V\text{-sec}$ )	Standard Deviation (Percent)	Drift Velocity ( $10^4$ cm/sec)	Pressure (Torr)	Run Number
13.9	2.78	1.8	1.04	0.106	132
17.2	2.65	3.4	1.22	0.106	143
20.0	2.70	0.3	1.45	0.106	133
21.1	2.72	2.4	1.54	0.212	129
24.3	2.75	3.0	1.80	0.106	144
27.6	2.74	1.8	2.01	0.106	131
31.4	2.71	2.2	2.29	0.212	128
34.2	2.74	0.9	2.52	0.106	130
35.0	2.67	1.6	2.51	0.053	122
41.8	2.64	2.2	2.92	0.212	116
52.7	2.66	2.1	3.76	0.212	115
62.4	2.65	2.0	4.44	0.212	114
69.5	2.65	1.7	4.94	0.053	121
72.0	2.62	0.9	5.07	0.212	113
81.8	2.58	0.4	5.68	0.212	112
91.5	2.56	0.4	6.31	0.212	111
106.2	2.54	1.6	7.25	0.053	123
117.2	2.54	0.5	7.98	0.053	134
142.7	2.54	1.5	9.75	0.053	120
150.9	2.51	0.6	10.19	0.053	135
177.7	2.46	1.3	11.74	0.053	124
213.5	2.48	1.0	14.21	0.053	119
248.4	2.46	1.1	16.45	0.053	118
277.1	2.48	1.5	18.43	0.053	125
316.4	2.47	1.7	21.01	0.053	117
343.3	2.52	1.7	23.28	0.026	142
346.8	2.50	1.7	23.29	0.053	126
381.9	2.53	1.8	25.96	0.053	127
408.8	2.58	0.9	28.31	0.026	141
474.9	2.60	0.9	33.24	0.026	140
544.3	2.76	1.0	40.35	0.026	138
609.2	2.73	1.8	44.66	0.026	139
676.9	2.85	1.2	51.88	0.026	137
745.1	2.86	1.0	57.33	0.026	136

Table 6. Mobility and Drift Velocity Results for  $K^+$  Ions  
in Carbon Monoxide

E/N (Td)	Reduced Mobility ( $\text{cm}^2/\text{V-sec}$ )	Standard Deviation (Percent)	Drift Velocity ( $10^4 \text{ cm/sec}$ )	Pressure (Torr)	Run Number
3.94	2.31	0.5	0.245	0.795	106
5.02	2.29	0.2	0.310	0.530	94
5.91	2.31	0.3	0.366	0.795	105
6.70	2.30	0.3	0.414	0.530	75
7.87	2.29	0.4	0.483	0.795	104
8.83	2.29	0.3	0.545	0.795	103
10.0	2.31	0.2	0.623	0.530	73
10.0	2.28	0.3	0.616	0.212	71
13.4	2.30	0.3	0.830	0.530	76
15.0	2.31	0.3	0.930	0.212	62
20.1	2.31	0.3	1.25	0.212	59
20.1	2.31	0.2	1.25	0.530	77
25.1	2.31	0.2	1.56	0.212	60
30.1	2.31	0.1	1.86	0.212	69
30.2	2.32	0.2	1.88	0.530	78
40.1	2.30	0.2	2.48	0.212	91
40.2	2.32	0.3	2.50	0.212	72
50.2	2.32	0.2	3.12	0.212	70
50.2	2.33	0.2	3.14	0.212	79
60.2	2.32	0.3	3.75	0.212	93
70.1	2.35	0.3	4.42	0.212	68
80.2	2.39	0.5	5.16	0.212	66
90.2	2.38	0.3	5.77	0.212	92
100.4	2.45	0.7	6.60	0.053	80
125.0	2.51	0.6	8.42	0.053	86
133.9	2.54	0.3	9.13	0.053	97
150.5	2.58	0.3	10.43	0.053	96
175.1	2.65	0.2	12.47	0.053	87
200.5	2.73	0.4	14.69	0.053	82
225.2	2.74	0.1	16.59	0.053	88
248.1	2.74	0.3	18.24	0.026	102
250.7	2.78	0.5	18.76	0.053	95
275.4	2.75	0.1	20.35	0.053	89
275.4	2.74	0.1	20.32	0.053	90
297.6	2.74	0.4	21.95	0.026	101
301.1	2.74	0.5	22.13	0.053	83
343.6	2.73	0.2	25.23	0.026	107
395.0	2.68	0.4	28.48	0.026	100
442.0	2.66	0.3	31.56	0.026	108
492.9	2.61	0.3	34.58	0.026	99
541.0	2.54	0.1	36.95	0.026	109
592.5	2.48	0.6	39.54	0.026	98
639.9	2.46	0.2	42.21	0.026	110

## APPENDIX II

## TABULATION OF THE LONGITUDINAL DIFFUSION COEFFICIENT RESULTS

The following pages list the results of the longitudinal diffusion coefficient determinations described in Chapter V. The results appear in order of increasing E/N for each ion species. The column headings, E/N, Pressure, and Run Number have the same meaning as in Appendix I. ND<sub>L</sub> gives the gas number-density normalized longitudinal diffusion coefficient for comparison between various pressures, in units of  $10^{18}$ /cm-sec. Mean Deviation is the mean deviation in percentage by which the D<sub>L</sub> values for the three or four positions differed from the average. D<sub>L</sub> is the longitudinal diffusion coefficient as determined by the curve-fitting program. The value is the average of the values obtained from (usually) four drift positions. Posns are the ion-source drift positions used (see Chapter IV).

Table 7. Longitudinal Diffusion Results for  $\text{CO}^+$  Ions  
in Carbon Monoxide

E/N (Td)	$\text{ND}_L$ ( $10^{18}/\text{cm-sec}$ )	Mean Deviation (Percent)	$\text{D}_L$ ( $\text{cm}^2/\text{sec}$ )	Pressure (Torr)	Run Number	Posns
13.8	1.68	12.2	980	0.053	224	321
20.0	1.73	8.3	1010	0.053	223	321
23.8	2.01	11.8	1180	0.053	238	321
26.7	1.83	13.6	1070	0.053	222	321
33.4	2.00	11.0	1170	0.053	221	32 <sup>3</sup> <sub>1</sub>
40.1	1.69	3.1	990	0.053	211	6543
46.7	2.13	15.1	1240	0.053	220	4321
53.5	1.82	2.8	1050	0.053	210	6543
62.7	2.27	7.2	1320	0.053	225	543
66.8	1.88	6.8	1100	0.053	209	6543
73.2	2.18	7.2	1270	0.053	226	543
93.4	1.99	0.7	1160	0.053	207	6543
93.6	2.17	4.1	2540	0.026	199	6543
94.1	2.08	3.7	1220	0.053	206	6543
107.4	2.07	3.1	1220	0.053	205	6543
120.3	2.32	1.3	2720	0.026	198	6543
120.7	2.15	0.9	1260	0.053	204	6543
134.0	2.28	3.6	1330	0.053	203	6543
134.5	2.44	4.9	1440	0.053	159	5432
147.0	2.34	3.3	2740	0.026	197	6543
167.5	2.60	3.5	1520	0.053	202	6543
187.2	2.29	4.7	2780	0.026	188	6543
199.8	2.43	1.4	1420	0.053	161	6543
213.8	2.40	3.4	2810	0.026	187	6543
227.6	3.00	2.0	3510	0.026	195	6543
233.1	2.63	1.5	1530	0.053	162	6543
240.6	2.66	1.9	3110	0.026	186	6543
266.6	2.78	2.6	1620	0.053	163	6543
267.2	2.60	3.3	3040	0.026	185	6543
281.8	2.78	2.5	1630	0.053	201	6543
293.7	2.67	2.1	3120	0.026	184	6543
300.0	2.84	2.7	1660	0.053	164	6543
308.4	2.85	3.3	1670	0.053	200	6543
320.2	3.13	2.5	3650	0.026	183	6543
333.6	3.13	3.3	1820	0.053	165	6543
333.7	3.67	1.8	4290	0.026	169	6543
346.8	3.25	2.8	3790	0.026	182	6543
374.2	3.24	2.9	3790	0.026	181	6543

Table 7. (Continued)

E/N (Td)	$ND_L$ ( $10^{18}$ /cm-sec)	Mean Deviation (Percent)	$D_L$ ( $cm^2$ /sec)	Pressure (Torr)	Run Number	Posns
400.6	3.83	5.3	4480	0.026	170	6543
427.4	3.35	2.9	3910	0.026	180	6543
454.6	3.66	3.4	4280	0.026	179	6543
467.4	4.07	4.0	4750	0.026	171	6543
481.0	3.71	3.6	4340	0.026	178	6543
507.3	4.05	3.5	4730	0.026	177	6543
534.4	4.35	4.5	5090	0.026	172	6543
566.8	4.09	1.8	4780	0.026	176	6543
600.7	5.05	3.0	5900	0.026	173	6543
633.3	4.61	4.1	5370	0.026	175	6543
667.5	5.48	5.6	6400	0.026	174	6543

Table 8. Longitudinal Diffusion Results for  $K^+$  Ions in Carbon Monoxide

E/N (Td)	$ND_L$ ( $10^{18}/\text{cm-sec}$ )	Mean Deviation (Percent)	$D_L$ ( $\text{cm}^2/\text{sec}$ )	Pressure (Torr)	Run Number	Posns
3.94	1.76	1.5	69	0.795	106	53
5.02	1.53	4.4	89	0.530	94	654
5.91	1.69	6.1	66	0.795	105	7654
6.70	1.64	1.1	96	0.530	75	654
7.87	1.52	1.2	60	0.795	104	543
8.83	1.61	3.4	63	0.795	103	6543
10.0	1.66	3.2	97	0.530	73	6543
10.0	1.62	1.3	237	0.212	71	654
13.4	1.68	5.0	99	0.530	76	7654
15.0	1.70	2.3	248	0.212	62	654
20.1	1.73	2.0	255	0.212	59	654
20.1	1.76	5.0	104	0.530	77	765
25.1	1.85	4.2	270	0.212	60	654
30.1	1.91	2.9	278	0.212	69	654
30.2	1.99	0.8	117	0.530	78	765
40.1	2.15	4.0	314	0.212	91	654
40.2	2.09	2.5	307	0.212	72	765
50.2	2.72	4.7	399	0.212	70	654
50.2	2.52	1.3	369	0.212	79	654
60.2	2.93	2.6	428	0.212	93	7654
70.1	3.59	3.1	524	0.212	68	765
80.2	4.63	5.3	677	0.212	66	765
90.2	5.29	2.2	772	0.212	92	7654
100.4	7.12	2.3	4170	0.053	80	765
125.0	10.5	2.1	6130	0.053	86	7654
133.9	12.2	2.2	7160	0.053	97	7654
150.5	14.7	1.3	8590	0.053	96	7654
175.1	19.2	2.7	11200	0.053	87	7654
200.5	25.9	0.8	15200	0.053	82	7654
225.2	27.9	1.1	16300	0.053	88	7654
248.1	32.8	0.5	38500	0.026	102	7654
250.7	33.9	3.9	19800	0.053	95	7654
275.4	36.4	2.3	21200	0.053	89	7654
275.4	35.2	2.7	20600	0.053	90	7654
297.6	40.3	3.1	47200	0.026	101	765
301.1	38.5	7.8	23300	0.053	83	7654
343.6	51.4	0.9	60000	0.026	107	54
395.0	55.4	3.5	64900	0.026	100	765
442.0	68.1	3.7	80900	0.026	108	765
492.9	76.3	3.8	89300	0.026	99	7654
541.0	92.9	6.0	108600	0.026	109	765
592.5	94.2	2.4	110500	0.026	98	765



## APPENDIX III

## TABULATION OF THE ION-MOLECULE REACTION RATES

The following table lists the results of the ion-molecule reaction rate determination discussed in Chapter VI. The results appear in order of increasing E/N. The Rate Coefficient is the coefficient  $k$ , in units of  $\text{cm}^6/\text{sec}$ , for  $\text{CO}^+$  reacting to form  $\text{CO}^+\cdot\text{CO}$ . The Pressure Range is the range of pressure, in units of Torr, used in obtaining product ion arrival-time spectra for the curve-fitting procedure. The  $\text{CO}^+$  Mobility lists the values of reduced mobility of the  $\text{CO}^+$  ions, in units of  $\text{cm}^2/\text{V}\cdot\text{sec}$ . These values were determined experimentally by the standard mobility measurements. The  $\text{CO}^+\cdot\text{CO}$  Mobility lists the values of reduced mobility of the  $\text{CO}^+\cdot\text{CO}$  ions, in units of  $\text{cm}^2/\text{V}\cdot\text{sec}$ . These values were determined from fitting the width of the product ion arrival-time spectra.

Table 9. Reaction Rate Coefficient Results for the Reaction  
 $\text{CO}^+ + 2 \text{CO} \rightarrow \text{CO}^+ \cdot \text{CO} + \text{CO}$

E/N (Td)	Rate Coefficient ( $\text{cm}^6/\text{sec}$ )	Pressure Range (Torr)	$\text{CO}^+$ Mobility ( $\text{cm}^2/\text{V-sec}$ )	$\text{CO}^+ \cdot \text{CO}$ Mobility ( $\text{cm}^2/\text{V-sec}$ )
75.0	$1.35 \times 10^{-28}$	0.078-0.132	1.56	1.97
87.5	$1.18 \times 10^{-28}$	0.078-0.159	1.52	2.00
100.0	$1.21 \times 10^{-28}$	0.078-0.159	1.48	2.06
112.5	$1.05 \times 10^{-28}$	0.078-0.159	1.45	2.11
125.0	$1.05 \times 10^{-28}$	0.078-0.159	1.43	2.16
137.5	$1.12 \times 10^{-28}$	0.053-0.132	1.40	2.27
150.0	$1.12 \times 10^{-28}$	0.078-0.132	1.37	2.33

## APPENDIX IV

## IONIC FLUX NEAR THE GUARD RINGS

In the solution of the transport equation in Chapter III, it was assumed that the ions were drifting in an unbounded volume containing only the low pressure gas. It was also assumed that the electric field was uniform over this unbounded space. These assumptions are violated if an ion diffuses near the guard rings. The purpose of this appendix is to present an analysis that can be used to determine if a significant number of ions are approaching the guard rings and thereby distorting the ionic flux density at the exit aperture.

Through the mathematics of this appendix, the percentage of ions that are within a certain radius  $r_1$  of the axis of the drift tube at a time  $t$  after being released into the drift tube will be determined. We will consider the restricted situation where only one ion species is introduced to the drift tube and that it undergoes only a depleting reaction. The differential equation governing the motion of this ion swarm is

$$\frac{\partial n}{\partial t} = D_T \left( \frac{\partial^2 n}{\partial x^2} + \frac{\partial^2 n}{\partial y^2} \right) + D_L \left( \frac{\partial^2 n}{\partial z^2} \right) - v_d \frac{\partial n}{\partial z} - \alpha n. \quad (A4-1)$$

The solution to this differential equation is (from Chapter III)

$$n(\vec{x}) = \int d^4 x' G(\vec{x}-\vec{x}') \beta(\vec{x}') \quad (A4-2)$$

where

$$G(\vec{x}) = \left[ (4\pi D_T t)^2 4\pi D_L t \right]^{-\frac{1}{2}} \exp \left[ -\alpha t - \frac{x^2 + y^2}{4D_T t} - \frac{(z - v_d t)^2}{4D_L t} \right] \quad (A4-3)$$

and

$$\vec{\beta}(\mathbf{x}) = \frac{b}{\pi r_0} S(r_0 - r) \delta(z) \delta(t). \quad (\text{A4-4})$$

If we define  $F$  to be the fraction of ions that lies within  $r_1$  centimeters from the axis, then

$$F = \int_{-\infty}^{+\infty} dz \int_0^{r_1} r dr \int_0^{2\pi} d\theta n(r, \theta, z, t) \quad (\text{A4-5})$$

$$= \frac{b}{\pi r_0} \left[ (4\pi D_T t)^2 4\pi D_L t \right]^{-\frac{1}{2}} \exp[-\alpha t] \int_{-\infty}^{\infty} dz \exp\left(-\frac{(z - v_d t)^2}{4D_L t}\right) \quad (\text{A4-6})$$

$$\times \int_0^{r_1} r dr \int_0^{2\pi} d\theta \int_0^{r_0} r' dr' \int_0^{2\pi} d\theta' \exp\left[-\frac{r^2 + r'^2 - 2rr' \cos(\theta - \theta')}{4D_T t}\right].$$

If we make the following definitions

$$x = \frac{r^2}{4D_T t}, \quad x_0 = \frac{r_1^2}{4D_T t}, \quad y = \frac{r'^2}{4D_T t}, \quad y_0 = \frac{r_0^2}{4D_T t}, \quad \text{and } \varphi = \theta - \theta', \quad (\text{A4-7})$$

and perform the  $z$  integration, we obtain

$$F = b \exp(-\alpha t) y_0^{-1} \int_0^{x_0} dx \int_0^{y_0} dy \frac{1}{2\pi} \int_0^{2\pi} d\varphi \exp[-x - y + \sqrt{4xy} \cos\varphi]. \quad (\text{A4-8})$$

Since the following equality holds:

$$\frac{1}{\pi} \int_0^{\pi} \exp(\sqrt{4xy} \cos\varphi) d\varphi = \sum_{n=0}^{\infty} \frac{x^n}{n!} \frac{y^n}{n!} \quad (\text{A4-9})$$

one obtains

$$F = b \exp(-\alpha t) y_0^{-1} \sum_{n=0}^{\infty} \left( \int_0^{x_0} \frac{x^n}{n!} e^{-x} dx \right) \left( \int_0^{y_0} \frac{y^n}{n!} e^{-y} dy \right). \quad (\text{A4-10})$$

The integrals can be evaluated for a given value of  $n$  by the following equality:

$$\int_0^{x_0} \frac{x^n}{n!} e^{-x} dx = e^{-x_0} \sum_{i=n+1}^{\infty} \frac{x_0^i}{i!}. \quad (\text{A4-11})$$

Combining equations (A4-10) and (A4-11) we find that

$$F = b \exp(-\alpha t) \exp[-(x_0+y_0)] \sum_{n=1}^{\infty} \left( \sum_{i=n}^{\infty} \frac{x_0^i}{i!} \right) \left( \sum_{j=n}^{\infty} \frac{y_0^{j-1}}{j!} \right). \quad (\text{A4-12})$$

Using a computer program written for the purpose, the above expression was evaluated for various values of  $x_0$  and  $y_0$ , with  $\alpha=0$ . To conform to the actual geometry of the ion source,  $r_0$  was set equal to 0.9525 centimeter. Since  $x_0 = r_1/4D_T t$  and  $y_0 = r_0/4D_T t$ , the actual parameters of interest are  $r_1$  and the quantity  $(4D_T t)$ . In Figure 17,  $F$  is plotted for various values of  $r_1$  and  $(4D_T t)$ .

As calculated in the report by Albritton, et al.,<sup>61</sup> the electric field strength in the drift tube is uniform to within one percent for radial distances less than 6.02 centimeters. Diffusion is produced by a random walk process caused by the random thermal motion of the ions and gas molecules. In the theoretical model of an infinite drift space with an electric field of uniform field strength, the probability of an ion diffusing radially a distance  $r$  from the axis and then diffusing back to reach the axis is the same as an ion diffusing radially a distance  $2r$ .

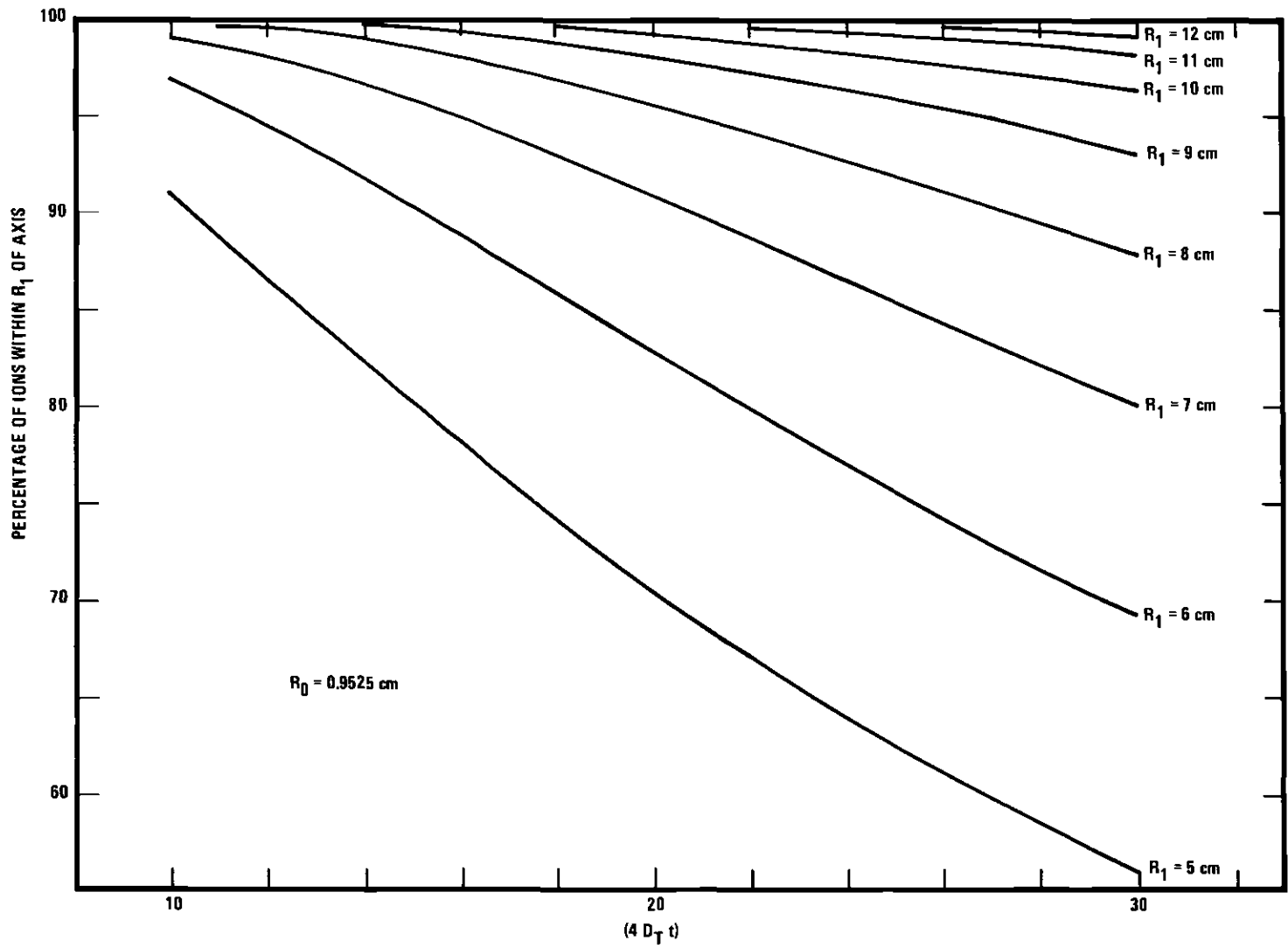


Figure 17. Plot of the Percentage of Ions Within a Given Radius versus  $(4 D_T t)$

On this basis, the number of ions that diffuse past 6 centimeters in the drift tube and then diffuse back to the region near the exit aperture would be the number predicted by this model to diffuse more than 12 centimeters from the axis. From Figure 17, this would be less than one percent of the total number of ions for values of the quantity  $(4D_T t)$  that are less than 30.

In the research just performed, the largest amount of transverse diffusion occurred for  $K^+$  ions at large values of  $E/N$ . At these high values of  $E/N$ , the random energy added to the ions by the presence of the electric field greatly increased the transverse diffusion coefficient. In addition, position 7 was used for the high  $E/N$  work, thereby increasing the drift time  $t$ . Even at this extreme, the value of  $(4D_T t)$  is estimated to be less than 19. Very few of the ions, well less than one percent, could have diffused to a point near the drift tube walls and then diffused back to the axis and been detected.

## BIBLIOGRAPHY\*

1. E. W. McDaniel, Collision Phenomena in Ionized Gases (John Wiley and Sons, New York, 1964), pp. 491.
2. G. H. Wannier, Bell System Tech. J. 32, 170 (1953).
3. A. M. Tyndall, The Mobility of Positive Ions in Gases (Cambridge University Press, London, 1938), p. 54.
4. R. N. Varney, Phys. Rev. 89, 708 (1953).
5. M. Saporoschenko, J. Chem. Phys. 49, 768 (1968).
6. S. Chong and J. L. Franklin, J. Chem. Phys. 54, 1487 (1971).
7. D. A. Parkes, Trans. Faraday Soc. 67, 711 (1971).
8. L. G. McKnight, K. B. McAfee, and D. P. Sipler, Phys. Rev. 164, 62 (1967).
9. D. S. Burch and R. Geballe, Phys. Rev. 106, 188 (1957).
10. D. Edelson and K. B. McAfee, Rev. Sci. Instr. 35, 187 (1964).
11. D. Edelson, J. A. Morrison, and K. B. McAfee, J. Appl. Phys. 35, 1682 (1964).
12. L. Frommhold, Fortschritte der Physik 12, 597 (1964).
13. E. C. Beaty and P. L. Patterson, Phys. Rev. 137, 346 (1965).
14. W. S. Barnes, Phys. Fluids 10, 1941 (1967).
15. D. Edelson, J. A. Morrison, L. G. McKnight, and D. P. Sipler, Phys. Rev. 164, 71 (1967).
16. D. Edelson, J. Appl. Phys. 39, 3497 (1968).
17. J. H. Whealton and S. B. Woo, Phys. Rev. Letters 20, 1137 (1968).

---

\*Abbreviations used herein conform to those in the American Institute of Physics Style Manual, 1965.



## BIBLIOGRAPHY (Continued)

18. J. T. Moseley, D. W. Martin, E. W. McDaniel, R. M. Snuggs, and T. M. Miller, Technical Report, Georgia Institute of Technology, Atlanta, Georgia (1968), Chap. IV.
19. J. T. Moseley, I. R. Gatland, D. W. Martin, and E. W. McDaniel, Phys. Rev. 178 (1969).
20. S. B. Woo and J. H. Whealton, Phys. Rev. 180, 314 (1969). Errata published Phys. Rev. A 1, 1558 (1970).
21. G. E. Keller, M. R. Sullivan, and M. D. Kregel, Phys. Rev. A 1, 1556 (1970).
22. R. M. Snuggs, D. J. Volz, J. H. Schummers, R. D. Laser, I. R. Gatland, D. W. Martin, and E. W. McDaniel, Technical Report, Georgia Institute of Technology, Atlanta, Georgia (1970), Chap. III.
23. R. M. Snuggs, D. J. Volz, I. R. Gatland, J. H. Schummers, D. W. Martin, and E. W. McDaniel, Phys. Rev. A 3, 487 (1971).
24. S. B. Woo and J. H. Whealton, Phys. Rev. A 4, 1046 (1971).
25. D. L. Albritton, D. W. Martin, E. W. McDaniel, T. M. Miller, and J. T. Moseley, Technical Report, Georgia Institute of Technology, Atlanta, Georgia (1967), Chap. II.
26. T. M. Miller, D. W. Martin, E. W. McDaniel, J. T. Moseley, and R. M. Snuggs, Technical Report, Georgia Institute of Technology, Atlanta, Georgia (1968), Chap. II.
27. J. T. Moseley, et al., Technical Report, Chap. II.
28. R. M. Snuggs, et al., Technical Report, Chap. II.
29. L. J. Puckett, M. W. Teague, and D. G. McCoy, Rev. Sci. Instr. 42, 580 (1971).
30. E. W. McDaniel and D. W. Martin, Rev. Sci. Instr. 42, 157 (1971).
31. J. T. Moseley, et al., op. cit., Chap. IV.
32. E. W. McDaniel and J. T. Moseley, Phys. Rev. A 3, 1040 (1971).
33. Snuggs, et al., op. cit., Appendix V.
34. Ibid., Chap. III.

## BIBLIOGRAPHY (Continued)

35. R. C. Amme and N. G. Utterback, Proc. Intern. Conf. Phys. of Electron. Atomic Collisions, 1st Univ. Coll. London, 1963 (North-Holland Publishing Company, Amsterdam, 1964), p. 847.
36. J. W. McGowan and L. Kerwin, Can. J. Phys. 42, 2086 (1964).
37. R. E. Fox and W. M. Hickam, J. Chem. Phys. 22, 2059 (1954).
38. T. R. Hogness and R. W. Harkness, Phys. Rev. 32, 936 (1928).
39. A. L. Vaughan, Phys. Rev. 38, 1687 (1931).
40. W. W. Lozier, Phys. Rev. 46, 268 (1934).
41. H. D. Hagstrum and J. T. Tate, Phys. Rev. 59, 354 (1941).
42. H. D. Hagstrum, Rev. Mod. Phys. 23, 185 (1951).
43. C. R. Lagergren, Dissertation, Univ. of Minnesota (1955).
44. M. A. Fineman and A. W. Petrocelli, J. Chem. Phys. 36, 25 (1962).
45. E. W. McDaniel, Collision Phenomena in Ionized Gases, p. 732.
46. M. S. B. Munson, F. H. Field, and J. L. Franklin, J. Chem. Phys. 37, 1790 (1962).
47. J. T. Moseley, et al., op. cit., pp. 125-126.
48. D. L. Albritton, et al., op. cit., Appendix VI.
49. J. T. Moseley, et al., op. cit., p. 123.
50. D. L. Albritton, et al., op. cit., Chap. IV.
51. J. T. Moseley, et al., op. cit., Appendix IV.
52. E. W. McDaniel and E. A. Mason, The Mobility and Diffusion of Ions in Gases (Wiley, New York, 1973).
53. J. O. Hirschfelder, C. F. Curtis, and R. B. Bird, Molecular Theory of Gases and Liquids (Wiley, New York, 1964), p. 950.
54. G. M. Thomson (to be published).
55. J. T. Moseley, et al., op. cit., pp. 97-99.
56. Ibid., p. 163.

## BIBLIOGRAPHY (Concluded)

57. R. M. Snuggs, et al., op. cit., p. 134.
58. D. J. Volz, J. H. Schummers, R. D. Laser, D. W. Martin, and E. W. McDaniel, Phys. Rev. A 4, 1106 (1971).
59. H. Fahr and K. G. Müller, Z. Physik 200, 343 (1967).
60. J. Heimerl, R. Johnson, and M. A. Biondi, J. Chem. Phys. 51, 5041 (1969).
61. D. L. Albritton, et al., op. cit., Appendix IV.

## VITA

John Herman Schummers was born in San Mateo, California, on August 28, 1946. He is the second of three sons of Lt. Col. and Mrs. W. M. Schummers. He was married to Claris Ann Farmer on September 18, 1970.

Mr. Schummers was graduated from Mount Vernon High School in Alexandria, Virginia, in 1964. He entered the Georgia Institute of Technology in that year. During the summers as an undergraduate student, he was employed by the Data Services Center of the Department of the Air Force. He received the degree of Bachelor of Science in Physics, with Highest Honor, in 1968. Through the AFROTC, he was commissioned a Second Lieutenant in the United States Air Force Reserve. He immediately began graduate study, and received the degree of Master of Science in Physics in 1969.

Mr. Schummers is a member of Sigma Xi, the American Physical Society, Tau Beta Pi, Phi Kappa Phi, and Sigma Pi Sigma.